THESIS REPORT

Ph.D.

Design and Optimization of Planar Leg Mechanisms Featuring Symmetrical Foot-Point Paths

by W-B. Shieh
Advisor: L-W. Tsai

Ph.D. 96-5

Sponsored by
the National Science Foundation
Engineering Research Center Program,
the University of Maryland,
Harvard University,
and Industry

Design and Optimization of Planar Leg Mechanisms Featuring Symmetrical Foot-Point Paths

by

Win-Bin Shieh

Dissertation submitted to the Faculty of the Graduate School
of The University of Maryland in partial fulfillment
of the requirements for the degree of
Doctor of Philosophy
1996

Advisory Committee:

Professor Lung-Wen Tsai, Chairman/Advisor
Associate Professor Shapour Azarm (Co-Advisor)
Professor André Tits (Co-Advisor)
Professor Nariman Farvardin
Assistant Professor Gregory C. Walsh

Abstract

Title of Dissertation: Design and Optimization of Planar Leg Mechanisms Featuring Symmetrical Foot-Point Paths

Win-Bin Shieh, Doctor of Philosophy, 1996

Dissertation directed by: Professor Lung-Wen Tsai[1] (Advisor)
Associate Professor Shapour Azarm[2] (Co-Advisor)
Professor André Tits[3] (Co-Advisor)
Department of Mechanical Engineering[1,2]
Department of Electrical Engineering[3]
Institute for Systems Research[1,3]

Design and optimization of planar leg mechanisms featuring symmetrical foot-point paths are presented in this study. These leg mechanisms are designed in such a way that a corresponding walking machine has the flexibility required for walking on a rough terrain, while it can achieve fast locomotion, is easy to control, and requires minimal actuation for walking on a flat ground. In addition, such leg mechanisms are compact in size with respect to a specified horizontal stride.

Based on a set of functional requirements, the concept generation of a set of leg mechanisms is accomplished via a systematic methodology. By temporarily excluding the degree-of-freedom (DOF) associated with the up-and-down motion of the leg, and based on a set of evaluation criteria, six admissible one-DOF planar four-, six-, and eight-bar leg mechanisms are found to have the desirable features to be used as a leg mechanism.

It is argued that a symmetrical foot-point path can be advantageous in reducing the maximum driving torque and making the motion control of the leg easier. While the four- and eight-bar compound mechanisms have been studied, a new class of six-bar linkages with an embedded (skew-) pantograph featuring a symmetrical foot-point path is introduced. Construction and design limitations for such six-bar mechanisms are explored. The guidelines to prevent double point(s) are derived and the conditions to select between the propelling and non-propelling portions of the path are established.

For the dimensional synthesis, the admissible mechanisms with and without an adjustable pivot are investigated. For those mechanisms with an adjustable pivot, one DOF is used for normal walking to provide an ovoid path which emulates that of humans, while the other (the motion of the adjustable pivot) is used only when necessary to walk over obstacles. For those mechanisms without an adjustable pivot, the sole DOF provides a large Δ-shaped path, with which the leg mechanisms are capable of performing the up-and-down as well as the back-and-forth motions. To exploit these to the fullest, a multi-objective optimization-based design problem formulation is developed to minimize the following three design objectives: (i) peak crank torque, (ii) maximum actuating force, and (iii) leg size. Results from the optimization model show that an eight-bar compound mechanism with an adjustable pivot and a six-bar mechanism without an adjustable pivot are the two best leg designs among those studied here.

Finally, further reduction of the actuating force and crank torque is successfully demonstrated by placing tension spring elements onto an already optimized eight-bar leg mechanism.

Dedication

To my parents and

my beloved country - Taiwan

Acknowledgements

I would like to express my sincere thanks to my advisor, Professor Lung-Wen Tsai, and co-advisors, Professors Shapour Azarm and André Tits, for their invaluable advice and guidance in the preparation of this dissertation. I would also like to thank the other members of the dissertation committee, Professors Nariman Farvardin and Gregory C. Walsh for reviewing and correcting the final transcript. This research is supported in part by the National Science Foundation under Grant No. EID-9212126. This support is gratefully acknowledged.

Table of Contents

List of Tables

List of Figures

Nomenclature

$\mathtt{C}i$:= ith constraint.

$\mathbf{e}_i$:= unit vector with an orientation angle θ_i,
i.e., $\mathbf{e}_i = [\cos(\theta_i), \sin(\theta_i)]^T$.

$\mathbf{e}_{(P_1)(P_2)}$:= unit vector of $\overrightarrow{(P_1)(P_2)}$.

$\mathbf{e}_X$:= unit vector associated with the X-axis.

$\mathbf{e}_Y$:= unit vector associated with the Y-axis.

Ei := ith evaluation criterion for four- and six-bar linkages.

Ei' := ith evaluation criterion for eight-bar linkages.

f_a := actuation force along a specified direction.

f_{ijX} := X-component of $\mathbf{f}_{ij}$.

f_{ijY} := Y-component of $\mathbf{f}_{ij}$.

$\mathbf{f}_{ij}$:= force (vector) applied by links i on j.

Fi := ith functional requirement.

$\mathtt{FC}i$:= ith functional constraint.

$\mathtt{FO}i$:= ith functional objective.

g := gravitational constant, 9.8 m/s^2.

h_p := path height.

$\mathtt{H}_{\mathtt{C}i}$:= threshold value for the ith hard constraint.

$\mathtt{H}_{\mathtt{FC}i}$:= threshold value for the ith hard functional constraint.

J_{ij} := joint that connects links i and j.

k_i := spring constant of the ith spring.

l_i := stretched length of the ith spring.

l_{0i} := unstretched length of the ith spring.

L_h := height of a leg mechanism.

L_w := width of a leg mechanism.

m := design variable of a skew-pantograph.

n := amplification factor of a pantograph.

$\mathtt{O}i$:= ith objective.

R_p := crank angle range of the propelling portion of the foot-path.

s_1 := $\overline{B_0C'}$ (see Fig. 4.17).

s_{21} := $\overline{FF'}$ (see Fig. 4.17).

s_{22} := $\overline{FG'}$ (see Fig. 4.17).

s_3 := $\overline{B_0F_0'}$ (see Fig. 4.17).

s_4 := $\overline{C''C'''}$ (see Fig. 4.17).

s_h := horizontal stride length, 0.30 m.

s_v := vertical stride length, 0.20 m.

t := time, sec.

T := crank torque, N-m.

w := walking machine weight.

$\mathbf{x}$:= $\mathbf{x} = (x_1, x_2, ..., x_5)^T$

$X_{(P)}$:= X coordinate of point (P).

Y_1 := $(Y)_{\alpha=0}$ (see Fig. 3.4).

Y_2 := $(Y)_{\alpha=\pi}$ (see Fig. 3.4).

$Y_{(P)}$:= Y coordinate of point (P).

α := crank angle (independent variable for the first-DOF motion).

$\pm\,\alpha_e$:= crank angles at the two horizontal extreme positions of a foot-point curve (see Section 3.1.3).

α_c := crank angle at the mid-point of the propelling path.

α_s := crank angle at one of the intersection points between a coupler-point path and the axis of symmetry (see Section 3.1.3).

β := (see Fig. 4.2 or 4.8).

γ := $\angle FGE$ (see Fig. 4.7).

δ := adjustable pivot displacement (independent variable for the second-DOF motion (see Fig. 4.8).

$\delta_{\max}$:= maximum value of δ.

δP := virtual potential energy.

δW := virtual work.

ϵ := lower bound of four-bar transmission angle.

θ_s := maximum slope angle (see Fig. 3.5).

θ_i := orientation angle of link i.

$\theta_{(P_1)(P_2)}$:= orientation angle of $\overrightarrow{(P_1)(P_2)}$.

κ_1 := $(1 - l_{01}/l_1)$.

κ_2 := $[(s_{21}s_{22})/{x_4}^2](1 - l_{02}/l_2)$.

μ := four-bar transmission angle.

$\mu_{\max}$:= maximum four-bar transmission angle.

$\mu_{\min}$:= minimum four-bar transmission angle.

ν := pantograph transmission angle.

$\nu_{\max}$:= maximum pantograph transmission angle.

$\nu_{\min}$:= minimum pantograph transmission angle.

ν' := skew-pantograph transmission angle.

$\nu'_{\max}$:= maximum skew-pantograph transmission angle.

$\nu'_{\min}$:= minimum skew-pantograph transmission angle.

ρ := pantograph size factor (see Fig. 3.6).

ϕ := coupler-plate angle $\angle ABC$ (see Fig. 3.1).

ϕ' := $\phi + \psi_2$.

ψ_1 := $\angle AB_0A_0$ (see Fig. 3.1).

ψ_2 := $\angle GFE$ (see Fig. 4.7).

$\overrightarrow{(P_1)(P_2)}$:= vector from point (P_1) to (P_2).

$\overline{(P_1)(P_2)}$:= length between points (P_1) and (P_2).

$\angle(P_1)(P_2)(P_3)$:= angle measured counterclockwise from $\overrightarrow{(P_2)(P_1)}$ to $\overrightarrow{(P_2)(P_3)}$.

$\|(\cdot)\|$:= absolute value of inner quantity.

$\overrightarrow{(L_1)}\|\overrightarrow{(L_2)}$:= vector $\overrightarrow{(L_1)}$ parallel to $\overrightarrow{(L_2)}$.

$\square$:= parallelogram .

Chapter 1

Introduction

1.1 Background

In terms of mobility and energy efficiency, walking machines are potentially superior to the conventional wheeled and tracked vehicles on off-road terrains (Bekker, 1969). Over the past few decades, many researchers have attempted to build walking machines that are capable of performing certain tasks on rough terrains. However, most of such walking machines were either laboratory-scaled machines (Klein et al., 1983; Todd, 1985a) or inefficient in terms of energy consumption (Mosher, 1968; Sutherland and Ullner, 1984). Due to the complexity involved in a legged locomotion system, only a few walking machines, such as the ODEX Hexapod (Byrd and DeVries, 1990) which was developed for nuclear power plant maintenance and the Adaptive Suspension Vehicle (ASV) (Waldron et al., 1984; Pugh et al., 1990) which was designed for field transportation, were considered close to realistic applications. Further studies in many subject areas of a legged locomotion system are required. Among them, design of a leg mechanism remains a challenge because the performance of a walking machine largely depends on it.

A wide variety of leg mechanisms for walking machines have been proposed and reported in the literature over the past few decades (Todd, 1985b). Depending on the desirable features (flexibility, speed, etc.) and the walking environment, machines with up to eight legs and a total of eighteen active degrees of freedom (DOFs) have been considered (Morecki et al., 1985). For example, the GE Quadruped (Mosher, 1968) and the Carnegie Mellon University's Hexapod (Sutherland and Ullner, 1984), both with two DOFs on each leg, had a total of eight and twelve active DOFs, respectively. On the other hand, the Ohio State University's Hexapod (Klein et al., 1983) with three DOFs on each leg had a total of eighteen active DOFs. These three walking machines used open-chain linkages as their leg mechanisms and were able to walk on a rough terrain. Fig. 1.1 (a) shows a typical two-DOF open-chain leg mechanism. Since, for this type of leg, the actuators on both the hip and knee joints of the leg linkage have to be actuated simultaneously to work against the gravity even for walking on a flat ground, this type of mechanism does not have a mechanical advantage. In addition, the hip and knee actuators of such leg mechanisms may even produce 'work' against each other, resulting in unnecessary energy loss (Waldron et al., 1984). Therefore, leg mechanisms of this type are very inefficient in terms of energy consumption.

Unlike a manipulator which can be operated with its controller and power supply unit installed on the ground, a walking machine has to carry all these loads in addition to the external loads (payloads) and the weight of the machine body [1]. Hence, a leg mechanism should be designed with high energy

[1]If a walking machine is wired (or piped) to a ground-stationed power supply unit, its activities will be restricted to a small reachable area, which is an undesirable feature.

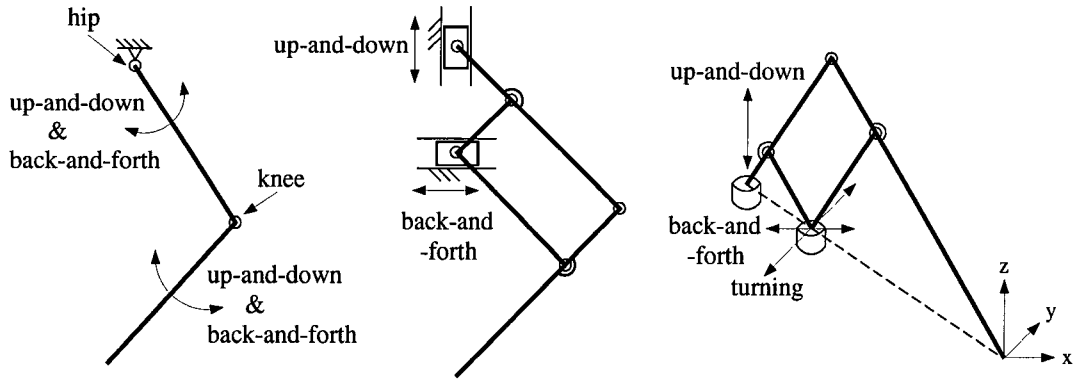

(a) Open-chain leg (b) 2-DOF pantograph leg (c) 3-DOF pantograph leg

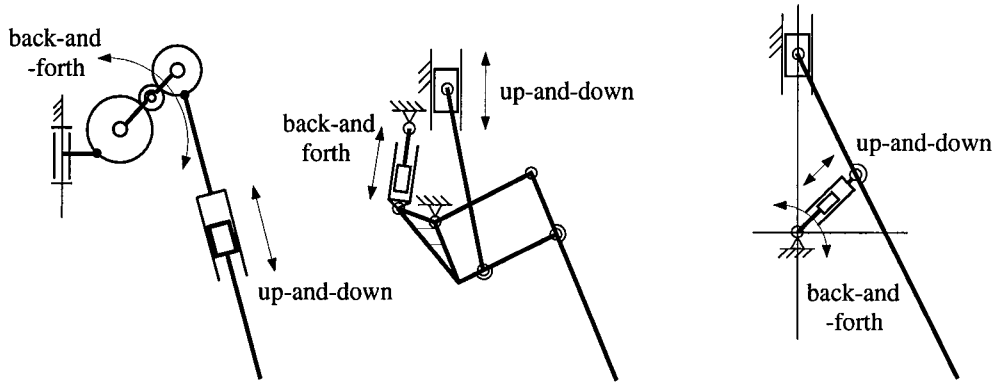

(d) Planetary leg (e) Odetics leg (f) Five-bar leg

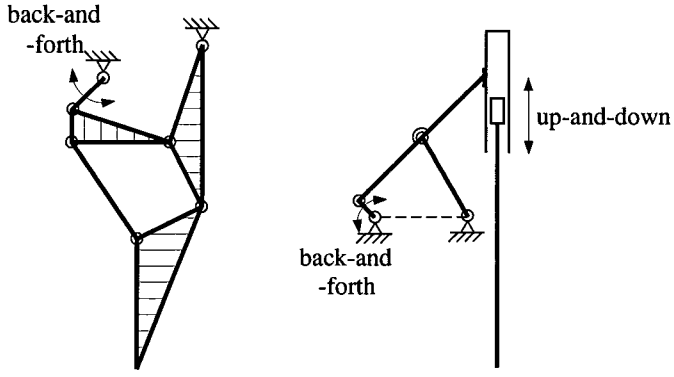

(g) Six-bar leg (h) Four-bar leg with a shank

FIGURE 1.1: Some of the existing leg mechanisms

efficiency. An energy efficient walking machine can be achieved by designing a leg mechanism which has a gravitationally decoupled actuation system (Hirose and Umetani, 1980). Having the actuation system decoupled into three mutually independent directions, each of the back-and-forth, up-and-down, and turning motion of a leg mechanism can be individually controlled by separate actuators. A leg mechanism employing a perfect gravitationally decoupled actuation system can generate a straight foot-point path in the horizontal direction and ideally results in zero energy loss during the entire walking cycle. Cartesian- and pantograph-type leg mechanisms belong to this type of legs. Fig. 1.1 (b) shows the schematic of a two-DOF pantograph leg mechanism used in the six-legged ASV (Waldron et al., 1984; Pugh et al., 1990), while Fig. 1.1 (c) shows a three-DOF pantograph (cylindrical type pantograph) leg mechanism adopted in the PVII and the more-sophisticated TITAN III quadrupeds (Hirose, 1984; Hirose and Kunieda, 1991).

Literature also reports on leg mechanisms that generate an approximately straight line. These include: a planetary-gear leg (Chen and Song, 1992), the Odetics leg (Russell, 1983; Byrd and DeVries, 1990), and a five-bar leg (Adachi et al., 1990) - all two-DOF planar mechanisms as shown in Figs. 1.1 (d), (e), and (f), respectively. Other experimental leg mechanisms that generate near-straight line path can also be found in Ryan and Hunt (1985). The above mentioned leg mechanisms in Figs. 1.1 (b), (d), (e), and (f) have three DOFs (the third DOF is not shown) and that the back-and-forth, up-and-down, and the turning motions can be individually controlled. Hence, these mechanisms have high flexibility on a rough terrain and are energy efficient on a flat terrain. Such leg mechanisms, however, require at least two DOFs to be actively controlled even for walking

on a flat terrain. This, in turn, may result in a machine with slow speed and a complex control architecture.

For a walking machine to achieve fast locomotion with a simple control algorithm, the leg mechanism should be able to generate an ovoid foot-point path with a continuously rotating crank (motor). Funabashi's biped machine achieves this by means of a one-DOF six-bar linkage (Funabashi et al., 1985a; Funabashi et al., 1985b) as shown in Fig. 1.1 (g). That mechanism, however, lacks the flexibility required for walking over obstacles and climbing stairs. On the other hand, Fig. 1.1 (h) shows a leg mechanism used in the MELCRAB-2 hexapod walking machine (Koyachi et al., 1990). Such a leg mechanism generates an ovoid foot-point path to accomplish fast locomotion and easy control for normal walking. Also, this mechanism is energy efficient, it is able to generate an approximately straight path in the propelling portion [2] of the foot path. Moreover, it has a second and a third DOF (the third DOF is not shown) to walk over obstacle. This mechanism, however, can become bulky if a large stride is required.

1.2 Motivation and Objective

It is desired that a walking machine has the flexibility required for walking on a rough terrain, while it can achieve fast locomotion, is easy to control, and requires minimum actuation load for walking on a flat ground. In addition, the leg mechanism should be compact in size with respect to a prespecified horizontal stride.

[2]The propelling portion of a foot-point path refers to the portion of the path when the foot is in contact with the ground. The other portion is called the non-propelling portion.

For a walking machine to be capable of walking on various terrains, each leg requires three DOFs. Since the turning motion is the least frequently used degree-of-freedom, for most of the walking machines, the turning motion have been separated from the other two in the leg design. Typically, one may employ a two-DOF planar mechanism to provide for the back-and-forth and up-and-down motions, while the turning motion is obtained by rotating the planar mechanism as a whole about a vertical (or horizontal) axis fixed to the frame of the walking machine. Therefore, the design of a leg mechanism can be simplified to that for a two-DOF planar leg mechanism.

Among the planar two-DOF leg designs, the Cartesian and pantograph-type mechanisms that employ a linear actuation system and those that use oscillatory actuation system are not considered in this study. This is because the back-and-forth swing of a leg requires an actuator to change its direction cyclicly when the leg switches from a propelling to a non-propelling phase, and vice versa. In addition, in order to prevent the foot from hitting the ground during transition from the propelling phase to the non-propelling phase, both DOFs must be actively controlled so that the foot point can be lifted slightly during the non-propelling phase. Because of these two reasons, the Cartesian and the pantograph-type leg mechanisms tend to result in a slow locomotion.

Hence, a continuous rotating actuation system that produces a closed, ovoid-shaped, foot-point path is sought for the leg mechanisms. Also, to maximize the energy efficiency, the propelling path of a leg mechanism has to approximate a straight line. In addition, since a symmetrical foot-path can be advantageous in reducing the maximum driving torque and simplifying the motion control of the legs, leg mechanisms featuring symmetrical coupler curves are of interest.

Therefore, the objective of this study is to search and design two-DOF, planar leg mechanisms with the above-mentioned features. Under the overall goal, we will:

1. identify all the admissible two-DOF planar leg mechanisms with the desirable features;

2. create a new class of leg mechanisms that produce symmetrical foot paths and are easy to be analyzed and synthesized;

3. perform dimensional synthesis of all the admissible mechanisms and reveal the advantages and disadvantages of the synthesized leg designs;

4. investigate the use of passive elements (tension springs) for the purpose of reducing the driving force and torque.

1.3 Approach

The approaches used to fulfill the above mentioned four objectives are described as follows:

1. In this study, a systematic methodology (Tsai, 1995) for the mechanical concept design is used to identify the admissible mechanisms for a leg design. According to the desired features, a planar leg mechanism should have two DOFs: one for the back-and-forth motion and the other for the up-and-down motion. Since adjusting the height of a leg can be easily accomplished through an adjustable, base-connected pivot, the design problem can be simplified by temporarily excluding the DOF associated with

the up-and-down motion of a leg. This way, only the search for one-DOF planar mechanisms is necessary.

2. Although the sufficient conditions for a four-bar coupler point to trace a symmetrical curve are well studied (Hartenberg and Denavit, 1964), there are only a few studies on symmetrical coupler curves associated with mechanisms with more than four links (Dijksman, 1976; Antuma, 1978; Dijksman, 1984). However, because these mechanisms can be bulky if a fairly large coupler curve is required, they are not suitable to be used as leg designs. In order to obtain slender leg mechanisms that feature symmetrical coupler curves and are easy to be analyzed and synthesized, a new class of six-bar mechanisms and an eight-bar compound mechanism are developed with the use of a symmetrical four-bar linkage.

3. The most common methodologies associated with the dimensional synthesis of a mechanism are the precision point synthesis (Freudenstein and Sandor, 1961; Roth and Freudenstein, 1963; Suh and Radcliffe, 1967; McLarnan, 1963) and approximate synthesis (Han, 1966; Sutherland and Roth, 1974; Tull and Lewis, 1968). Although these two synthesis techniques are well applied to many mechanism design problems, they are not suitable for the leg design considered in this thesis because of the following reasons. First, it is desired to simultaneously minimize several design objectives: the crank torque, actuating force and the leg size. Second, a number of design specifications (or constraints) have to be accommodated in the design process. Therefore, the dimensional synthesis of such mechanisms can only be formulated as a constrained multi-objective optimization problem.

Due to the complexity of such a multi-objective optimization model, the Consol-Optcad (Fan et al., 1990), an interactive optimization-based design package, is used to solve this problem.

4. Spring elements have been used in leg mechanism both to store kinetic energy (Alexander, 1990; Dhandapani and Ogot, 1994) and to reduce actuating forces (Shin and Streit, 1993). Since there is no general guidelines for mounting springs to a leg mechanism, the spring placement configuration should take the advantage of some of the special features of a mechanism. For our leg mechanism, since symmetry is a significant feature, all spring elements are arranged in such a way that the actuator force and crank torque are reduced in a symmetrical manner.

1.4 Outline of the Thesis

The concept design of a leg mechanism is presented in Chapter 2. To generate all admissible two-DOF planar leg mechanisms, a systematic methodology is used. First, the functional requirements of a leg mechanism are established. Some of the functional requirements are translated into mechanism structural characteristics from which possible candidate mechanisms are enumerated. Finally, based on the remaining functional requirements and certain structural considerations, a set of evaluation criteria is developed to screen out the unwanted mechanisms. As a result, several planar, one-DOF, four-, six-, and eight-bar linkages with adjustable pivots are obtained as the admissible mechanisms.

In Chapter 3, admissible leg mechanisms featuring symmetrical foot-point path are studied. The construction of such linkages, the special features of

a symmetrical coupler curve, and how such a coupler curve can be used as a foot path in a walking machine are discussed. The symmetry properties of a coupler curve associated with a four-bar mechanism are explored. Several existing six-bar mechanisms that can generate symmetrical coupler curves are surveyed. A new class of six-bar linkages made up of a four-bar linkage with an embedded regular or skew pantograph are introduced. The advantages and the disadvantages of such six-bar mechanisms are explored. Finally, an eight-bar compound mechanism consisting of a four-bar linkage and a simple pantograph is presented.

In Chapter 4, optimization-based dimensional synthesis of the admissible mechanisms with symmetrical foot-point path is performed. Following a literature review on a dimensional synthesis, an optimization-based model is described, the design objectives and design specifications are defined, the optimization software is explained, and the assumptions are made for the optimization models. Then, each of the four-, six-, and eight-bar mechanisms with and without an adjustable pivots are investigated. Spring elements are added, in case of an eight-bar mechanism for further reduction of actuating force and cranking torque in excess of the values obtained by the optimization-based dimensional synthesis.

Finally, some concluding remarks, main contributions of this study, and the future works are given in Chapter 5.

Chapter 2

Concept Design of a Leg Mechanism

The performance of a walking machine is closely related to its leg design. In this chapter, the concept design of a planar leg mechanism based on certain desirable features of a walking machine is presented.

In Section 2.1, functional requirements of a planar leg mechanism are identified. In Section 2.2, a systematic methodology for the enumeration of a class of leg mechanisms is described. While the search of four- and six-bar mechanisms is presented in Section 2.3, the search of eight-bar mechanisms is carried out in Section 2.4. In the search of the mechanisms, structure specifications are used to enumerate all candidate mechanisms. Then, a set of evaluation criteria is developed to screen out the unwanted linkages. Finally, all admissible leg mechanisms are discussed in Section 2.5.

2.1 Functional Requirements of a Leg Mechanism

It is desired that a walking machine has the flexibility required for walking on a rough-terrain, while it can still achieve fast locomotion, remain easy to control, and require minimal actuation for walking on a flat terrain (hereafter called normal walking).

For a walking machine to be capable of walking on various terrains, each leg requires three DOFs to carry out the back-and-forth, up-and-down, and turning motions. Since the turning motion can be separated from the other two motions in a leg design, a two-DOF planar mechanism which provides the back-and-forth and up-and-down motions is of interest.

If all three DOFs need to be simultaneously actuated for rough-terrain walking, then the walking machine's speed can be slow and the control algorithm becomes complex. On the contrary, if a leg mechanism is designed such that only one DOF is required to be actuated for normal walking, then the speed of a walking machine can be fast and the control algorithm becomes simple.

For normal walking, the motion of a leg can be divided into two phases, a propelling and a non-propelling phase. Figs. 2.1 (a) and (b) show the propelling and non-propelling phases of a normal walking cycle where two extreme leg postures are labeled as postures 1 and 2. At postures '1' and '2', one foot begins to contact the ground (posture 1) while the other foot is to leave the ground (posture 2). Referring to Fig. 2.1 (a), during the propelling phase, the body is propelled forward from the posture 1 to 2 with a stride length s_h. Referring to Fig. 2.1 (b), during the non-propelling phase, the leg swings forward from the

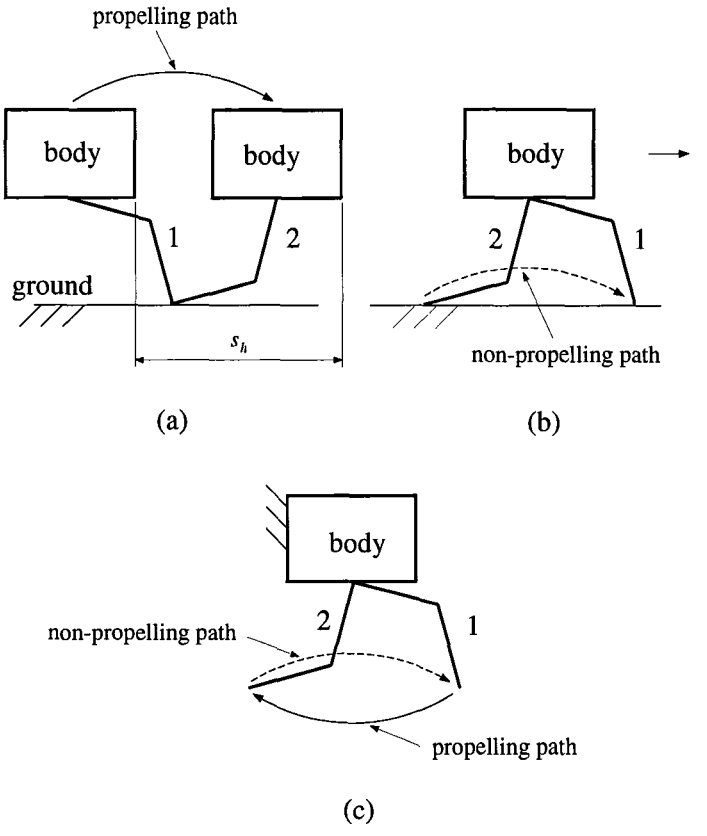

FIGURE 2.1: Normal walking in two phases: (a) propelling and (b) non-propelling. These two walking phases are equivalent to (c) swing the leg while body is fixed

posture 2 back to 1, while the body is supported by the other legs (not shown). As these two phases alternate, the walking machine moves forward. The relative movement between the body and its leg as shown in Figs. 2.1 (a) and (b) is equivalent to the case for which the body is fixed and the leg swings backward from the posture 1 to 2 and then forward from the posture 2 back to 1 as shown in Fig. 2.1 (c).

Leg designs, such as the Cartesian or pantograph-type mechanisms, that employ a linear actuation system or other mechanisms that use oscillatory actuation system, feature certain undesirable characteristics. First, for the back-and-forth

motion, the actuator of such a leg mechanism has to change its moving direction cyclically when the leg switches from the propelling to the non-propelling phase, and vice versa. Second, in order to prevent the foot point from hitting the ground during the non-propelling phase, both degrees of freedom must be actively controlled such that the foot point can be lifted slightly in the non-propelling (returning) phase. Because of these two reasons, this type of leg mechanisms tend to result in a slow locomotion. In order to overcome this disadvantage, a continuously rotating actuation system that produces a closed, ovoid-shaped, foot-point path is sought. For a walking machine to be energy efficient, a leg mechanism has to produce a nearly straight propelling path. Therefore, the functional requirements of a desirable planar leg mechanism can be summarized as follows:

F1. The leg mechanism, in addition to being able to move forward and backward, should have the capability to lift the foot point up and down.

F2. The back-and-forth motion of the foot point is to be driven by a continuously rotary crank.

F3. The foot-point path has to be a closed ovoidal curve.

F4. The propelling portion of the foot-point path is approximately a straight line.

2.2 Design Methodology

A systematic methodology for the concept generation of mechanisms can be found in Tsai (1995). An outline of the methodology is as follows:

1. Determine the desirable functional requirements of a mechanism.

2. Identify mechanism structural specifications:

   (a) select a type of mechanism that has the most potential to meet the functional requirements;

   (b) determine the degree-of-freedom, nature of motion (i.e., planar, spherical, or spatial), and the complexity of mechanism (e.g., number of links, joints, loops, and type of joints, etc.);

   (c) identify as many structural features [1] associated with the functional requirements as possible.

3. Enumerate mechanism structures:

   (a) enumerate topological graphs [2] according to the mechanism structure specifications;

   (b) label each structure according to the various types of joints and choice of fixed, input, and output links and sketch the corresponding mechanism for each topological graph.

4. Use the remaining functional requirements and certain evaluation guidelines to screen out unacceptable mechanisms.

The mechanisms produced from such procedure represent the potential solutions of the mechanism design problem. These mechanisms can then be analyzed in great details and their dimensions synthesized by design optimization techniques.

---

[1] An example of a desirable feature for a leg mechanism is a straight propelling path.

[2] In a graph representation, links are represented by vertices and joints are represented by edges. Since all the joints are restricted to revolute joints, the edges are not labeled.

2.3 Search of Four- and Six-Link Mechanisms

2.3.1 General Structure Specifications

According to functional requirement **F1**, a planar leg mechanism should have two DOFs: one for the back-and-forth motion and the other for the up-and-down motion. To simplify the design problem, the DOF associated with the up-and-down motion of a leg is temporarily excluded. Since adjusting the height of a leg via a floating pivot is not desired, the change of the leg height will be accomplished through the adjustment of a fixed pivot. This way, we only need to search for one-DOF planar mechanisms.

It is well known that the number of DOF and the number of loops (L) in a mechanism is related to the number of links (n), number of joints (j), and joint types (f) by the Grübler's mobility criterion:

$$F = \lambda(n - j - 1) + \sum_i f_i \tag{2.1}$$

and the Euler equation:

$$L = j - n + 1 \tag{2.2}$$

where $\lambda = 3$ for planar mechanism and f_i indicates the number of DOFs associated with joint i. From Eqs. (2.1) and (2.2), for a one-DOF planar mechanism with all the joints being revolute joints, we obtain: $n = 4$ and $j = 4$ for L=1; $n = 6$ and $j = 7$ for L=2; $n = 8$ and $j = 10$ for L=3; etc.

In summary, the search is focused on one-DOF planar mechanisms with all the joints being revolute joints. The number of links and the number of joints should obey both the Grübler's mobility criterion and the Euler equation.

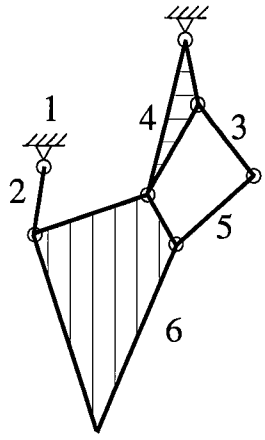

FIGURE 2.2: Six-bar mechanism with two no-load carrying links

2.3.2 Special Structure Specifications

In order to avoid the unnecessary complication associated with a large number of links, the search begins with one- ($L = 1$) and two-loop ($L = 2$) mechanisms, i.e., four-bar linkages with four joints and six-bar linkages with seven joints.

According to the functional requirement **F2**, the input link must be a base-connected crank, while according to **F3**, the output link must be a floating link, i.e., not directly connected to the base.

In addition, any mechanism with a ternary input link is to be excluded. This is because a ternary crank requires complex arrangements of its joints in order to avoid mechanism interference with other links.

Moreover, six-bar mechanisms with no-load carrying loop are excluded. For example, consider the Watt-I six-bar mechanism shown in Fig. 2.2. In this mechanism, if we assign link 2 as the input link and link 6 as the output link, then only the link members of the four-bar linkage formed by links 1, 2, 4, and 6 will carry loads. The other two links (links 3 and 5) carry no load. Elimination

1	Mechanism type	:	planar
2	Degree-of-freedom	:	*F=1*
3	Joint type	:	revolute
4	Link number	:	four and six
5	Input link	:	base-connected binary crank
6	Output link	:	floating
7	No-load carrying links	:	not permitted

TABLE 2.1: Structure specifications for four- and six-bar leg mechanisms

of links 3 and 5 has no effect on the desired input-output relationship. This type of mechanisms, with no-load carrying links, can be replaced with a mechanism with fewer number of links. Therefore, any mechanism with no-load carrying links are excluded from our study.

Based on the above discussion, the mechanism structure specifications (both general and special) are summarized in Table 2.1.

2.3.3 Enumeration

Following the structure specifications listed in Table 2.1, one four-bar linkage and twelve six-bar linkages are obtained. The four-bar linkage is a crank-and-rocker mechanism with a binary crank as its input link. The twelve six-bar linkages belong to Watt-I and -II and Stephenson-II and -III type mechanisms, where notations 'I', 'II', and 'III' refer to different selections of the base link. The topological graphs of these six-bar linkages are shown in Fig. 2.3, while the corresponding schematic drawings are shown in Fig. 2.4.

The following notations apply to all diagrams shown in Figs. 2.3 and 2.4:

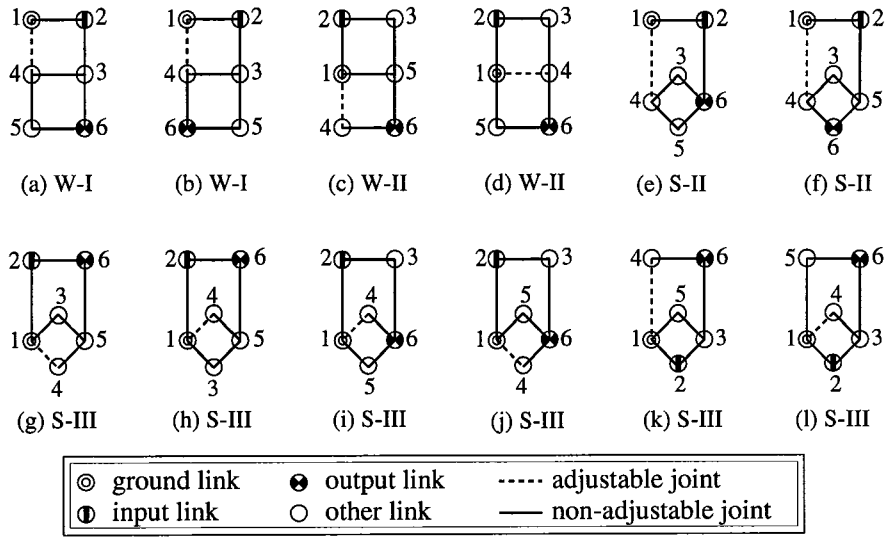

FIGURE 2.3: Topological graphs of the Watt- (W-) and Stephenson-type (S-) six-bar leg mechanisms

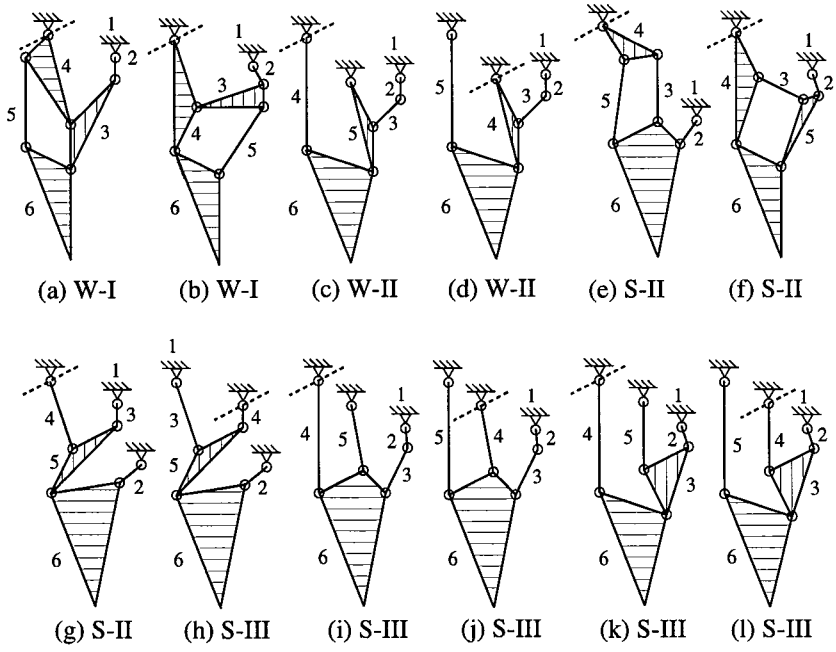

FIGURE 2.4: Schematic drawings of the Watt- (W-) and Stephenson-type (S-) six-bar leg mechanisms

1 : base

2 : input link (crank)

4 : link connected to the adjustable pivot

6 : output link (lower limb)

Notations '3' and '5' are assigned to the remaining two links. Note that, in Fig. 2.4, each adjustable pivot path is symbolically indicated by a slanted dotted line. Also note that, the mechanisms in the following pairs, (c) and (d), (g) and (h), (i) and (j), and (k) and (l) are structurally identical to each other, except for the selection of the adjustable pivots.

2.3.4 Evaluation Criteria

After a set of linkages is enumerated, all mechanisms have to be evaluated according to the remaining functional requirements and other structural considerations, e.g., complexity or awkwardness of the mechanisms, etc.

In the mechanism structure specifications, we have used **F2** and **F3** as the necessary conditions to establish the input link as a base-connected crank and the output link as a floating link. However, a floating link is not a sufficient condition for generating a closed ovoidal curve. Therefore, we have to carefully examine all the mechanisms against **F3**. Accordingly, the following evaluation criteria have been developed:

E1: Any mechanism with its output link connected to two rockers should be excluded. This is because an output link connected to two rockers is most likely to generate an arc at the foot point, which is a violation of **F3**.

E2: It is desired that there are two major limbs, resembling the upper and lower limbs of a leg. In addition, the input link can not be used as the upper

limb, because (i) a crank rotates while an upper limb oscillates, and (ii) the crank length usually is short, but the length of a major limb is long.

From these two criteria, **E1** is following the functional requirement **F3**, while **E2** is based on the structural consideration. Note that, since **E2** is not as essential as **E1**, violation of **E2** will only make a leg mechanism awkward.

Since the foot point of all mechanisms in Fig. 2.4 can be moved up and down by the adjustable pivot, the functional requirement **F1** is satisfied. However, it is not clear whether or not the movement of the adjustable pivot provides a sufficient up-and-down motion at the foot point. It is also not clear at this stage whether or not the propelling portion of the foot-point path can produce a nearly straight line (**F4**).

2.3.5 Evaluation

Using the criteria **E1** and **E2** to evaluate all the candidate mechanisms in Fig. 2.4, we obtain the following results: Mechanisms (c), (d), (i) and (j) are removed for the violation of **E1**. Since mechanisms (b), (c), (d), (f), (i), (j), (k), and (l) have two major limbs that can resemble the motion of a human leg, while others have more than two links between the base and the foot point, mechanisms (a), (e), (g), and (h) are excluded due to the violation of **E2**. The evaluation results for the six-bar leg mechanisms are tabulated in Table 2.2 where only mechanisms (b), (f), (k) and (l) are the admissible mechanisms. Note that, since the crank-and-rocker type four-bar linkage, with the coupler plate as its output link, does not violate either of criterion **E1** or **E2**, it is also an admissible mechanism.

Mechanism	Status	Reason(s)
(a)	rejected	violation of **E2**
(b)	admissible	
(c) and (d)	rejected	violation of **E1**
(e)	rejected	violation of **E2**
(f)	admissible	
(g) and (h)	rejected	violation of **E2**
(i) and (j)	rejected	violation of **E1**
(k) and (l)	admissible	

TABLE 2.2: Evaluation of the six-bar mechanisms shown in Fig. 2.4

2.4 Search of Mechanisms with Eight Links

In the previous subsection, one four-bar and four six-bar mechanisms are admitted for further study. However, these mechanisms have a common shortcoming associated with the up-and-down motion of a leg. Let's take mechanism (b) of Fig. 2.4 as an example. If the input link (link 2) of this mechanism is held stationary and the adjustable pivot J_{14} is adjusted for the up-and-down motion, the link length ratios within the input loop (loop 1-2-3-4) will be altered. As a result, the force transmission characteristics of the input loop as well as the foot-point path will also be changed. In addition, since it is desirable to maintain the propelling portion of a foot-point path to be as close to a straight line as possible regardless of the position of the adjustable pivot, a leg mechanism with such a feature is undesirable. Therefore, in this subsection, the search of three-loop mechanisms with eight links and ten joints is conducted.

2.4.1 Mechanism Structure Specifications

In addition to the general structure specifications described in Sections 2.3.1 and 2.3.2, the following special structure specifications for the eight-bar mechanisms are required. To simplify the search, prevent complex mechanism structure, and make a leg compact, a mechanism with a quaternary link (link connected with four joints) will be excluded. As mentioned earlier, it is desirable to have a mechanism in which the link length ratios of an input loop [3] remain constant regardless of the movement of the adjustable pivot. Hence, a leg mechanism should be connected to the base with three pivots, two of them (the input and supporting pivots) belongs to the input loop, while the other (the adjustable pivot) does not.

For a planar one-DOF eight-bar mechanism, the input loop can be a four-, five-, or six-bar loop. This search begins with those mechanisms having a four-bar input loop, simply because the kinematic synthesis and analysis of a four-bar linkage are well studied and understood. As a result, we may apply the knowledge associated with a four-bar mechanism to the synthesis of an eight-bar mechanism. If those mechanisms with a four-bar input loop can not satisfy all the functional requirement and the structural considerations, the search will then be extended to those with five- and six-bar input loops. Both general and specific structure specifications of admissible eight-bar leg mechanisms based on the above discussion are summarized in Table 2.3.

[3]Here, an input loop is referred to the loop which has the smallest number of links and contains the base and the input links.

1	Mechanism type	:	planar
2	Degree-of-freedom	:	*F=1*
3	Joint type	:	revolute
4	Link number	:	eight
5	Input link	:	base-connected binary crank
6	Output link	:	floating
7	Quartenary link	:	not permitted
8	Base link	:	ternary
9	Input loop	:	four-bar
10	No-load carrying links	:	not permitted

TABLE 2.3: Structure specifications for leg mechanisms with eight links

2.4.2 Enumeration

Based on the structure specifications listed in Table 2.3, nineteen eight-bar linkages are enumerated from seven different topological graphs. Fig. 2.5 shows the graph representations of the eight-bar mechanisms, where each of the following mechanism groups, (a)-(b), (c)-(f), (g)-(h), (i)-(k), (l)-(n), (o)-(q), and (r)-(s), belongs to a different topological graph.

Fig. 2.6 shows the schematic drawings of the leg mechanisms. The following notations apply to all the diagrams shown in Figs. 2.5 and 2.6 are:

1 : base

2 : input link (crank)

3 : coupler of the input loop

4 : rocker of the input loop

5 : link connected to the adjustable pivot

8 : output link (lower limb)

The notations '6' and '7' are assigned to the remaining two links. Note that, in Fig. 2.6, each adjustable pivot path is symbolically indicated by a dotted line.

2.4.3 Evaluation Criteria

Similar to the enumeration of six-bar mechanisms, a set of evaluation criteria for eight-bar leg mechanisms is developed. In addition to the criteria listed for six-bar linkages, we add the following additional criteria for the evaluation of eight-bar leg mechanisms:

E1′: For any mechanism, when the input link (link 2) is held stationary, the output link should not simply rotate about a point due to the motion of the adjustable pivot. For example, referring to the mechanism (d) of Fig. 2.6, if link 2 is held stationary, the output link (link 8) is simply hinged about the axis of joint J_{48}. When the adjustable pivot moves, link 8 rotates about pivot J_{48}, generating an arc at the foot point. This arc, when projected to the direction of up-and-down motion, is usually short, mostly, because of the output link orientation. Therefore, it is not a desired feature for a leg mechanism.

E2′: Mechanisms that consist of two four-bar loops, a base-connected loop and a floating loop, are preferred. As an eight-bar mechanism is split into two four-bar sub-mechanisms, the analysis and synthesis procedures can be largely simplified.

E3′: Among the mechanisms selected by **E2′**, those with their floating four-bar loops driven by a coupler point are more desirable than those driven by a rocker point. For a driving curve, a closed curve is usually preferable over an arc because of the design flexibility.

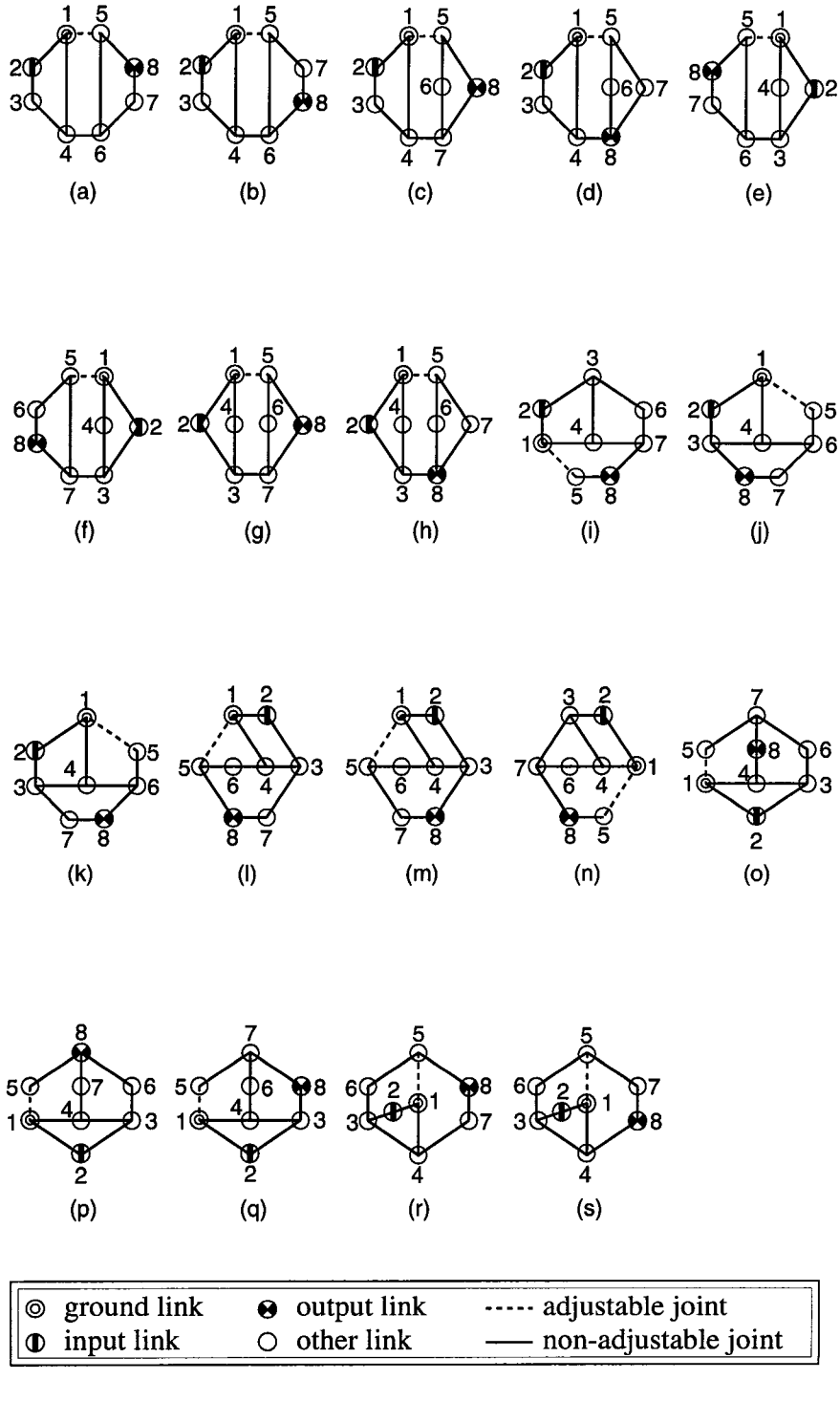

FIGURE 2.5: Structural diagrams of eight-bar leg mechanisms

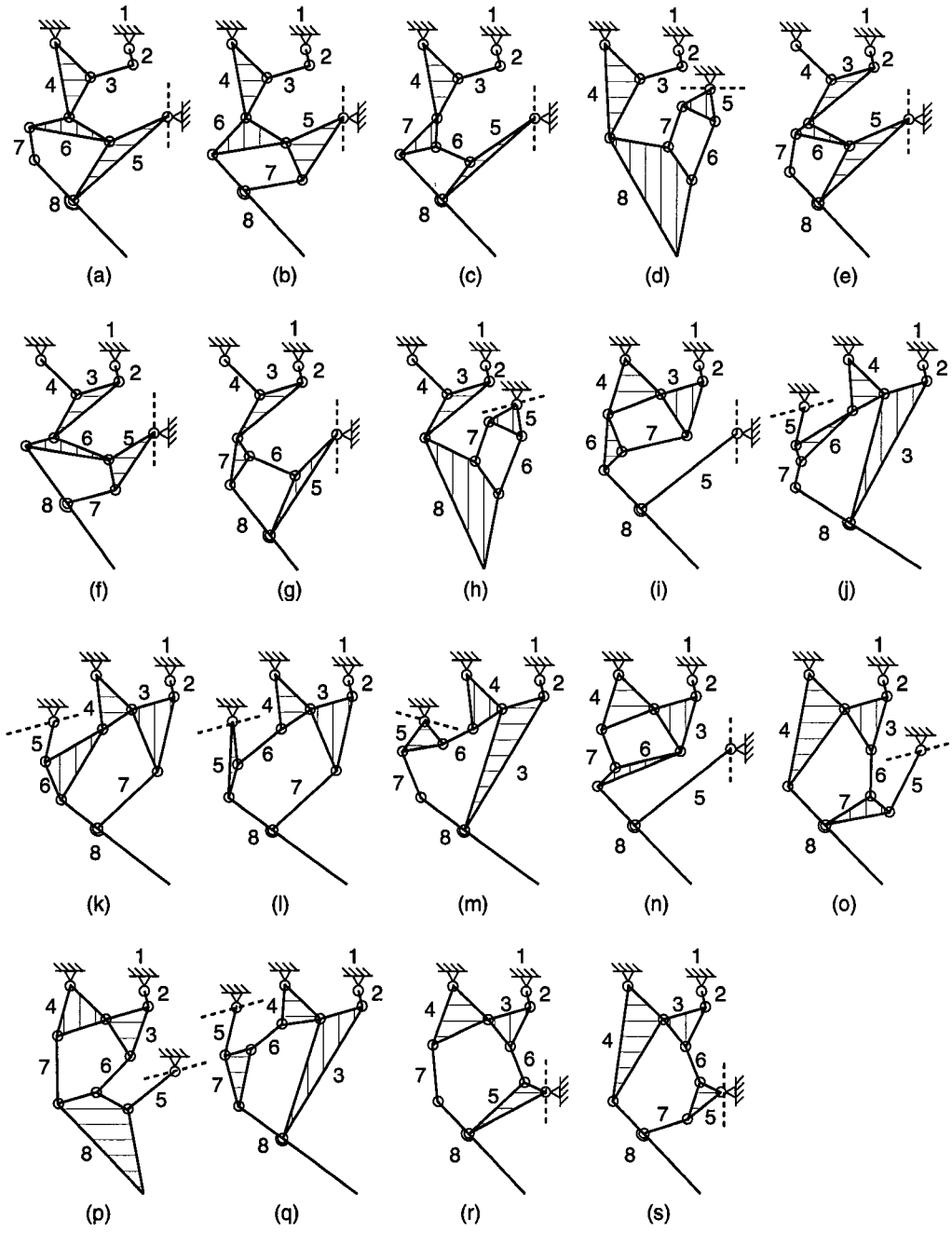

FIGURE 2.6: Schematic drawings of eight-bar leg mechanisms

Among the above three criteria, since **E1′** is based on a more stringent functional requirement **F1**, it is the most significant one. Although **E2′** has nothing to do with the functional requirements, it will simplify the analysis and synthesis of the feasible mechanism. Criterion **E3′** is mainly based on the view point of increasing the design flexibility. Note that, at this point, it is not clear whether **F4** is satisfied, As to **F2** and **F3**, they are satisfied because these two functional requirements have been included in the structure specifications.

2.4.4 Evaluation

Mechanisms (d), (h), (j), (m), (o), (q), and (s) in Fig. 2.6 are excluded because their output links are connected to the input four-bar 1-2-3-4, resulting in violation of **E1′**. Although the output links of mechanisms (i) and (n) are connected to link 6 (instead of the input four-bar 1-2-3-4), links 6 and 7 of these mechanisms are also considered stationary when the input link is held stationary. Hence, mechanisms (i) and (n) are also excluded due to the violation of **E1′**. According to **E2′**, mechanisms (i) through (s) are less desirable than mechanisms (a) through (h), and hence they are removed. Because of the lack of design flexibility, mechanisms (a) through (d) are excluded because of the **E3′** violation.

Based on the above discussion, only mechanisms (e), (f), and (g) of Fig. 2.6 are considered as the admissible leg mechanisms. However, the floating four-bar loops 5-6-7-8 of mechanisms (f) and (g) can be constructed as a pantograph, while that of mechanism (e) can not.

The evaluation results of the nineteen eight-bar mechanisms are summarized in Table 2.4. Since admissible eight-bar mechanisms have been obtained, the

Mechanism	Status	Reason(s)
(a)	rejected	violation of **E3′**
(b)	rejected	violation of **E3′**
(c)	rejected	violation of **E3′**
(d)	rejected	violation of **E1′**, **E3′**
(e)	rejected	(see Section 2.4.4)
(f)	admissible	
(g)	admissible	
(h)	rejected	violation of **E1′**
(i)	rejected	violation of **E1′**, **E2′**
(j)	rejected	violation of **E1′**, **E2′**
(k)	rejected	violation of **E2′**
(l)	rejected	violation of **E2′**
(m)	rejected	violation of **E1′**, **E2′**
(n)	rejected	violation of **E1′**, **E2′**
(o)	rejected	violation of **E1′**, **E2′**
(p)	rejected	violation of **E2′**
(q)	rejected	violation of **E1′**, **E2′**
(r)	rejected	violation of **E2′**
(s)	rejected	violation of **E1′**, **E2′**

TABLE 2.4: Evaluation of the eight-bar linkages shown in Fig. 2.6

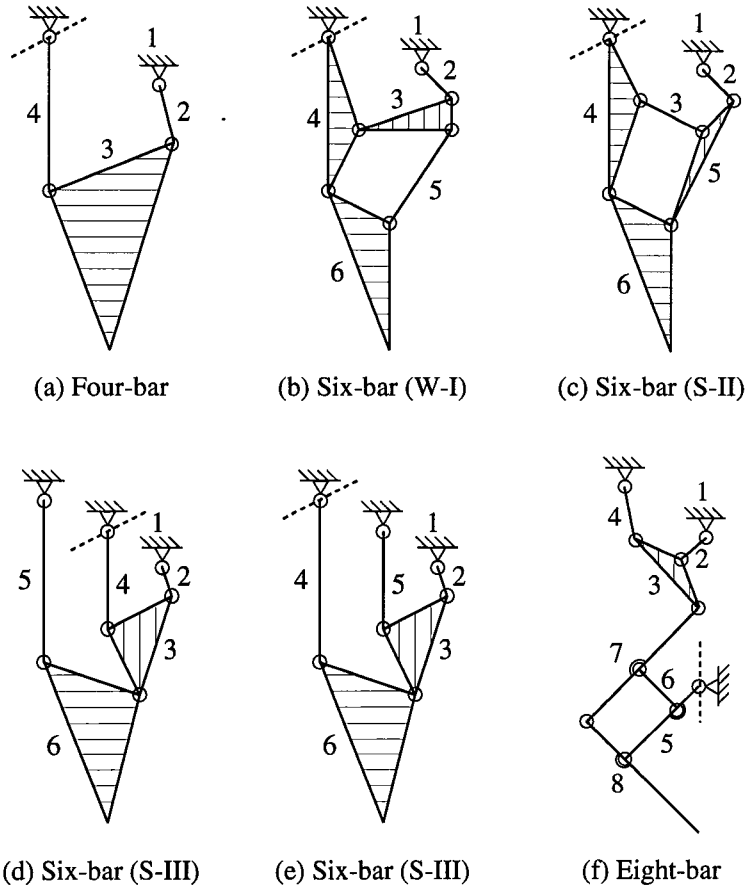

(a) Four-bar (b) Six-bar (W-I) (c) Six-bar (S-II)

(d) Six-bar (S-III) (e) Six-bar (S-III) (f) Eight-bar

FIGURE 2.7: Admissible leg mechanisms, (a) four-bar mechanism, (b)-(e) six-bar mechanisms, (f) eight-bar mechanism

search of eight-bar mechanisms with five- and six-bar input loop is not needed.

2.5 Summary

In this chapter, a systematic methodology for the concept design of a leg mechanism is used to identify the admissible mechanisms for a leg design. First, some of the functional requirements of a leg mechanism are transformed into a set of structural specifications from which all possible candidate mechanisms

are enumerated. Then, the remaining functional requirements and other design guidelines are included in a set of evaluation criteria from which unwanted mechanisms are screened out.

Using this methodology, six leg mechanisms are admitted for further studies. These mechanisms include one four-bar, four six-bar, and one eight-bar mechanisms as shown in Figs. 2.7 (a), (b)-(e), and (f), respectively. Although both mechanisms (f) and (g) of Fig. 2.6 are selected as two admissible eight-bar mechanisms, they become the same mechanisms when their floating four-bar loop is replaced by a pantograph. Hence, the only admissible eight-bar mechanism is a compound mechanism consisting of a four-bar linkage and a pantograph as shown in Fig. 2.7 (c).

Chapter 3

Leg Mechanisms with Symmetrical Foot Paths

Design of a leg mechanism with a symmetrical foot path can be advantageous in reducing the maximum driving torque and making the motion control of the leg easier. Hence, in this chapter, all admissible leg mechanisms are examined for the feasibility of producing symmetrical foot-point path. The construction of such linkages, the properties of a symmetrical coupler curve, and how such a coupler curve can be used as a foot-point path in a walking machine are discussed in details.

In Section 3.1, the symmetry properties of a coupler curve associated with a crank-and-rocker type four-bar linkage is explored. The derivation of a symmetrical coupler curve, the prevention of double points, the selection of the propelling and non-propelling portions of a walking cycle, and the derivation of crank torque are discussed.

In Section 3.2, several existing six-bar mechanisms that can generate symmetrical coupler curves are surveyed. Although these six-bar linkages are capable of tracing symmetrical coupler paths, none of them is judged to be suited as a leg mechanism. Thus, a new class of six-bar mechanisms with symmetrical coupler-point curves is presented. This class of mechanisms is made up of a four-bar

linkage with an additional dyad to form an embedded regular or skew pantograph. Because the coupler curve generated at an output point is amplified from that of a four-bar, a compact mechanism with a relatively large coupler curve can be obtained. In addition, due to their structure arrangement, the analysis and synthesis of such mechanisms can be easily achieved. The construction of such a new class of six-bar linkages with an embedded regular and skew pantograph is described in Section 3.3. The mechanism characteristics such as the transmission angles and the coupler curves are investigated in Section 3.4.

Finally, an eight-bar compound mechanism consisting of a four-bar linkage and a regular pantograph is presented in Section 3.5.

3.1 Four-Bar Mechanism with Symmetrical Foot-Point Path

Referring to the four-bar linkage $A_0 - A - B - B_0$ shown in Fig. 3.1, it is well known (Hartenberg and Denavit, 1964) that $\overline{AB} = \overline{BC} = \overline{B_0B}$ is a sufficient condition for the coupler point C to trace a symmetrical curve about the Y axis which passes through joint B_0. The angle which the Y axis makes with the four-bar linkage baseline $\overrightarrow{B_0A_0}$ is equal to $\phi/2$, where $\phi = \angle CBA$. It is noted that, hereafter, all the angles, unless otherwise indicated, are measured counter-clockwise, e.g., $\angle CBA$ is the angle measured counter-clockwise from $\overrightarrow{BC}$ to $\overrightarrow{BA}$, as shown in Fig. 3.1.

The crank-and-rocker type four-bar linkage under study must satisfy the Grashof criteria: (i) its shortest link serves as the crank, and (ii) the sum of the longest and shortest link lengths has to be less than the sum of the remaining

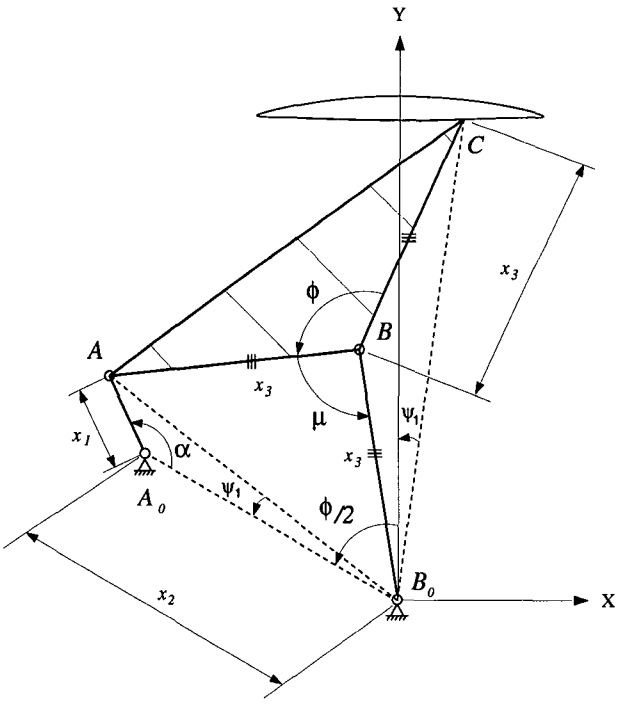

FIGURE 3.1: Symmetric four-bar linkage

two link lengths (Hartenberg and Denavit, 1964). Property (i) leads to the constraints,

$$\texttt{C1} : x_2 - x_1 \geq 0$$

$$\texttt{C2} : x_3 - x_1 \geq 0$$

and property (ii) is equivalent to

$$\texttt{C3} : (x_2 + x_1) \leq 2x_3$$

Since the above constraints $\texttt{C1} - \texttt{C3}$ are the necessary conditions for a crank-and-rocker mechanism, they must be satisfied for all four-bar mechanisms discussed hereafter.

3.1.1 Coordinate of the Foot Point

For convenience, an $X-Y$ reference coordinate system with its $Y-$axis coinciding with the axis of symmetry and with its origin located at joint B_0 is defined as shown in Fig. 3.1.

Theorem 3.1 *Referring to the four-bar linkage in Fig. 3.1, if the angle measured from* $\overrightarrow{B_0A}$ *to* $\overrightarrow{B_0A_0}$ *is* ψ_1, *the angle* $\angle CB_0Y$ *measured from* $\overrightarrow{B_0C}$ *to the axis of symmetry* $\overrightarrow{Y}$ *is equal to*

$$\angle CB_0Y = \begin{cases} \text{(i) } \psi_1, & \text{if } \mu+\phi < 2\pi \\ \text{(ii) } \pi+\psi_1, & \text{if } \mu+\phi > 2\pi \end{cases} \tag{3.1}$$

where

$$\psi_1 = \sin^{-1}\frac{x_1 \sin\alpha}{(x_2^2+x_1^2-2x_1x_2\cos\alpha)^{1/2}} \tag{3.2}$$

Proof

Referring to the angle $\angle CB_0A_0$ in Fig. 3.1,

$$\angle CB_0A_0 = \angle CB_0A + \angle AB_0A_0 = \angle CB_0Y + \angle YB_0A_0 \tag{3.3}$$

where Y is referred to a point on the positive $Y-$axis and $\angle CB_0A_0$ is the angle measured counter-clockwise from $\overrightarrow{B_0C}$ to $\overrightarrow{B_0A_0}$.

Since B_0 is a point on a circle centered at point B and passing through A, B_0, and C, we have (i) $\angle CB_0A = \angle CBA/2 = \phi/2$, if $\mu+\phi < 2\pi$, and (ii) $\angle CB_0A = 2\pi - (2\pi - \angle CBA)/2 = \pi + \phi/2$, if $\mu+\phi > 2\pi$. (Note that, when $\mu+\phi = 2\pi$, $\angle AB_0C$ is not defined.) Substituting $\angle AB_0A_0 = \psi_1$, $\angle YB_0A_0 = \phi/2$,

and

$$\angle CB_0A = \begin{cases} \phi/2, & \text{if } \mu+\phi < 2\pi \\ \phi/2+\pi, & \text{if } \mu+\phi > 2\pi \end{cases} \tag{3.4}$$

into Eq. (3.3) yields

$$\angle CB_0Y = \begin{cases} \psi_1, & \text{if } \mu+\phi < 2\pi \\ \pi+\psi_1, & \text{if } \mu+\phi > 2\pi \end{cases} \tag{3.5}$$

(QFD)

Since the coordinates of the coupler point C can be obtained by projecting the vector $\overrightarrow{B_0C}$ onto the $X-$ and $Y-$ axes, respectively, we have:

Case (i): $\mu+\phi < 2\pi$

$$X_C = \overline{B_0C}\cos(\pi/2-\psi_1) = \overline{B_0C}\sin\psi_1 \tag{3.6}$$

$$Y_C = \overline{B_0C}\sin(\pi/2-\psi_1) = \overline{B_0C}\cos\psi_1 \tag{3.7}$$

where

$$\overline{B_0C} = 2x_3\sin(\phi/2+\mu/2) \tag{3.8}$$

Case (ii): $\mu+\phi > 2\pi$

$$X_C = \overline{B_0C}\cos[\pi/2-(\pi+\psi_1)] = -\overline{B_0C}\sin\psi_1 \tag{3.9}$$

$$Y_C = \overline{B_0C}\sin[\pi/2-(\pi+\psi_1)] = -\overline{B_0C}\cos\psi_1 \tag{3.10}$$

where

$$\overline{B_0C} = -2x_3\sin(\phi/2+\mu/2) \tag{3.11}$$

Note that the 'minus' sign in Eq. (3.11) is due to the fact that the term $\sin(\phi/2+\mu/2)$ is negative. Substituting either Eq. (3.8) into (3.6) and (3.7) for the case

of $\mu + \phi < 2\pi$ or Eq. (3.11) into (3.9) and (3.10) for the case of $2\pi < \mu + \phi$ yields the same result

$$X_C = 2x_3 \sin(\phi/2 + \mu/2) \sin\psi_1 \tag{3.12}$$

$$Y_C = 2x_3 \sin(\phi/2 + \mu/2) \cos\psi_1 \tag{3.13}$$

Substituting Eqs. (3.2) into (3.12) and (3.13) gives

$$X_C = x_1 \sin\alpha \frac{\sin(\phi/2 + \mu/2)}{\sin\mu/2} \tag{3.14}$$

$$Y_C = (x_2 - x_1 \cos\alpha) \frac{\sin(\phi/2 + \mu/2)}{\sin\mu/2} \tag{3.15}$$

where

$$\mu/2 = \sin^{-1}(\frac{\overline{AB_0}}{2x_3}) \tag{3.16}$$

$$\overline{AB_0} = (x_2^2 + x_1^2 - 2x_1x_2\cos\alpha)^{1/2} \tag{3.17}$$

Thus the coordinates of the point C can be obtained by substituting Eqs. (3.16) and (3.17) in (3.14) and (3.15), respectively

$$X_C = x_1 \sin\alpha\{\cos\frac{\phi}{2} + [\frac{4x_3^2}{(x_2^2 + x_1^2 - 2x_1x_2\cos\alpha)} - 1]^{1/2} \sin\frac{\phi}{2}\} \tag{3.18}$$

$$Y_C = (x_2 - x_1\cos\alpha)\{\cos\frac{\phi}{2} + [\frac{4x_3^2}{(x_2^2 + x_1^2 - 2x_1x_2\cos\alpha)} - 1]^{1/2} \sin\frac{\phi}{2}\} \tag{3.19}$$

3.1.2 Double Point(s)

Although the path of a coupler curve is fully described by Eqs. (3.18) and (3.19), several issues still remain to be resolved before a coupler curve can be used as a foot path of a walking machine.

First, it is noted that the propelling portion of foot-path cannot contain any double point [1]. Because, at a double point, there exist two crank torque values.

[1] A double point is a point where a curve crosses over itself once.

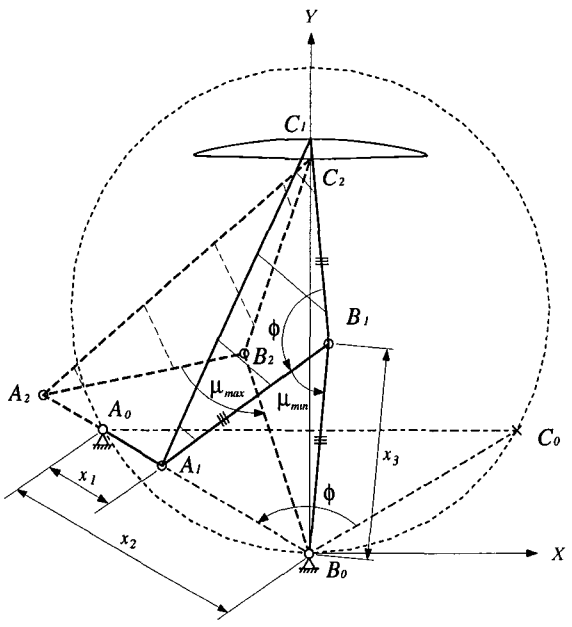

FIGURE 3.2: Circle of singular foci and two configurations of the symmetrical four-bar linkage with crank angle α at 0 and π

This, in turn, will potentially cause the foot point to slip on the ground. In addition, when a walking machine is instructed to walk along a given direction, the existence of a double point may periodically cause the walking machine to hesitate or walk back and forth. Thus, for simplicity, we exclude coupler curves with double point(s) from our designs. It is well known (Hartenberg and Denavit, 1964) that, in a four-bar linkage, a double point occurs at the positions where the coupler curve intersects with the circle of singular foci which passes through A_0, B_0, and C_0 as shown in Fig. 3.2. Because the triangle formed by points A_0, B_0, and C_0 is similar to the coupler plate ABC, accordingly, the center and the radius of the circle of singular foci can be obtained as $(0, x_2 \sec(\phi/2)/2)$ and $(\|x_2 \sec(\phi/2)/2\|)$, respectively. The symbol $\|\cdot\|$ refers to the absolute value of

the inner quantity. Thus, the equation of the circle can be written as

$$\hat{C}(X,Y) = X^2 + [Y - x_2 \sec(\phi/2)/2]^2 - [x_2 \sec(\phi/2)/2]^2 = 0 \qquad (3.20)$$

where the quantity (X, Y) represents the coordinates of any point on the circle of singular foci. To prevent the coupler curve from forming double points, any point C on the coupler curve must fall entirely inside or outside of the circle, i.e., $\hat{C}(X_C, Y_C) \neq 0$, for $\alpha \in [0, 2\pi]$.

Once the double points are excluded from a coupler curve, the selection of the propelling and non-propelling portions of the foot path becomes the next issue to be resolved.

3.1.3 Propelling and Non-Propelling Portions of a Foot Path

(a) Extreme positions ($\alpha = \pm\alpha_e$)

In order to achieve a maximal horizontal stride, the two extreme positions of a coupler curve that separate the propelling and the non-propelling portions of the curve must be identified. These two extreme positions can be found by setting

$$\frac{dX_C}{d\alpha} = 0 \qquad (3.21)$$

Substituting Eq. (3.18) into (3.21) and through a series of operation on the rationalization of the resulting equation yields

$$\sum_{i=0}^{6} a_i Z^i = 0 \qquad (3.22)$$

where $Z = \cos\alpha$ and a_i is the constant coefficient of the polynomial. The formulation for a_i, obtained with the aid of MATHMATICA - a symbolic language,

can be found in Appendix A. Since Eq. (3.22) is a sixth degree polynomial, it can only be solved numerically. Because of $Z = \cos\alpha$, the solutions of Z should be real and their absolute values should be less than or equal to 1 to be meaningful. The crank angles are then obtained as $\alpha = \pm \cos^{-1} Z$. Among the solutions, the two solutions for α that result in the two extreme values of X_C are denoted as $\pm \alpha_e$.

It is worthy noting that, if the coupler angle ϕ is equal to π, Eq. (3.22) degenerates into a third-degree polynomial, from which closed-form solutions can be obtained. The coefficients of the third-degree polynomial are also listed in Appendix A.

(b) Symmetrical Positions ($\alpha = 0$ and $\alpha = \pi$)

After the crank angles corresponding to the two extreme positions which are symmetrical about the $Y-$axis are obtained, the crank angles at the points of intersection between the coupler curve and the $Y-$axis have to be obtained so that the crank angle ranges corresponding to the propelling and non-propelling portions of a foot-point path can be identified.

Theorem 3.2 *If the coupler curve intersects the axis of symmetry more than twice, then the curve will pass through point B_0 twice, a double point. If there are only two intersection points, the two corresponding crank angles are $\alpha = 0$ and $\alpha = \pi$.*

Proof

Since the X-coordinate of the coupler point at the intersection points of the axis of symmetry and the coupler curve are zero, solving Eq. (3.18) for $X_C = 0$

yields four solutions, $\alpha = 0$, π, α_s, or $(2\pi - \alpha_s)$, where

$$\alpha_s = \cos^{-1}\{\frac{(x_2/x_1)^2 + 1 - [2(x_3/x_1)\sin(\phi/2)]^2}{2(x_2/x_1)}\} \tag{3.23}$$

For the solutions $\alpha = \alpha_s$ and $\alpha = 2\pi - \alpha_s$ to exist, the following two conditions must be satisfied:

$$\pi \leq \phi < 2\pi \tag{3.24}$$

$$-1 \leq \{\frac{(x_2/x_1)^2 + 1 - [2(x_3/x_1)\sin(\phi/2)]^2}{2(x_2/x_1)}\} \leq 1 \tag{3.25}$$

Simplifying Eq. (3.25) yields

$$\frac{x_2 - x_1}{2x_3} \leq \sin(\phi/2) \leq \frac{x_2 + x_1}{2x_3} \tag{3.26}$$

or simply

$$\sin(\frac{\mu_{\min}}{2}) \leq \sin(\phi/2) \leq \sin(\frac{\mu_{\max}}{2}) \tag{3.27}$$

where $\mu_{\min} = 2\sin^{-1}[(x_2 - x_1)/(2x_3)]$ and $\mu_{\max} = 2\sin^{-1}[(x_2 + x_1)/(2x_3)]$ are the minimum and maximum transmission angles (see Fig. 3.2). Solving Eq. (3.27) yields two solutions for ϕ, for which one is smaller and the other is greater than π. Since, according to Eq. (3.24), ϕ has to be greater than π, therefore, we have

$$\pi/2 < \pi - \frac{\mu_{\max}}{2} \leq \frac{\phi}{2} \leq \pi - \frac{\mu_{\min}}{2} \tag{3.28}$$

or

$$\pi < 2\pi - \mu_{\max} \leq \phi \leq 2\pi - \mu_{\min} \tag{3.29}$$

If ϕ satisfies Eq. (3.29), the two solutions α_s and $2\pi - \alpha_s$ exist and there are four intersection points between the coupler curve and the axis of symmetry.

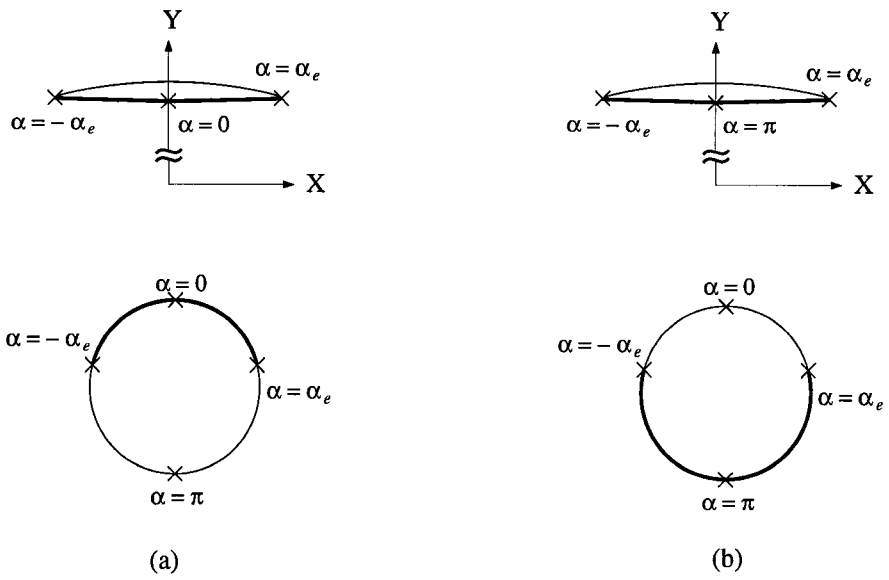

FIGURE 3.3: A symmetrical coupler curve (above) and its corresponding crank angle range (below); (a) propelling (solid bold line) portion includes $\alpha = 0$ (b) propelling portion includes $\alpha = \pi$

Substituting $\alpha = \alpha_s$ and $\alpha = (2\pi - \alpha_s)$ into Eq. (3.19) yields $(Y_C)_{\alpha=\alpha_s} = (Y_C)_{\alpha=2\pi-\alpha_s} = 0$. This indicates that the coupler point C passes through joint B_0 twice, i.e., joint B_0 is a double point. Since any coupler curve with a double point is excluded from our leg design, there should be only two points of intersection between the coupler curve path and the axis of symmetry. Therefore, the crank angle α at the points of intersection between the symmetrical axis and the coupler curve is either 0 or π. (QFD)

Hence, without any double point, a symmetrical coupler curve can be divided to two portions: one includes $\alpha = 0$ and the other includes $\alpha = \pi$. Therefore, the crank angle ranges for the propelling or non-propelling portion can be represented by a single value of α, i.e., $\alpha = 0$ or $\alpha = \pi$. For example, if the propelling portion includes the point at $\alpha = 0$, then the corresponding crank angle range,

R_p, should be equal to $[-\alpha_e, \alpha_e]$ as shown in Fig. 3.3(a). Otherwise, if the propelling portion includes the point at $\alpha = \pi$, R_p should be equal to $[\alpha_e, 2\pi - \alpha_e]$ as shown in Fig. 3.3(b).

(c) Selection of the Propelling and Non-Propelling Portions

Since the coupler curve intersects the axis of symmetry at $\alpha = 0$ and $\alpha = \pi$, the corresponding $Y-$coordinates can be obtained via Eq. (3.19)

$$Y_1 = (Y_C)_{\alpha=0} = 2x_3 \sin(\frac{\mu_{\min} + \phi}{2}) \tag{3.30}$$

$$Y_2 = (Y_C)_{\alpha=\pi} = 2x_3 \sin(\frac{\mu_{\max} + \phi}{2}) \tag{3.31}$$

Subtracting Y_2 from Y_1 yields

$$Y_1 - Y_2 = -4x_3 \sin(\frac{\mu_{\max} - \mu_{\min}}{4}) \cos(\frac{\mu_{\max} + \mu_{\min} + 2\phi}{4}) \tag{3.32}$$

Since the quantity $\sin[(\mu_{\max} - \mu_{\min})/4]$ on the right-hand side of Eq. (3.32) is always positive, the sign of $(Y_1 - Y_2)$ depends on the sign of $\cos[(\mu_{\max} + \mu_{\min} + 2\phi)/4]$. Since no double point is allowed in our design, the angle ϕ should fall out of the range defined by Eq. (3.29), i.e., ϕ should be in

$$\text{(i) } 2\pi - \mu_{\max} > \phi \tag{3.33}$$

$$\text{(ii) } \phi > 2\pi - \mu_{\min} \tag{3.34}$$

When ϕ falls into these two ranges, the relationship between Y_1 and Y_2 is investigated as follows:

Case (i): $2\pi - \mu_{\max} > \phi$ **or** $(\mu_{\min} + \phi)/2 < (\mu_{\max} + \phi)/2 < \pi$

According to Eqs. (3.30) and (3.31), both Y_1 and Y_2 are positive. Furthermore, in this case, we have $(\mu_{\max} + \mu_{\min} + 2\phi)/4 < \pi$. Two sub-cases exist:

Sub-Case (i-a): if $[(\mu_{\max} + \mu_{\min} + 2\phi)/4] \leq \pi/2$ or simply $0 < \phi \leq \pi - (\mu_{\max} + \mu_{\min})/2$, based on Eq. (3.32), we have

$$0 < Y_1 \leq Y_2 \tag{3.35}$$

Sub-Case (i-b): if $\pi/2 < [(\mu_{\max} + \mu_{\min} + 2\phi)/4] < \pi$ or simply $\pi - (\mu_{\max} + \mu_{\min})/2 < \phi < 2\pi - \mu_{\max}$, based on Eq. (3.32), we have

$$0 < Y_2 < Y_1 \tag{3.36}$$

Case (ii): $\phi > 2\pi - \mu_{\min}$ **or** $\pi < (\mu_{\min} + \phi)/2 < (\mu_{\max} + \phi)/2$

From Eqs. (3.30) and (3.31), both Y_1 and Y_2 are negative. Furthermore, in this case, we have $\pi < (\mu_{\max} + \mu_{\min} + 2\phi)/4$. Since $0 < \mu_{\min} < \mu_{\max} < \pi$ and $0 < \phi < 2\pi$, $[(\mu_{\max} + \mu_{\min} + 2\phi)/4]$ can not exceed $3\pi/2$. Therefore, $\pi < [(\mu_{\max} + \mu_{\min} + 2\phi)/4] < 3\pi/2$ or simply $2\pi - \mu_{\min})/2 < \phi < 2\pi$ for which we have

$$Y_2 < Y_1 < 0 \tag{3.37}$$

In summary, the relations between the value of ϕ and the values of Y_1 and Y_2, that are described in Eqs. (3.35)-(3.37), are depicted in Fig. 3.4. For example, if $\phi \in \{\phi \mid \pi - (\mu_{\max} + \mu_{\min})/2 < \phi < 2\pi - \mu_{\max}\}$, and if the lower portion of the coupler curve is selected as the propelling portion, the crank angle range for the propelling portion should include $\alpha = \pi$.

3.1.4 Crank Torque Analysis

Assuming that the transmission loss between the input crank and the output foot point is negligible, the input and output powers are equal:

$$T\frac{d\alpha}{dt} = (\mathbf{f}_{fg} \cdot \mathbf{e}_X)\frac{dX_C}{dt} + (\mathbf{f}_{fg} \cdot \mathbf{e}_Y)\frac{dY_C}{dt} \tag{3.38}$$

(a) $0 < \phi \leq \pi - (\mu_{max} + \mu_{min}) / 2$ (b) $\pi - (\mu_{max} + \mu_{min}) / 2 < \phi < 2\pi - \mu_{max}$

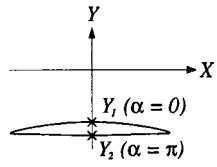

(c) $2\pi - \mu_{min} < \phi < 2\pi$

FIGURE 3.4: Three cases for the relations between the range of ϕ and the values of Y_1 and Y_2.

where T denotes the input torque on the crank, $\mathbf{f}_{fg}$ denotes the force acting on the ground by the foot at point C, and $\mathbf{e}_X$ and $\mathbf{e}_Y$ denote the two unit vectors in the $X-$ and $Y-$ directions, respectively.

Dividing both sides of Eq. (3.38) by $d\alpha/dt$ and using $\mathbf{f}_{fg} = -\mathbf{f}_{gf}$ results in

$$T = -f_{gfX}\frac{dX_C}{d\alpha} - f_{gfY}\frac{dY_C}{d\alpha} \tag{3.39}$$

where f_{gfX} and f_{gfY} are the $X-$ and $Y-$ components of the force exerted on the foot point by the ground, respectively. In general, they can be expressed as a sum of the gravitational force and the inertia force as shown in Fig. 3.5:

$$f_{gfX} = -w\sin\theta_s + \frac{w}{g}\frac{d^2X_C}{dt^2} \tag{3.40}$$

$$f_{gfY} = -w\cos\theta_s + \frac{w}{g}\frac{d^2Y_C}{dt^2} \tag{3.41}$$

where g is the gravitational constant, w is the walking machine weight, θ_s is the

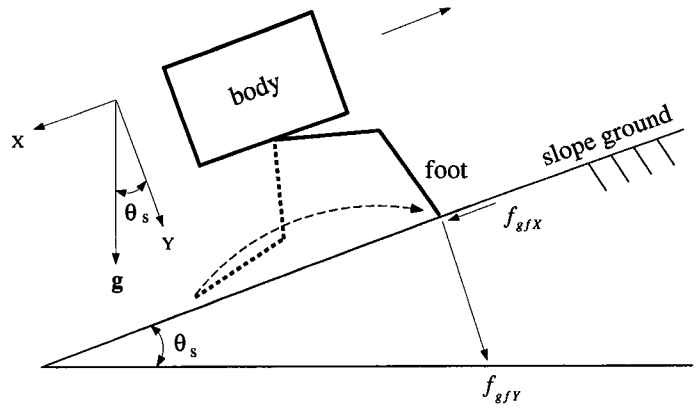

FIGURE 3.5: Reaction force from the ground at the foot point

slope angle of the terrain at the contact point and

$$\frac{d^2X_C}{dt^2} = \frac{d^2X_C}{d\alpha^2}(\frac{d\alpha}{dt})^2 + \frac{dX_C}{d\alpha}\frac{d^2\alpha}{dt^2} \tag{3.42}$$

$$\frac{d^2Y_C}{dt^2} = \frac{d^2Y_C}{d\alpha^2}(\frac{d\alpha}{dt})^2 + \frac{dY_C}{d\alpha}\frac{d^2\alpha}{dt^2} \tag{3.43}$$

where the first and second derivatives of X_C and Y_C with respect to α can be found in Appendix B. In the above derivation, we have assumed that the $X-$axis is parallel to the terrain.

Note that the reaction force in Eqs. (3.40) and (3.41) becomes nearly constant if it is assumed that the rotational speed of the crank is constant and comparatively low. Under this assumption, the crank torque in Eq. (3.39) only depends on the first derivatives $dX_C/d\alpha$ and $dY_C/d\alpha$. As a result, the calculation of crank torque is greatly simplified.

3.2 Literature Review on Six-Bar Mechanisms Featuring Symmetrical Foot-Point Path

Unlike the four-bar linkage, there are only a few studies on symmetrical coupler curves associated with six-bar linkages. For examples, sufficient conditions for the Watt-I mechanisms with symmetrical coupler curves were investigated by Dijksman (1976; 1980a; 1980b; 1981; 1984). Stephenson-I and -III mechanisms that generated symmetrical coupler curves were reported by Dijksman (1979) and Antuma (1978), respectively. All of the above mechanisms were developed with the use of a four-bar linkage with a symmetrical coupler curve. Among them, most were derived according to Roberts-Chebychev cognate theorem, while others were developed from the Chebychev's dyad or a combination of the two. Although these six-bar mechanisms all generate symmetrical coupler curves, their characteristics are different from one another. For example, using a four-bar linkage as the source linkage, Hain's six-bar mechanism can trace a symmetrical coupler curve at any point on its translational coupler link (Dijksman, 1976). Note that Hain's six-bar coupler curve is identical to that of the source four-bar. Using the Kempe's over-constrained focal mechanism as the source mechanism, Dijksman's Watt-I mechanism can generate a series of symmetrical curves at various points of its floating link (Dijksman, 1984). A Stephenson-III mechanism derived from the Chebychev's dyad is capable of generating a symmetrical curve whose order is higher than that of a four-bar linkage (Antuma, 1978). The construction of these three mechanisms and the properties of their coupler curves are discussed in details in Appendixes C.1, C.2, and C.3, respectively. Although the above-mentioned six-bar linkages are

capable of tracing symmetrical coupler curves, none is capable of amplifying the four-bar coupler curve.

In the following sections, we will present a new class of six-bar linkages made up of a four-bar mechanism with an embedded regular or skew pantograph. This class of six-bar mechanisms is capable of generating amplified symmetrical four-bar coupler curves at their output points. This is particularly useful in applications such as walking machine leg mechanisms for which a compact mechanism with a relatively large output coupler curve is needed (Funabashi et al., 1985a; Shieh et al., 1995). Furthermore, unlike the Funabashi's leg design (Funabashi et al., 1985) that uses a general six-bar mechanism, the analysis or synthesis of a six-bar mechanism with an embedded regular or skew pantograph can be easily accomplished in two steps. First, a four-bar linkage is analyzed or synthesized with a desired coupler curve. This is then followed by adding a dyad to form an embedded pantograph. In this way, the analysis or synthesis of the six-bar is essentially simplified to that of a four-bar. In addition, this new class of six-bar mechanisms can be transformed into Watt-I and Stephenson-II and -III type mechanisms - the admissible mechanisms are shown in Fig. 2.7.

3.3 Construction of Six-Bar Mechanisms with Symmetrical Coupler Curves

The basic idea for creating a new class of six-bar mechanisms with symmetrical coupler curves is to combine the functions of a four-bar linkage and a pantograph into one. Since there are four links in each of the four-bar mechanism and the pantograph, it is necessary for these two mechanisms to share two com-

mon links. By embedding a pantograph in a six-bar linkage, the coupler curve of a four-bar linkage can be amplified at the output point. As it will be described in more details, two different types of six-bar linkages with an embedded regular or skew pantograph are possible. For Type A mechanisms, the upper link of the embedded pantograph is a new link passing through B_0 and is parallel to line BC of the four-bar linkage shown in Fig. 3.1, while the lower link is parallel to the rocker link BB_0. On the other hand, for Type B mechanisms, the upper link of the embedded pantograph is the extension of the rocker link, while the lower link is parallel to line BC.

3.3.1 Construction of Six-Bar Mechanisms with an Embedded Regular Pantograph

In what follows, we first review the function of a regular pantograph. Then, the constructions of Types A and B six-bar linkages are described.

(a) Description of a Regular Pantograph

A pantograph is usually used to amplify an input curve at its output point. Referring to the pantograph shown in Fig. 3.6, points D, C, and E always remain collinear and points H, C, G, and F form a parallelogram. The link lengths of a pantograph are related by two factors n and ρ, where n refers to an amplification factor, while ρ, a size factor, only effects the size of the pantograph.

Provided that point D is fixed and C traces an input curve, point E will trace a similar curve which is amplified by a factor n with respect to the input curve without changing its orientation as shown in Fig. 3.6. On the other hand, if point C is fixed and point D traces an input curve, point E will trace a similar

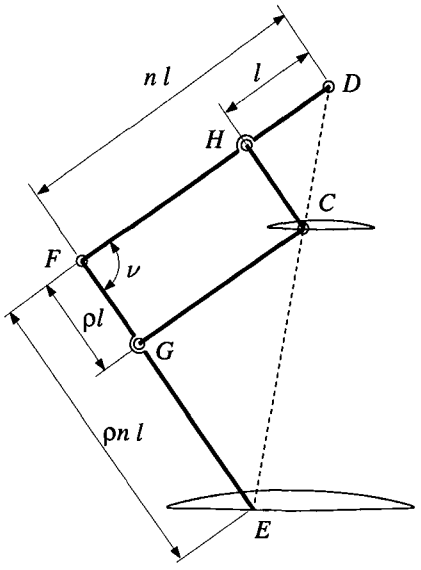

FIGURE 3.6: Regular pantograph

curve which is amplified by a factor $(n-1)$, and rotated by an angle of π about point C.

(b) Construction of Type A Mechanisms

For Type A mechanisms as shown in Figs. 3.7(a), (b), and (c), the embedded pantograph is B_0HFGEC, and points C and E are the input and output points, respectively. The construction of such mechanisms is carried out through the following steps:

1. Construct a four-bar linkage $A_0 - ABC - B_0$ such that $\overline{AB} = \overline{BC} = \overline{B_0B}$.

2. Starting from point B_0, draw a dashed-line passing through point C.

3. Construct a four-bar parallelogram B_0BGF by adding two binary links B_0F and FG such that $B_0F \| BG$ and $FG \| B_0B$. (The length of B_0F is determined by the amplification factor n.)

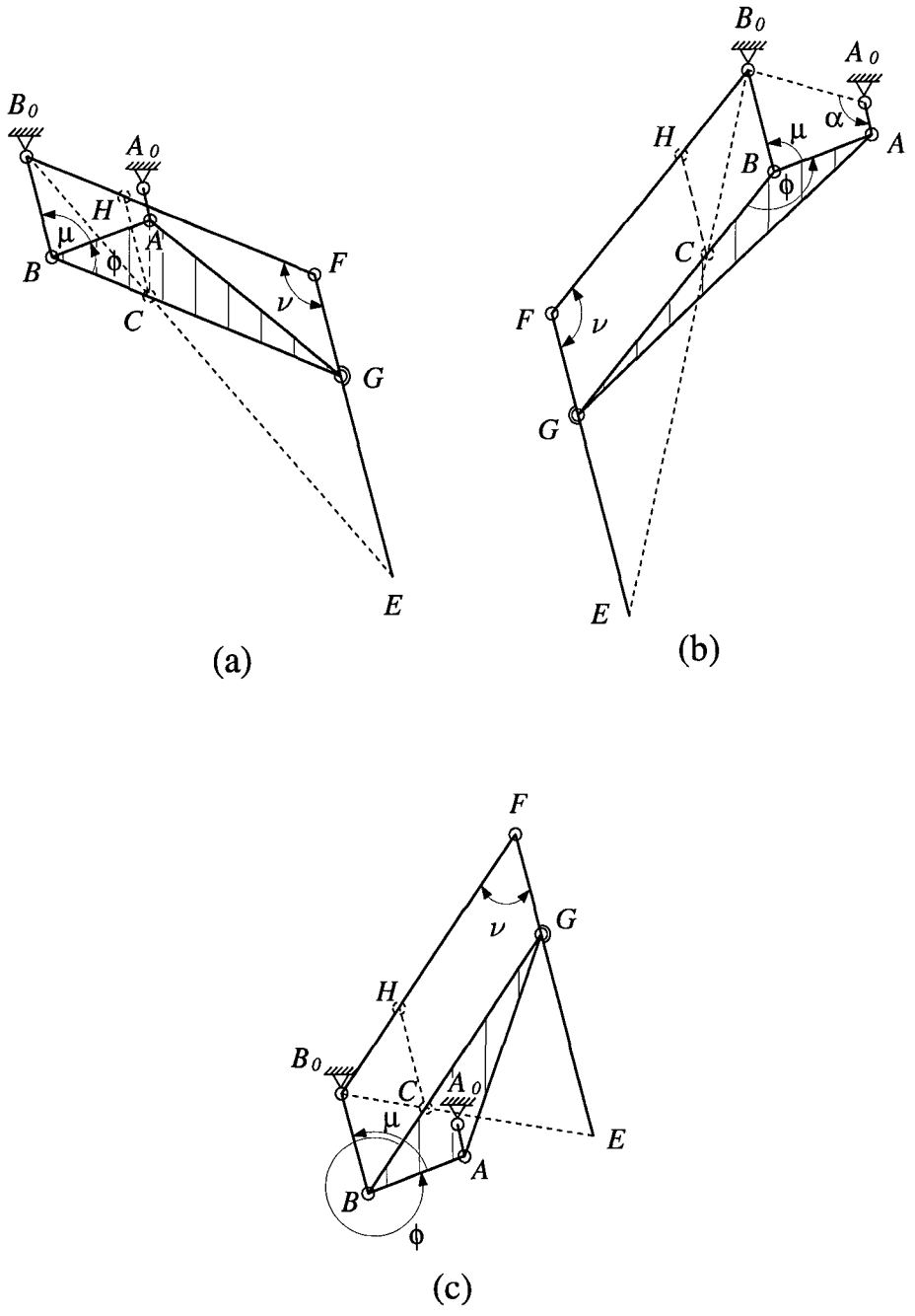

FIGURE 3.7: Type A six-bar linkages with an embedded regular pantograph: (a) $0 < \mu + \phi < \pi$;(b) $\pi < \mu + \phi < 2\pi$; (c) $2\pi < \mu + \phi < 3\pi$.

4. Locate the intersection point E between the extended lines of B_0C and FG and extend link FG to FE.

5. Reshape the coupler plate from ABC to ABG.

For this type of mechanisms, if point B_0 is considered as two concentric binary pivots, then the mechanism becomes a special case of the Stephenson-III mechanism. Referring to the mechanism shown in Fig. 3.7(b), if link B_0B is replaced by a parallel link of the same length, e.g., link CH, a Stephenson-II mechanism is obtained. If link B_0F of Fig. 3.7(b), instead of link B_0B, is replaced by a parallel link of the same length, then a Watt-I mechanism is obtained.

For this type of six-bar linkages, the size factor $\rho = 1$ and the link lengths are related by:

$$\overline{B_0F} = \overline{BG} = \overline{FE} = n\overline{B_0B} \quad \text{and} \quad \overline{FG} = \overline{B_0B} \tag{3.44}$$

(c) Construction of Type B Mechanisms

For Type B mechanisms as shown in Figs. 3.8(a), (b), and (c), the embedded regular pantograph is B_0BFGEC and points C and E are the input and output points, respectively. Type B mechanisms are constructed through a similar (as in Type A) procedure:

1. Construct a four-bar linkage $A_0 - ABC - B_0$ such that $\overline{AB} = \overline{BC} = \overline{B_0B}$.

2. Starting from point B_0, draw a dashed-line passing through point C.

3. Extend the rocker link from B_0B to B_0F. (The choice of joint F is determined by the amplification factor n.)

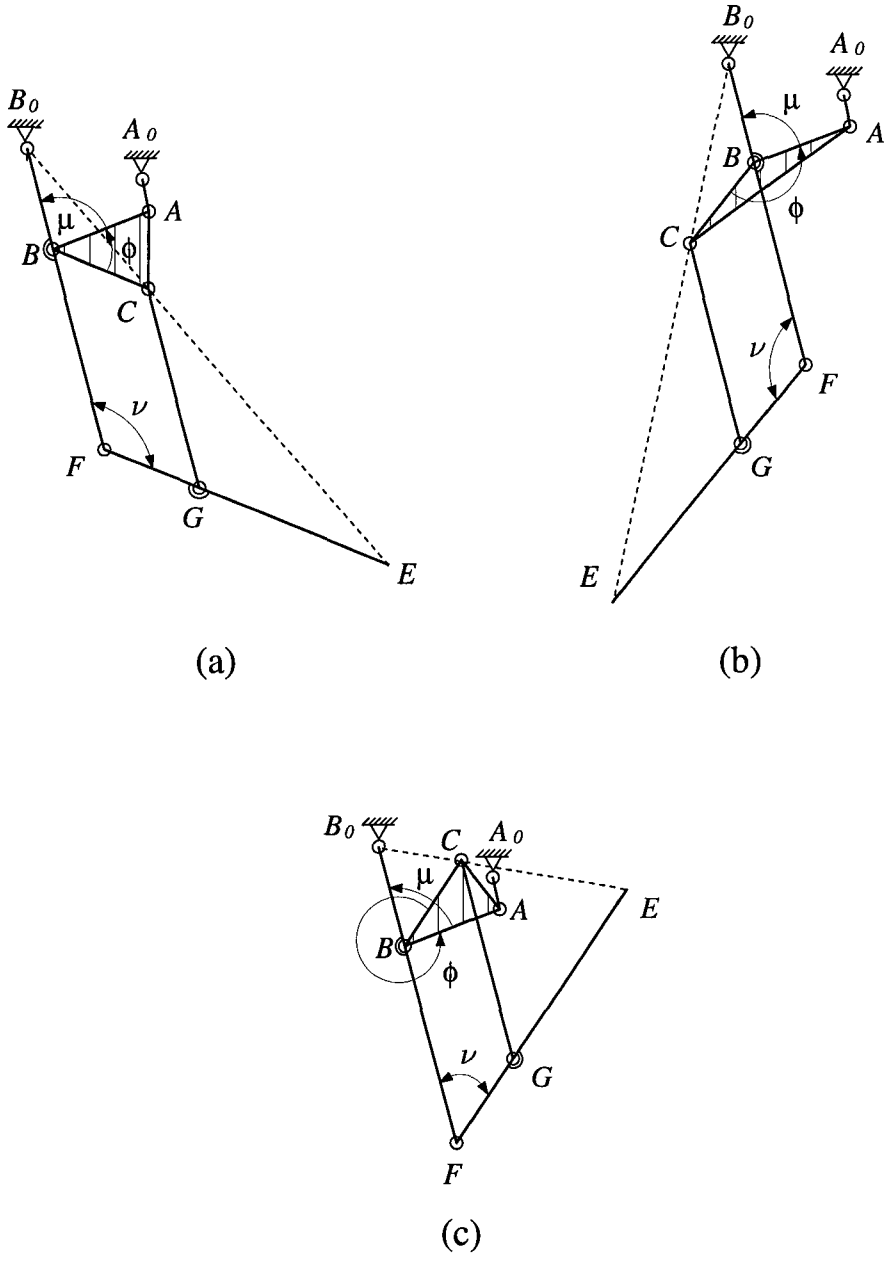

FIGURE 3.8: Type B six-bar linkages with an embedded pantograph: (a) $0 < \mu + \phi < \pi$;(b) $\pi < \mu + \phi < 2\pi$; (c) $2\pi < \mu + \phi < 3\pi$.

4. Add a binary link FE such that $\overline{FE} \parallel \overline{BC}$. ($E$ is the intersection of $\overrightarrow{B_0C}$ and $\overrightarrow{FE}$.)

5. Create a binary link CG to connect the coupler plate ABC and link FE at points C and G, respectively, such that $\overline{CG} \parallel \overline{BF}$.

For this type of mechanisms, the size factor $\rho = 1$ and the link lengths are related by:

$$\overline{BF} = \overline{CG} = (n-1)\,\overline{B_0B} \quad \text{and} \quad \overline{B_0F} = \overline{FE} = n\,\overline{B_0B} \tag{3.45}$$

Note that, Type B mechanisms are Watt-I mechanisms.

3.3.2 Six-Bar Mechanisms with an Embedded Skew Pantograph

In this section, we first review the function of a skew pantograph. Then, the constructions of Types A and B six-bar mechanisms are described.

(a) Description of a Skew Pantograph

Referring to the skew pantograph shown in Fig. 3.9, points H, C, G, and F form a parallelogram and the triangular link DHF is similar to FGE. It is shown (Song et al., 1987) that if point D is fixed and point C traces a given curve, then point E will trace a similar curve which is amplified by a ratio n, and rotated clockwise about the fixed point D through an angle ψ_2 with respect to the given curve as shown in Fig. 3.9. On the other hand, if point C is fixed and point D traces a given curve, then point E will trace a similar curve which

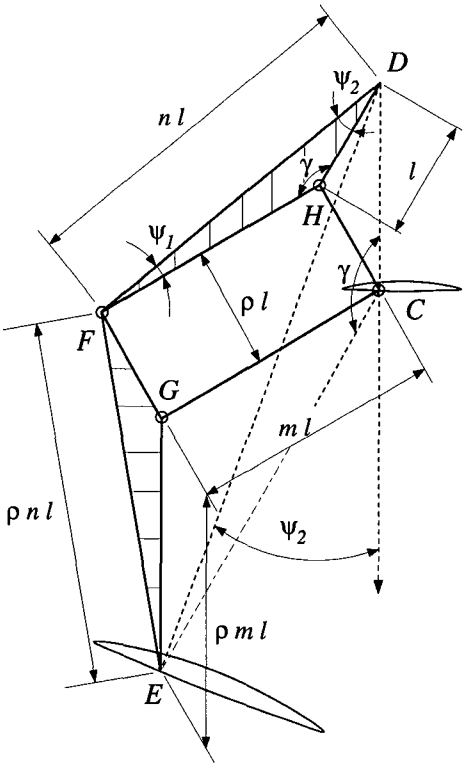

FIGURE 3.9: Skew pantograph

is amplified by a ratio m, and rotated counter-clockwise about the fixed point C through an angle γ, where

$$m = (n^2 - 2n\cos\psi_2 + 1)^{1/2} \quad \text{and} \quad \gamma = \sin^{-1}(\tfrac{n\sin\psi_2}{m}) \tag{3.46}$$

Note that, in Fig. 3.9, ρ effects the size of a skew pantograph.

(b) Construction of Type A Mechanisms

For Type A mechanisms as shown in Figs. 3.10(a), (b), and (c), the embedded pantograph is B_0HFGEC where point B_0 is a fixed pivot while C and E are the input and output points, respectively. The construction of Type A linkages is carried out through the following steps:

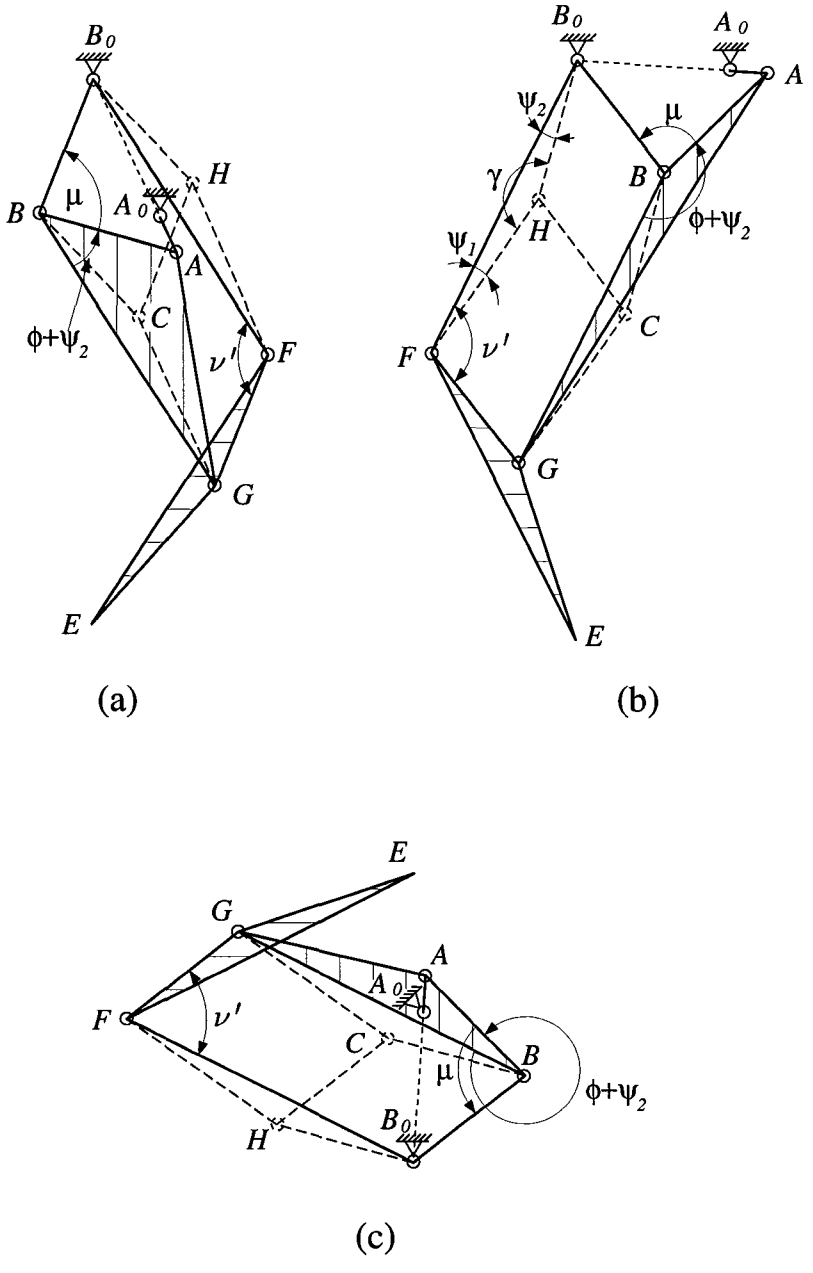

FIGURE 3.10: Type A six-bar linkages with an embedded skew pantograph: (with $\phi' = \phi + \psi_2$) (a) $0 < \mu + \phi' < \pi$; (b) $\pi < \mu + \phi' < 2\pi$; and (c) $2\pi < \mu + \phi' < 3\pi$.

1. Construct a four-bar linkage $A_0 - ABC - B_0$ such that $\overline{AB} = \overline{BC} = \overline{B_0B}$.

2. Add a binary link B_0F. (Note that, the length of link B_0F determines the amplification factor while the orientation of link B_0F determines the orientation of the output curve.)

3. Form a four-bar parallelogram B_0BGF by reshaping the coupler plate from ABC to ABG and adding a binary link FG.

4. Reshape link FG to a triangular plate FGE such that ΔFGE is identical to ΔBCG.

For this type of mechanisms, if point B_0 is considered as two concentric binary pivots, then such a mechanism becomes a special case of Stephenson-III mechanism. If link B_0B is replaced by a parallel link of the same length, a Stephenson-II mechanism is obtained. In addition, if link B_0F (instead of link B_0B) is substituted by a parallel link of the same length, a Watt-I mechanism is obtained. For Type A mechanisms, the size factor $\rho = 1$ and the link lengths are related by:

$$\overline{B_0F} = \overline{BG} = \overline{FE} = n\overline{B_0B} \quad \text{and} \quad \overline{FG} = \overline{B_0B} \tag{3.47}$$

(c) Construction of Type B Mechanisms

For Type B mechanisms as shown in Fig. 3.11, the embedded skew pantograph is B_0BFGEC. The construction of Type B mechanisms is carried out through a procedure as follows:

1. Construct a four-bar linkage $A_0 - ABC - B_0$ such that $\overline{AB} = \overline{BC} = \overline{B_0B}$.

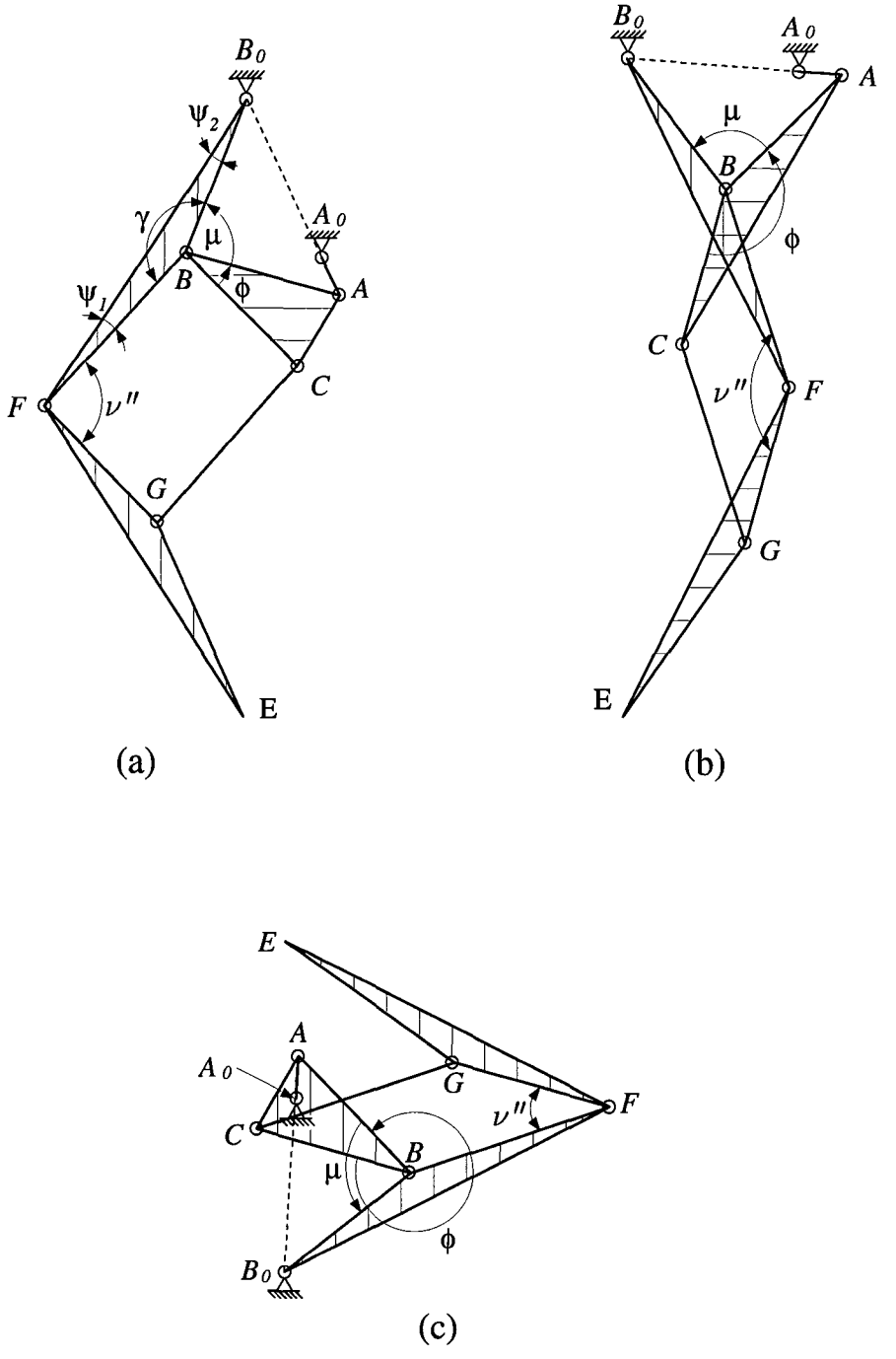

FIGURE 3.11: Type B six-bar linkages with an embedded skew pantograph: (with $\phi'' = \phi - \psi_1 - \psi_2$) (a) $0 < \mu + \phi'' < \pi$; (b) $\pi < \mu + \phi'' < 2\pi$; and (c) $2\pi < \mu + \phi'' < 3\pi$.

2. Reshape the binary link B_0B to a triangular plate B_0BF. (Similar to Type A mechanisms, the choice of point F determines the amplification factor and the orientation of the output curve.)

3. Create a four-bar parallelogram $BCGF$ by adding two binary links CG and GF.

4. Reshape link FG to a triangular plate FGE such that ΔFGE is identical to ΔB_0BF.

Note that, Type B mechanisms belong to Watt-I mechanisms and their link lengths are related by:

$$\overline{B_0F} = \overline{FE} = n\overline{B_0B}\,,\ \overline{BF} = \overline{CG} = \overline{GE} = m\overline{B_0B}\,,\ \text{and}\ \overline{FG} = \overline{B_0B} \quad (3.48)$$

3.4 Characteristics of Six-Bar Mechanisms with Symmetrical Coupler Curve

3.4.1 Six-Bar Linkages with an Embedded Regular Pantograph

Although Types A and B mechanisms with an embedded regular pantograph are different in structure, the characteristics of their transmission angles and coupler curves are identical to each other.

(a)Transmission Angle

Referring to the mechanisms shown in Fig. 3.7 or 3.8, the transmission angles of the four-bar linkage and the embedded regular pantograph are denoted as μ

and ν, respectively. Although the singular condition [2] of such mechanisms can be avoided as long as μ and ν are kept between 0 and π, it is desirable to keep both of them as close to $\pi/2$ as possible. Thus, both transmission angles μ and ν should be constrained:

$$\epsilon < \mu < \pi - \epsilon \tag{3.49}$$

$$\epsilon < \nu < \pi - \epsilon \tag{3.50}$$

where ϵ is the minimum transmission angle for a mechanism to possess good force transmission characteristics. Usually, $\epsilon = 45°$ is assumed for both the four-bar linkage and the embedded regular pantograph.

According to Figs. 3.7 and 3.8, it is observed that the transmission angle ν of the embedded pantograph is determined by both the four-bar transmission angle μ and the coupler plate angle $\angle ABG$ (or ϕ). Since $0 < \mu < \pi$ and $0 < \phi < 2\pi$, we have $0 < \mu + \phi < 3\pi$. Referring to the mechanisms in Figs. 3.7(a), (b) or (c), the transmission angle ν can be expressed as

$$\nu = \begin{cases} \mu + \phi, & \text{for } 0 < \mu + \phi < \pi \\ 2\pi - (\mu + \phi), & \text{for } \pi < \mu + \phi < 2\pi \\ (\mu + \phi) - 2\pi, & \text{for } 2\pi < \mu + \phi < 3\pi \end{cases} \tag{3.51}$$

With the substitution of Eq. (3.51) into Eq. (3.50) and after simplification yields

$$\begin{array}{lll} \text{(i)} & \epsilon - \phi < \mu < \pi - \epsilon - \phi, & \text{for } 0 < \mu + \phi < \pi \\ \text{(ii)} & \epsilon + (\pi - \phi) < \mu < \pi - \epsilon + (\pi - \phi), & \text{for } \pi < \mu + \phi < 2\pi \\ \text{(iii)} & \epsilon + (2\pi - \phi) < \mu < \pi - \epsilon + (2\pi - \phi), & \text{for } 2\pi < \mu + \phi < 3\pi \end{array} \tag{3.52}$$

In order to satisfy both Eqs. (3.49) and (3.52), the transmission angle μ must

[2] A singular condition refers to the condition when μ or ν is equal to 0 or π.

fall in one of the following ranges:

$$\begin{array}{lll} \text{(i)} & \epsilon < \mu < \pi - \epsilon - \phi, & \text{for } 0 < \mu + \phi < \pi \\ \text{(iia)} & \epsilon + (\pi - \phi) < \mu < \pi - \epsilon, & \text{for } \pi < \mu + \phi < 2\pi \text{ and } \pi - \phi \geq 0 \\ \text{(iib)} & \epsilon < \mu < \pi - \epsilon + (\pi - \phi), & \text{for } \pi < \mu + \phi < 2\pi \text{ and } \pi - \phi < 0 \\ \text{(iii)} & \epsilon + (2\pi - \phi) < \mu < \pi - \epsilon, & \text{for } 2\pi < \mu + \phi < 3\pi \end{array} \tag{3.53}$$

Comparing the admissible range of μ in Eq. (3.53) for a six-bar mechanism with an embedded regular pantograph with that in Eq. (3.49) for a four-bar mechanism, we observe that the admissible ranges of μ for the four-bar linkages have been reduced by an amount of ϕ, $|(\pi - \phi)|$, and $(2\pi - \phi)$ for cases (i) through (iii), respectively. Such a reduction in the range of μ may be considered as a significant design limitation.

(b) Coupler-Point Curve

The coupler curve of a six-bar mechanism with an embedded regular pantograph satisfies the following theorem.

Theorem 3.3 *Referring to the six-bar mechanisms in Fig. 3.7 or 3.8, the amplified coupler curve generated by point E is bounded between two concentric circles centered at B_0 and with radii of $(\overline{B_0E})_{\alpha=0}$ and $(\overline{B_0E})_{\alpha=\pi}$, where*
(i) $(\overline{B_0E})_{\alpha=\pi} > (\overline{B_0E})_{\alpha=0}$, if $0 < \mu + \phi < \pi$ or $2\pi < \mu + \phi < 3\pi$, or
(ii) $(\overline{B_0E})_{\alpha=0} > (\overline{B_0E})_{\alpha=\pi}$, if $\pi < \mu + \phi < 2\pi$.

Proof

Referring to Fig. 3.7(b), $\overline{B_0E}$ can be obtained by applying the cosine law to ΔB_0EF,

$$\overline{B_0E} = \sqrt{2}\ \overline{B_0F}\,(1 - \cos\nu)^{1/2} \tag{3.54}$$

Since $\cos\nu$ is a monotonically decreasing function within the range of $0 < \nu < \pi$, the maximum and minimum of $\overline{B_0E}$ occur at $\nu = \nu_{\max}$ and $\nu = \nu_{\min}$, respectively.

(i) For $0 < \mu + \phi < \pi$ or $2\pi < \mu + \phi < 3\pi$, we observe from Eq. (3.51) that the maximum and minimum values of ν follow that of μ. Hence, $\nu_{\max}$ and $\mu_{\max}$ occur at $\alpha = \pi$; $\nu_{\min}$ and $\mu_{\min}$ occur at $\alpha = 0$. This, in turn, indicates that $(\overline{B_0E})_{\alpha=\pi}$ and $(\overline{B_0E})_{\alpha=0}$ are the longest and the shortest distances between points E and B_0 for $\alpha \in [0, 2\pi]$.

(ii) Similarly, for $\pi < \mu + \phi < 2\pi$ we observe from Eq. (3.51) that the maximum value of ν follows the minimum value of μ and vice versa. Hence, $\nu_{\max}$ and $\mu_{\min}$ occur at $\alpha = 0$; $\nu_{\min}$ and $\mu_{\max}$ occur at $\alpha = \pi$. This indicates that $(\overline{B_0E})_{\alpha=0}$ and $(\overline{B_0E})_{\alpha=\pi}$ are the longest and the shortest distances between points E and B_0 for $\alpha \in [0, 2\pi]$.

From (i) and (ii), we conclude that the entire coupler curve is bounded between two concentric circles centered at B_0 and with radii of $(\overline{B_0E})_{\alpha=\pi}$ and $(\overline{B_0E})_{\alpha=0}$, respectively. (QFD)

3.4.2 Six-Bar Linkages with an Embedded Skew Pantograph

For this class of six-bar mechanisms, the transmission angle characteristics between Type A and B mechanisms are different, while the characteristics of their coupler curves remain identical to each other.

(a) Transmission Angle of Type A Mechanism

Referring to Type A mechanisms shown in Fig. 3.10, the transmission angles of the four-bar linkage and the embedded skew pantograph are denoted as μ and

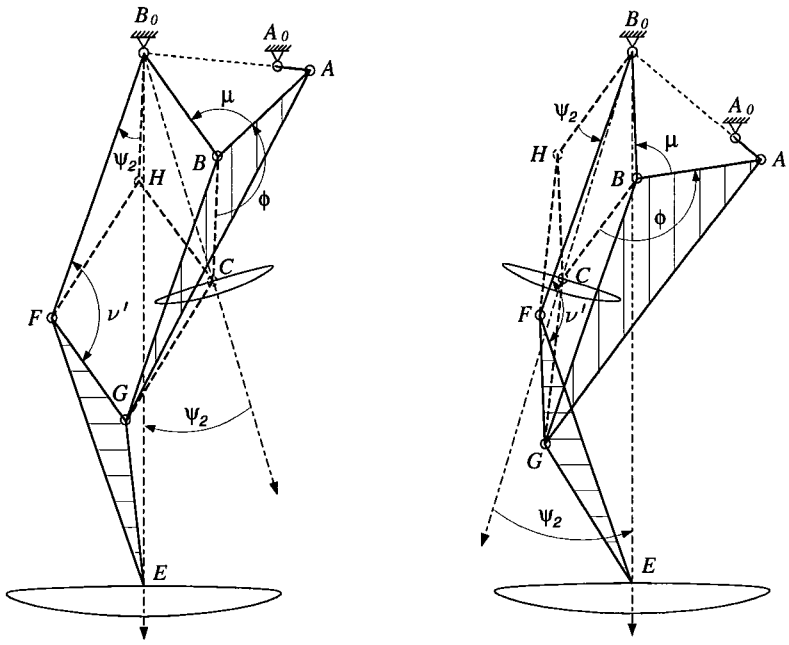

FIGURE 3.12: Coupler curve at C is rotated about point B_0 through an angle ψ_2 at point E: (a) clockwise rotation ($a = +1$) and (b) counter-clockwise rotation ($a = -1$)

ν', respectively. Similar to the six-bar mechanisms with an embedded regular pantograph, these transmission angles should be constrained:

$$\epsilon < \mu < \pi - \epsilon \tag{3.55}$$

$$\epsilon < \nu' < \pi - \epsilon \tag{3.56}$$

Referring to Fig. 3.12, the value of transmission angle ν' of the embedded skew pantograph is determined by both μ and the coupler plate angle $\angle ABG$. The value of $\angle ABG$ depends on the angle $\angle ABC$ and the relative orientation angle between $\overrightarrow{B_0F}$ and $\overrightarrow{B_0H}$ (or $\overrightarrow{B_0C}$). For instance, if the orientation of $\overrightarrow{B_0F}$ is achieved by rotating the vector $\overrightarrow{B_0H}$ clockwise about B_0 through an angle ψ_2

as shown in Fig. 3.12(a), then $\angle ABG = \angle ABC + \angle CBG = \phi + \psi_2$. Otherwise, if the orientation of $\overrightarrow{B_0F}$ is achieved by rotating the vector $\overrightarrow{B_0H}$ counter-clockwise about B_0 through an angle ψ_2 as shown in Fig. 3.12(b), then $\angle ABG = \angle ABC - \angle GBC = \phi - \psi_2$. Hence, denoting $\angle ABG$ as ϕ' yields

$$\phi' = \phi + a\psi_2 \tag{3.57}$$

where $a = \pm 1$. Note that, the coupler curve at E is obtained by rotating the curve at C clockwise or counter-clockwise about point B_0 through an angle ψ_2 according to $a = 1$ or $a = -1$. (see Figs. 3.12(a) and (b))

Since $0 < \mu < \pi$ and $0 < \phi < 2\pi$, we have $0 < \mu + \phi + a\psi_2 < 3\pi + a\psi_2$ or $0 < \mu + \phi' < 3\pi + a\psi_2$. Referring to the mechanisms in Figs. 3.10(a), (b) or (c), the transmission angle ν' of the embedded pantograph can be expressed as

$$\nu' = \begin{cases} \mu + \phi', & \text{for } 0 < \mu + \phi' < \pi \\ 2\pi - (\mu + \phi'), & \text{for } \pi < \mu + \phi' < 2\pi \\ (\mu + \phi') - 2\pi, & \text{for } 2\pi < \mu + \phi' < 3\pi \end{cases} \tag{3.58}$$

Note that, since the condition $\mu + \phi' > 3\pi$ is not desirable, such a condition is not considered. Substituting Eq. (3.58) into (3.56) and satisfying Eq. (3.55), the transmission angle μ of Type A mechanisms must fall in either of the following ranges:

$$\begin{array}{lll} \text{(i)} & \epsilon < \mu < \pi - \epsilon - \phi', & \text{for } 0 < \mu + \phi' < \pi \\ \text{(iia)} & \epsilon + (\pi - \phi') < \mu < \pi - \epsilon, & \text{for } \pi < \mu + \phi' < 2\pi \text{ and } \pi - \phi' \geq 0 \\ \text{(iib)} & \epsilon < \mu < \pi - \epsilon + (\pi - \phi'), & \text{for } \pi < \mu + \phi' < 2\pi \text{ and } \pi - \phi' < 0 \\ \text{(iii)} & \epsilon + (2\pi - \phi') < \mu < \pi - \epsilon, & \text{for } 2\pi < \mu + \phi' < 3\pi \end{array} \tag{3.59}$$

Eq. (3.59) shows that, when compared with a four-bar linkage, the admissible range of μ for Type A mechanism is reduced by an amount of ϕ', $|(\pi - \phi')|$,

and $(2\pi - \phi')$ for ranges (i) through (iii), respectively. Since $\phi' = \phi + a\psi_2$ and $a = \pm 1$, the admissible range of μ for a mechanism with an embedded skew pantograph is larger than that with an embedded regular pantograph, if the value of a is selected as -1, $+1$, -1, and $+1$ for cases (i), (iia), (iib), and (iii), respectively.

(b) Transmission Angle of Type B Mechanism

Referring to Type B mechanisms shown in Fig. 3.11, the transmission angle ν'' of the embedded skew pantograph can be expressed as

$$\nu'' = \begin{cases} \mu + \phi'', & \text{for } 0 < \mu + \phi'' < \pi \\ 2\pi - (\mu + \phi''), & \text{for } \pi < \mu + \phi'' < 2\pi \\ (\mu + \phi'') - 2\pi, & \text{for } 2\pi < \mu + \phi'' < 3\pi \end{cases} \tag{3.60}$$

where

$$\phi'' = \phi - a\psi_1 - a\psi_2 \tag{3.61}$$

and $a = \pm 1$. Note that, for the mechanisms in Fig. 3.11, we have $a = +1$.

For this type of mechanisms, since $\phi'' = \phi - a\psi_1 - a\psi_2$ and $a = \pm 1$, the admissible range of μ for a mechanism with an embedded skew pantograph will be larger than that with an embedded regular pantograph, if the value of a is properly selected.

(c) Coupler-Point Curve

Referring to Type A mechanism as shown in Fig. 3.10, the distance between the fixed point B_0 and the output point E can be written as

$$\overline{B_0E} = \sqrt{2}\ \overline{B_0F}\,[1 - \cos(\angle B_0FE)]^{1/2} \tag{3.62}$$

where $0 < \angle B_0FE < \pi$. Since $\angle B_0FE$ can be written as

$$\angle B_0FE = \nu' + \begin{cases} -a\psi_2, & \text{for } 0 < \mu + \phi' < \pi \\ +a\psi_2, & \text{for } \pi < \mu + \phi' < 2\pi \\ -a\psi_2, & \text{for } 2\pi < \mu + \phi' < 3\pi \end{cases} \tag{3.63}$$

Substituting Eq. (3.58) into (3.63) yields

$$\angle B_0FE = \begin{cases} \mu + \phi, & \text{for } 0 < \mu + \phi' < \pi \\ 2\pi - (\mu + \phi), & \text{for } \pi < \mu + \phi' < 2\pi \\ (\mu + \phi) - 2\pi, & \text{for } 2\pi < \mu + \phi' < 3\pi \end{cases} \tag{3.64}$$

In Eq. (3.64), it is possible that the maximum value of $\angle B_0FE$ is greater than π and the minimum value of $\angle B_0FE$ is less than 0. Hence, the maximum and minimum values of $\overline{B_0E}$ may not occur at the crank angle $\alpha = 0$ or $\alpha = \pi$. Therefore, Theorem 3.3 no longer holds for Type A six-bar mechanisms with an embedded skew pantograph. Similarly, it can be shown that Theorem 3.3 does not hold for Type B mechanisms.

3.4.3 Example Mechanism

To demonstrate the slenderness of the new class of six-bar mechanisms, an example mechanism from this class is illustrated and compared with a four-bar linkage with the same coupler curve.

Fig. 3.13(a) shows a six-bar mechanism with an embedded skew pantograph. Since this mechanism is designed with $\overline{AB} = \overline{B_0B} = \overline{BC}$, point C traces a symmetrical coupler-point curve while crank A_0A rotates about the fixed pivot A_0. By using the additional dyad B_0FGE to form an embedded skew pantograph, the coupler curve at point C is amplified by a factor of $n = \overline{B_0F}/\overline{B_0B}$ and is

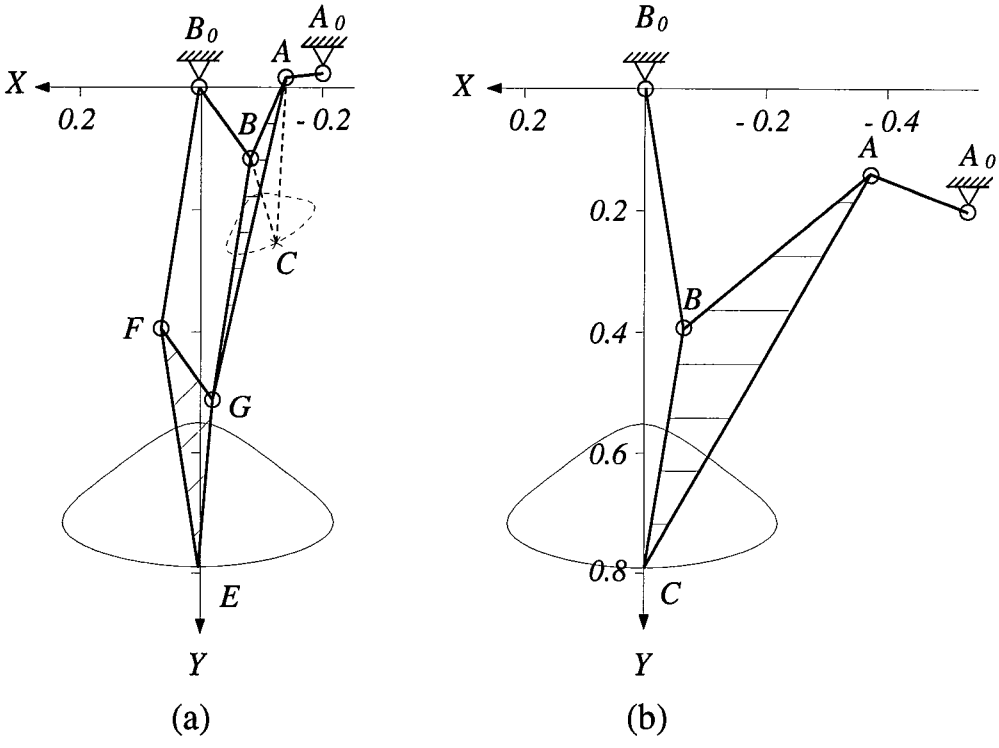

FIGURE 3.13: An identical coupler curve generated by (a) a six-bar mechanism with an embedded skew pantograph (b) a four-bar linkage

rotated clockwise about point B_0 through an angle of $\angle GFE$. Fig. 3.13(b) shows a four-bar linkage which generates a coupler curve identical to that of the six-bar mechanism. For the purpose of comparison, two X-Y reference coordinate systems with their Y-axes pointing downward along the line of symmetry and with their origins located at joint B_0 are defined in Figs. 3.13(a) and (b). It is clear that, when an identical curve is traced, the six-bar linkage shown in Fig. 3.13(a) is more compact than the four-bar mechanism shown in Fig. 3.13(b). Such a compactness is important in many applications, especially for a multi-legged walking machine where the interference between adjacent legs is crucial.

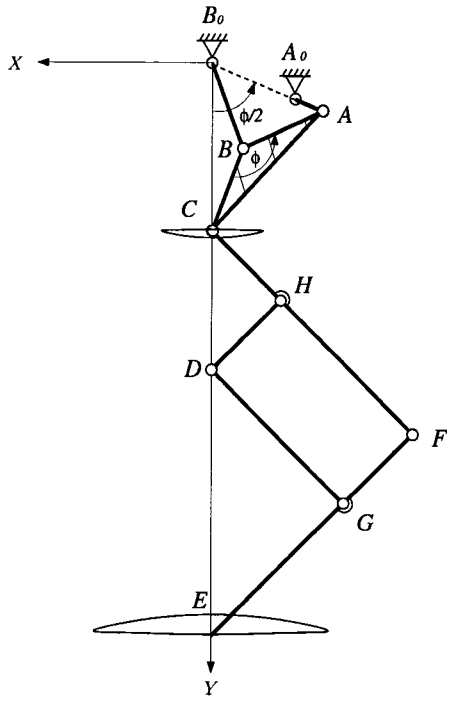

FIGURE 3.14: Eight-bar compound linkage

3.5 An Eight-Bar Compound Mechanism

An eight-bar compound mechanism consisting of a symmetrical four-bar linkage $A_0 - ABC - B_0$ and a regular pantograph $CDEFGH$ is shown in Fig. 3.14. For this compound mechanism, one end of the pantograph is connected to and driven by the coupler point C of a four-bar linkage, while the other end of the pantograph, point D, is fixed for walking on a flat ground. Therefore, the motion at point C provided by rotation of the crank is amplified through the pantograph by a factor of $(-n)$ at the foot-point E, where $n = \overline{FH}/\overline{CH}$ and the negative sign refers to the inverted shape of the curves at points E and C.

The differences between an eight-bar compound mechanism and a six-bar linkage with an embedded pantograph (for both regular and skew pantograph) are: (i) the compound mechanism amplifies the upper portion of the basic four-

bar coupler curve as the propelling path, while the six-bar linkage amplifies the lower portion of the coupler curve as the propelling path; (ii) the transmission angles μ and ν of the four-bar linkage and the pantograph in a compound eight-bar mechanism are independent of each other, while the transmission angles μ and ν (or ν' in case of skew pantograph) of a six-bar linkage discussed in Section 3.4 are related to each other by the angle ϕ (or ϕ' in case of skew pantograph).

Since $dX_E/d\alpha = -n(dX_C/d\alpha)$ and $dY_E/d\alpha = -n(dY_C/d\alpha)$, the crank torque for this compound mechanism can be obtained as

$$T = n(f_{gfX}\frac{dX_C}{d\alpha} + f_{gfY}\frac{dY_C}{d\alpha}) \tag{3.65}$$

where f_{gfX} and f_{gfY} are the same as those in Eqs. (3.40) and (3.41) except for replacing X_C and Y_C by X_E and Y_E, respectively.

3.6 Summary

In this chapter, all the admissible leg mechanisms obtained in Chapter 2 are examined for the feasibility of generating a symmetrical foot-point path.

For the symmetrical four-bar linkage, the coordinates of the foot point are formulated, the guidelines to prevent double point(s) are derived, and the equation for the crank torque is obtained. The relation between the coupler angle ϕ and the condition used to select the propelling and non-propelling portions of a foot-point path is also established.

A new class of six-bar mechanisms which are capable of generating relatively large symmetrical coupler curves at their output points is presented. For this class of mechanisms, the four-bar linkage generates a symmetrical coupler curve

which is then amplified via an embedded regular or skew pantograph to a desired size. As such, the analysis or synthesis of these mechanisms can be easily performed beginning with the four-bar linkage and followed by the pantograph. It is shown that the six-bar mechanisms in this class can be constructed in two different types (or structures). For those mechanisms with an embedded regular pantograph, both types of mechanisms are subject to the same transmission angle constraints. However, for those mechanisms with an embedded skew pantograph, the two types of mechanisms yield different transmission characteristics. The characteristics of the six-bar coupler curves are also investigated. Because of the different characteristics, six-bar mechanisms with an embedded skew pantograph are shown to exhibit better design flexibility.

Finally, an eight-bar compound mechanism consisting of a four-bar linkage and a pantograph is discussed.

Chapter 4

Optimization-Based Dimensional Synthesis of Leg Mechanisms

Optimization-based dimensional synthesis of a leg mechanism can be beneficial in reducing the actuating force and torque and making the leg mechanism slender, while a set of design specifications are met. Based on this approach, candidate four-, six-, and eight-bar mechanisms with symmetrical coupler curves are studied.

In Section 4.1, several dimensional synthesis methods used in the design of mechanisms are reviewed. In Section 4.2, an overall optimization-based model and the solution tool are described. The design objectives and design specifications are defined and the optimization software is briefly explained. Following that, a brief description of the admissible mechanisms, and the assumptions used in the optimization models are given. Then, the four-, six-, and eight-bar mechanisms are investigated in Sections 4.3, 4.4, and 4.5, respectively. For each of the three mechanisms, two types of legs mechanisms, with and without adjustable pivots, are studied. Their results are compared and discussed in Section 4.6. Finally, spring elements are added for further reduction of the actuating forces

and torques.

4.1 Literature Review

Dimensional synthesis is to obtain all the necessary design variables defining the geometry of a mechanism, while certain motion requirements are satisfied. Among the various dimensional synthesis problems, the input-output function generation, coupler path generation, and rigid-body guidance are the most intensively studied in the literature. The methodologies used for solving these three problems can be categorized as the precision point synthesis and the approximate synthesis.

The precision point synthesis is to synthesize a mechanism such that the foot path will pass through a number of pre-specified positions or points. Generally, in this approach, the maximum number of precision points depends on the number of design variables associated with the mechanism of interest. If the number of equations generated by the precision points is less than that of the design variables, a designer is free to choose the values of certain design variables. Early work related to precision point synthesis includes Freudenstein (1961), Roth and Freudenstein (1963), Roth (1967), Suh and Radcliffe (1967), and McLarnan (1963). More references can be found in Thompson (1975). While precision-point synthesis approach is well suited for certain mechanisms, this approach has several drawbacks. First, although the synthesized mechanism does pass through all the precision points, this technique has no control over the structural errors between any two successive precision points. Secondly, this approach is usually restricted by the number of precision points (or design specifications).

Furthermore, as the number of precision points increases, the synthesis problem becomes very nonlinear and extremely difficult to solve. For example, a maximum number of nine prescribed coupler points is allowed for synthesizing a planar four-bar linkage. However, because the nine-coupler-point synthesis problem is highly nonlinear and highly singular (Tsai and Lu, 1990), an attempt to synthesize such a four-bar linkage may not necessarily be successful. These shortcomings call for an alternative approach known as the approximate synthesis technique.

Since the approximate synthesis technique allows a designer to choose more precision points than that allowed by the precision point synthesis technique, it becomes an error minimization problem. In this method, an error function based on the difference between the generated and desired precision points is constructed. As the error function is minimized with respective to the design variables, an optimum linkage is obtained. Consequently, the approximate synthesis returns a better distribution of the error between the synthesized and desired paths over the entire range. The most widely used approximate synthesis technique is the least-squares method. Han (1966) employed the least square approach for the planar coupler curve synthesis, while Tull and Lewis (1968) used the least square method to solve a spatial synthesis problem. Arkhras and Angeles (1990) and Bhatia and Bagciad (1977) adopted this approach for a planar rigid-body guidance problem, while Sutherland and Roth (1974) formulated an iterative algorithm to solve the function generation problem. Sarkisyan et al. (1972) developed a least-squares method which could be regarded as a generalization of the classical Burmester theory to an unlimited number of design points. Their results were applied to both rigid-body guidance and function

generation problems.

The above mentioned studies are based on the kinematic synthesis alone. For many applications, however, the effect of external loads, in addition to the motion specifications, is crucial to the performance of a mechanism. Hence, the interactions between a mechanism and its environment should also be considered. With the inclusion of static loads into the classical dimensional synthesis techniques for mechanisms, Huang and Roth (1993; 1994) successfully synthesized a planar and a spatial mechanism to satisfy both the force and motion conditions for several pre-specified positions. Essentially, their approach is based on the so-called precision point theory.

Although the above mentioned approaches can be used to synthesize certain mechanisms, they are not suited for the mechanism design considered in this thesis. Here, it is desired to simultaneously minimize several design objectives: the crank torque, actuating force and the leg size. In addition, a number of design specifications (or constraints) have to be accommodated in the design process. Hence, the dimensional synthesis of such mechanisms is formulated as a constrained multi-objective optimization problem.

4.2 Overall Optimization Model and Tool

4.2.1 Design Objectives

For our leg mechanism design, three design objectives are simultaneously considered in the model. They are to minimize: (i) the peak crank torque, (ii) the maximum actuating force for an entire propelling portion, and (iii) the mechanism size.

4.2.2 Design Specifications

Based on the desired performance of a six-legged walking robot under study at the University of Maryland, the design specifications of the leg mechanism are given as follows:

1. A horizontal stride (s_h) of 0.3 m and a vertical lift (s_v) of 0.2 m are desired for the back-and-forth and the up-and-down motions, respectively. This means a working area of 0.3 m by 0.2 m is desired.

2. Based on the worst walking condition that a walking machine may encounter, the largest vertical reaction force on the foot point of a single leg is estimated to be 890 N (200 lb).

3. The maximum walking speed of the machine is designed to be 0.3 m/sec (or 1 ft/sec). This is equivalent to a rotational speed of 30 rpm for the crank.

4. The propelling and non-propelling portions of the foot-point path should not intersect each other. In addition, the foot-point path height is required to be no less than 0.03 m so that a small obstacle on the ground can be avoided without the need of activating the second-DOF motion.

5. In order to obtain a better force transmission within the leg mechanism, the transmission angles of any four-bar loop should fall between 45 and 135 degrees.

6. To avoid the lower limb of a leg to bump into the ground, the orientation angle between the lower limb and the ground is constrained to be no less than 20 degrees.

4.2.3 Optimization Tool

Optimization-based dimensional synthesis of a mechanism with a number of design objectives subject to several constraints can be formulated as a constrained multi-objective optimization problem. An interactive optimization-based design software package called Consol-Optcad (Fan et al., 1990) is used to solve the optimization problem.

Consol-Optcad implements a methodology developed by Nye and Tits (1986) and an optimization algorithm based on FSQP (Feasible Sequential Quadratic Programming) which is described and analyzed by Panier and Tits (1993), Bonnans et al. (1992), and Zhou and Tits (1993). The Consol-Optcad methodology allows for three qualitatively different types of design specifications. An *objective* is a specification of a quantity that should be minimized or maximized. A *hard constraint* is a specification of a quantity that must achieve a specified threshold or the corresponding design has no or little value. A *soft constraint* is a specification of a quantity that should achieve or at least approach a specified threshold, however, a small violation is acceptable. A mathematical meaning is given to the optimization problem by means of *good* and *bad* values assigned by the designer to each objective and soft constraint, according to the following uniform satisfaction/dissatisfaction rule: having any of the various objectives or soft constraints achieve its corresponding good value should provide the same level of satisfaction to the designer, whereas having any of them achieve its bad value should provide the same level of dissatisfaction. Also, the good value of a soft constraint must be the corresponding threshold. Each objective and soft constraint is scaled by Consol-Optcad using its good and bad values according

to the formula:

$$scaled\_value = \frac{raw\_value - good\_value}{bad\_value - good\_value} \tag{4.1}$$

The resulting optimization problem is as follows: minimize the scaled objectives ($obj_k(\mathbf{x})$) subject to scaled soft constraints on $\mathbf{x}$ ($soft_i(\mathbf{x})$ is non-positive) and scaled hard constraints on $\mathbf{x}$ ($hard_j(\mathbf{x})$ is non-positive). The quantity $\mathbf{x}$ represents an n-vector of design variables. In mathematical terms, one has to solve

$$\begin{cases} \min\limits_{\mathbf{x}} & obj_k(\mathbf{x}) & \forall k \\ \text{subject to} & soft_i(\mathbf{x}) \leq 0 & \forall i \\ & hard_j(\mathbf{x}) \leq 0 & \forall j \end{cases} \tag{4.2}$$

Functional objectives and functional constraints are handled whereby some quantity that depends on some free variables must be made small or large for all values of these free variables in their given ranges. Similar to *ordinary* (nonfunctional) specifications, these can be objectives, hard constraints, or soft constraints. They are normalized according to user-specified good and bad curves (i.e., functions of the free variables) according to the formula

$$scale\_value(\omega) = \frac{raw\_value(\omega) - good\_value(\omega)}{bad\_value(\omega) - good\_value(\omega)} \tag{4.3}$$

where ω represents the free variables. For example, in the design of a leg mechanism, while link lengths are the design variables, the crank angle is considered as a free variable.

Consol-Optcad first constructs a vector of design variables $\mathbf{x}$ that satisfies all the hard constraints (phase 1). Then a minimax optimization is performed on all scaled objectives and soft constraints, subject to satisfying the hard constraints

(phase 2). Finally, if and when all the scaled objectives and soft constraints become negative (i.e., all good values are achieved), Consol-Optcad performs a minimax optimization on all objectives subject to satisfying all constraints (phase 3). Typically most of the optimization run and user interaction will take place in phase 2 or 3.

Throughout this chapter, we shall use the notation `H` to specify the threshold for hard constraint functions.

4.2.4 Mechanisms to be Synthesized

As shown in Fig. 4.1, three one-DOF planar mechanisms, each with an adjustable pivot, are selected for optimization. While rotation of the cranks of these mechanisms provides the back-and-forth motion at the foot point, displacement of their adjustable pivots provide the up-and-down motion.

Fig. 4.1 (a) shows a crank-and-rocker type four-bar mechanism with point B_0 as the adjustable pivot. Fig. 4.1 (b) shows a Stephenson-III type six-bar mechanism with points B_0 of link 4 and F_0 of link 5 coincide. For this mechanism, either B_0 or F_0, or both of them can be considered as the adjustable pivot. Although the class of six-bar mechanisms with an embedded skew-pantograph can form a Watt-I, or Stephenson-II, or Stephenson-III type mechanism as discussed previously, Stephenson-III type mechanism is chosen for further study because it has one more base-connected pivot than the other two. Fig. 4.1 (c) shows a compound eight-bar mechanism consisting of a four-bar linkage and a pantograph. Point F_0 is the adjustable pivot. Basically, all three mechanisms are designed such that each generates either a symmetrical four-bar coupler curve or an amplified symmetrical four-bar coupler curve at the foot point. Note that

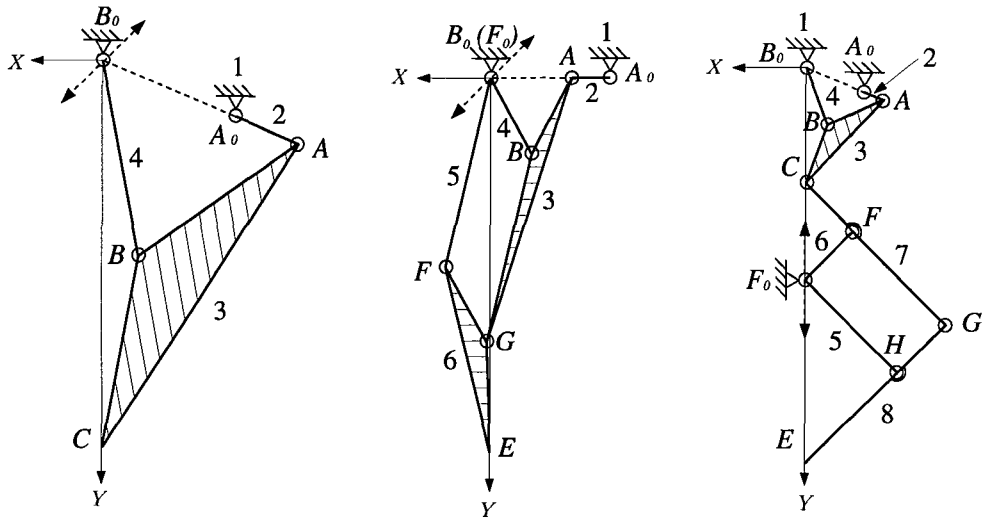

(a) Four-bar (b) Six-bar (S-III) (c) Eight-bar

FIGURE 4.1: Mechanisms to be synthesized (a) symmetrical four-bar mechanism (b) six-bar mechanism with an embedded skew-pantograph (c) eight-bar compound mechanism

it is possible for the mechanisms shown in Fig. 4.1 to generate a symmetrical delta-shaped (Δ-shaped) coupler curve. If such a delta-shaped curve has a sufficient height for a leg mechanism to step over obstacles, designing such a leg mechanism with an adjustable pivot becomes unnecessary. Hence, each of the three mechanisms shown in Fig. 4.1, can be divided into two types. Type I mechanisms, without an adjustable pivot, generate a delta-shaped path, while Type II mechanisms, with an adjustable pivot, generate a narrow ovoid path.

For the mechanisms to be synthesized, the following assumptions are made:

1. No transmission loss between the input and output ends of the mechanisms, i.e., no frictions in the joints.

2. Throughout the entire walking cycle, the vertical reaction force acting on

the foot point by the ground is constant and is equal to 890 N. (Since this value is estimated as the largest reaction force ever encountered, this assumption simplifies the synthesis process and makes the design a conservative one.)

3. Since fast locomotion is not expected for a machine walking on a rough terrain, the up-and-down motion of a leg mechanism can be relatively slow. (This assumption reduces the coupling effects between the first- and second-DOF motions substantially. Hence, the dynamic effects due to the coupling is neglected.)

4. Inertia forces are ignored due to their relatively small values compared to the ground reaction force on the foot point.

4.3 Optimization of Four-Bar Leg Mechanisms

4.3.1 Mechanism Description

(a) Type I Mechanism

Fig. 4.2 shows a four-bar Type I mechanism. This mechanism features a symmetrical coupler path with a large path height, h_p at its foot point. Having such a foot-point path, rotation of the input link (crank) not only provides the back-and-forth motion, but also enables the robot to step over obstacles.

For convenience, an X-Y reference coordinate system with its Y-axis pointing downward in the direction of the symmetrical axis $\overrightarrow{B_0C}$ and with its origin O located at joint B_0 is defined in Fig. 4.2. In our design, this four-bar mechanism is proportioned such that $\overline{AB} = \overline{B_0B} = \overline{BC}$ and the angle between the

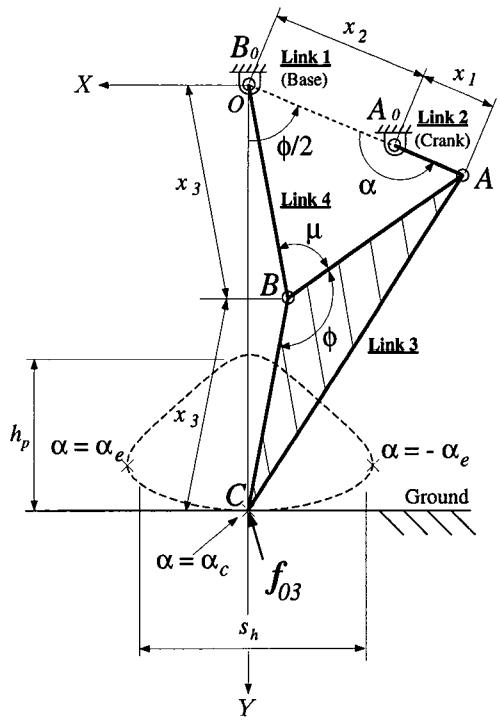

FIGURE 4.2: Four-bar Type I mechanism

symmetrical axis $\overrightarrow{Y}$ (or $\overrightarrow{B_0C}$) and the four-bar linkage baseline $\overrightarrow{B_0A_0}$ is equal to $\phi/2$, where $\phi = \angle ABC$. As a result, the coupler curve is symmetric. The distance between the two extreme positions of point C which are symmetrical about the Y-axis, is referred to as the horizontal stride. Note that the horizontal stride should not be shorter than the desired stride length s_h, as shown in Fig. 4.2.

(b) Type II Mechanism

Type II mechanism is similar to the mechanism shown in Fig. 4.2 except for the following differences. First, Type I mechanism does not have an adjustable pivot, while Type II mechanism has. Second, the foot-point path height of Type I mechanism is large, while that of Type II mechanism is not. Since the

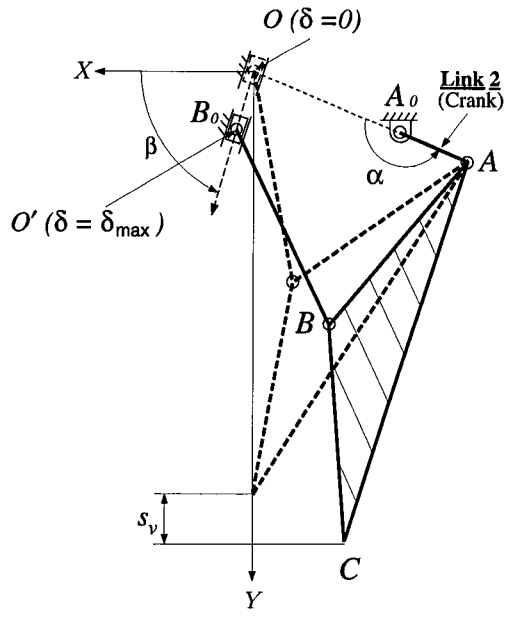

FIGURE 4.3: Four-bar Type II mechanism (with point B_0 as the adjustable pivot)

mechanism shown in Fig. 4.2 has only two supporting pivots A_0 and B_0, pivot B_0 is used as an adjustable pivot. Fig. 4.3 shows a Type II mechanism where point B_0 can be adjusted between two end positions O and O'.

For this type of mechanism, linear motion of the adjustable pivot between the two end positions O and O' provides the up-and-down motion, while rotation of the crank about the fixed pivot A_0 provides the back-and-forth motion on the foot point C. The maximum stroke of the up-and-down motion is defined as the vertical lift s_v as shown in Fig. 4.3.

4.3.2 Optimization Model

(a) Type I Mechanism

Since Type I mechanism as shown in Fig. 4.2 is a one-DOF mechanism, crank angle α is the only free variable. However, Type II mechanism shown in

Fig. 4.3 is two-DOF mechanisms, and hence it includes two free variables, crank angle α and the adjustable pivot displacement, in the model.

(a) Design Variables

Referring to Fig. 4.2, four design variables, link lengths x_1 through x_3 and angles ϕ, are required for Type I mechanism. In addition to the four variables, two additional design variables, δ_{max} and β, are required for Type II mechanism (see Fig. 4.3).

(b) Objective Functions

Three design objectives are simultaneously considered for Type II mechanisms. They are to minimize (i) the peak crank torque and (ii) the maximum actuating force for the entire propelling portion and (iii) the leg size at a particular configuration. For each of the design objectives (i) and (ii), two functions are considered: one is calculated at the normal configuration (i.e., $\delta = 0$), while the other is calculated at the extreme configuration (i.e., $\delta = \delta_{max}$). This is because both quantities at the normal configuration are different from those at the extreme configuration. However, for simplicity, the size of the leg is only calculated at the configuration as shown in Fig. 4.2. Therefore, four functional and one simple objective functions are included in the model. For Type I mechanism, since the ground reaction force at pivot B_0 is not of interest, only two design objectives are simultaneously considered. They are to minimize: (i) the peak crank torque and (ii) the leg size.

Objective 1: Minimizing peak crank torque. Since it is assumed that transmission loss between the input crank and the output foot point is negligible,

the input and output powers are equal:

$$T\frac{d\alpha}{dt} = f_{30X}\frac{dX_C}{dt} + f_{30Y}\frac{dY_C}{dt} \tag{4.4}$$

Rearranging Eq. (4.4) results in functional objectives for both types of mechanisms as

$$\begin{aligned} \texttt{FO1} :=&\ T = -f_{03X}\tfrac{dX_C}{d\alpha} - f_{03Y}\tfrac{dY_C}{d\alpha},\ \ \forall\, \alpha \in R_p,\, \delta = 0 \qquad \text{(I, II)} \\ \texttt{FO2} :=&\ T = -f_{03X}\tfrac{dX_C}{d\alpha} - f_{03Y}\tfrac{dY_C}{d\alpha},\ \ \forall\, \alpha \in R_p,\, \delta = \delta_{max} \quad \text{(II)} \end{aligned} \tag{4.5}$$

where the first derivatives of X_C and Y_C can be found in Appendix B. Note that, in Eq. (4.5), expression (I, II) indicates that FO1 is applicable for both Type I and II mechanisms, while expression (II) means that FO2 is only valid for Type I mechanism. Thus, such expression will be used for the sake of convenience hereafter.

Hence, the first design objective for Type I mechanism is $\min_{\mathbf{x}}\{\texttt{FO1}\}$, while first and second design objectives for Type II mechanism are $\min_{\mathbf{x}}\{\texttt{FO1}\}$ and $\min_{\mathbf{x}}\{\texttt{FO2}\}$, respectively.

Objective 2: Minimizing vertical actuating force.

Using the free-body diagram method, we obtain the following equations:

$$\mathbf{f}_{43} = f_{43}\,\mathbf{e}_{B_0B} \tag{4.6}$$

$$\mathbf{f}_{23} = -\mathbf{f}_{43} - \mathbf{f}_{06} \tag{4.7}$$

$$T = \overline{A_0A}\,(\mathbf{e}_{A_0A} \times \mathbf{f}_{23}) \tag{4.8}$$

where

$$f_{43} = -\frac{\overline{AC}}{\overline{BC}}\frac{(\mathbf{e}_{AC} \times \mathbf{f}_{06}) \cdot \mathbf{k}}{(\mathbf{e}_{AB} \times \mathbf{e}_{B_0B}) \cdot \mathbf{k}} \tag{4.9}$$

where $\mathbf{e}$ represents an unit vector, $\mathbf{k}$ is an unit vector perpendicular to the plane of the linkage, and '$\times$' means the cross product of two vectors. Note that, since

Eq. (4.8) is an alternative way of calculating the value of the crank torque, it can be used to validate the values of the functional objectives FO1 and FO2 obtained from Eqs. (4.5) and (4.5). Since point B_0 is adjusted between points O and O', the actuating force on point B_0 can be obtained as the projection of force $\mathbf{f}_{43}$ on the direction of $\overrightarrow{OO'}$, Hence, two functional objectives are obtained,

$$\begin{aligned} \texttt{FO3} &:= \mathbf{f}_{43} \cdot \mathbf{e}_{OO'}, \quad \forall\, \alpha \in R_p,\ \delta = 0 \qquad \text{(II)} \\ \texttt{FO4} &:= \mathbf{f}_{43} \cdot \mathbf{e}_{OO'}, \quad \forall\, \alpha \in R_p,\ \delta = \delta_{max} \qquad \text{(II)} \end{aligned} \tag{4.10}$$

Hence, our third and fourth design objectives are: $\underset{\mathbf{x}}{min}\ \{\texttt{FO3}\}$ and $\underset{\mathbf{x}}{min}\ \{\texttt{FO4}\}$, respectively.

Objective 3: Minimizing leg size. For both types of mechanisms, the leg size is only calculated at the configuration shown in Fig. 4.2. At this particular configuration, point B_0 is at point O and point C is at the center of the propelling portion. Hence, the leg height L_h can be written as,

$$L_h = Y_C|_{\alpha=\alpha_c} \tag{4.11}$$

and the width of leg mechanism, L_w, is defined as

$$L_w = \max(X_B|_{\alpha=\alpha_c}, X_{B_0}) - \min(X_A|_{\alpha=\alpha_c}, X_{A_0}) \tag{4.12}$$

Normalizing the rectangular leg size with respect to a pre-specified walking area $(s_v s_h)$ yields

$$\texttt{O1} := \frac{L_h L_w}{s_v s_h},\ \delta = 0 \qquad \text{(I, II)} \tag{4.13}$$

Therefore, this design objective is: $\underset{\mathbf{x}}{min}\ \{\texttt{O1}\}$.

(c) Constraint Functions

The mechanism constraint functions are referred to the constraints imposed on the geometry of the linkage and the shape of the foot-point path.

Stride length. The horizontal stride is defined as the distance between the two extreme positions where $dX_C/d\alpha = 0$. Due to symmetry, the corresponding crank angles at these two positions are denoted as $\alpha = \alpha_e$ and $\alpha = -\alpha_e$ (see Fig. 4.2). As a result, $X_C|_{\alpha=\alpha_e} - X_C|_{\alpha=-\alpha_e} = 2X_C|_{\alpha=\alpha_e}$. Hence, the constraint on the stride length is

$$\texttt{C1} := \frac{2X_C|_{\alpha=\alpha_e}}{s_h} \geq \texttt{H}_{\texttt{C1}}, \text{ for } \delta = 0 \quad \text{(I, II)} \tag{4.14}$$

Since the foot-path stride should be no smaller than the pre-specified stride length s_h, the threshold $\texttt{H}_{\texttt{C1}}$ is set to be one.

Vertical Lift. The vertical lift s_v is defined as the maximum change of the foot point C in the $Y-$direction due to the adjustment of pivot B_0 as shown in Fig. 4.3. Therefore,

$$\texttt{C2} := \frac{\|Y_C|_{\alpha=\alpha_c,\ \delta=0} - Y_C|_{\alpha=\alpha_c,\ \delta=\delta_{max}}\|}{s_h} \geq \texttt{H}_{\texttt{C2}} \quad \text{(II)} \tag{4.15}$$

where $\|\cdot\|$ returns the absolute value of the inside quantity. Here, the value of $\texttt{H}_{\texttt{C2}}$ is set to be $2/3$.

Foot-path height. The foot-path height h_p is defined as the distance between the two intersection points of the symmetrical $Y-$ axis and the foot-point path as shown in Fig. 4.2. Hence, the constraint of the foot-path height can be written as

$$\texttt{C3} := \frac{\|Y_C|_{\alpha=\alpha_c} - Y_C|_{\alpha=\pi-\alpha_c}\|}{s_h} \geq \texttt{H}_{\texttt{C3}} \quad \text{(I, II)} \tag{4.16}$$

For Type I mechanism, since the foot-point path provides the back-and-forth as well as the up-and-down motion of the leg mechanism, the height of the foot-point path should be higher than a pre-specified vertical lift ($s_v = 2/3 s_h$). Therefore, the value of $\texttt{H}_{\texttt{C2}}$ is set to be 0.8. However, for Type II mechanism,

a large foot-path height is not necessary and hence the value of H_{C3} is set to be 0.1.

Four-bar transmission angle. The transmission angle of the four-bar mechanism changes as a result of the adjustment of point B_0. Therefore, the transmission angle should be calculated at both extreme positions. Here, at $\delta = 0$, we have

$$\begin{aligned} C4 :=&\ \mu_{\min} = 2\sin^{-1}\left(\tfrac{x_2 - x_1}{2x_3}\right) \geq H_{C4}, \quad \text{for } \delta = 0 \quad \text{(I, II)} \\ C5 :=&\ \mu_{\max} = 2\sin^{-1}\left(\tfrac{x_2 + x_1}{2x_3}\right) \leq H_{C5}, \quad \text{for } \delta = 0 \quad \text{(I, II)} \end{aligned} \tag{4.17}$$

Similarly, at $\delta = \delta_{\max}$, we have

$$\begin{aligned} C6 :=&\ \mu_{\min} = 2\sin^{-1}\left(\tfrac{x'_2 - x_1}{2x_3}\right) \geq H_{C6}, \quad \text{for } \delta = \delta_{\max} \quad \text{(II)} \\ C7 :=&\ \mu_{\max} = 2\sin^{-1}\left(\tfrac{x'_2 + x_1}{2x_3}\right) \leq H_{C7}, \quad \text{for } \delta = \delta_{\max} \quad \text{(II)} \end{aligned} \tag{4.18}$$

where $x'_2 = \overline{A_0 O'}$. In order to achieve efficient force transmission in the four-bar linkage, the transmission angle should not deviate too much from $\pi/2$. Hence, the values of H_{C4} and H_{C6} are chosen to be 45 degrees, while those of H_{C5} and H_{C7} are selected to be 135 degrees. Note that under this constraint the Grashof criteria for the four-bar linkage are automatically satisfied.

Orientation angle of the lowest link. In order to prevent link 3 from bumping into the ground, the orientation angle of link 3 must be constrained:

$$\begin{aligned} FC1 :=&\ \|\theta_{BC} - \pi/2\| \leq H_{FC1}, \ \forall\alpha, \ \delta = 0 \qquad \text{(I, II)} \\ FC2 :=&\ \|\theta_{BC} - \pi/2\| \leq H_{FC2}, \ \forall\alpha, \ \delta = \delta_{max} \qquad \text{(II)} \end{aligned} \tag{4.19}$$

where both values of H_{FC1} and H_{FC2} are set to be 70 degrees, i.e., the angle between the lowest link and the ground has to keep at least 20 degrees.

Design Vaiables	Initial Values	Optimized Values	
		Type I Mechanism	Type II Mechanism
x_1 (m)	0.05	0.134	0.080
x_2 (m)	0.20	0.410	0.290
x_3 (m)	0.25	0.294	0.274
ϕ (rad)	3	2.768	2.359
δ_{max} (m)	0	N/A	0.135
β (rad)	0	N/A	-1.65

TABLE 4.1: Initial and optimized design variables

4.3.3 Results and Discussion

The optimization was carried out based on the design specifications outlined in Section 4.2.2 and the assumption of a flat walking terrain. Here, optimization-based dimensional syntheses of the four-bar Type I and II mechanisms are performed. For these two types of mechanisms, the initial and optimized leg dimensions are shown in Table 4.1, while the values of the optimized objective functions are listed in Table 4.2.

Figs. 4.4(a) shows the initial and optimized Type I mechanisms and their foot-point paths. The optimized design shows a $\Delta-$shaped foot-point path featuring a large path height, enabling a leg mechanism to step over obstacles. We note that the horizontal stride of the optimized path is larger than the the prespecified value, 0.3 m, while the path height is identical to the specified value of 0.24 m. This indicates that, for this optimized mechanism, the path height constraint is more crucial than the horizontal stride constraint. Fig. 4.4(b) shows an

Objective Functions		Type I	Type II
Peak crank torque (N-m)	$T\|_{\delta=0}$	73.5	25.7
Peak crank torque (N-m)	$T\|_{\delta=\delta_{max}}$	N/A	60.6
Maximum actuating force(kN)	$f_a\|_{\delta=0}$	N/A	1.36
Maximum actuating force(kN)	$f_a\|_{\delta=\delta_{max}}$	N/A	1.63
Normalized leg size		2.52	1.63

TABLE 4.2: Values of the optimized objective functions

optimized Type II mechanism with its adjustable pivot at two positions, $\delta = 0$ and $\delta = \delta_{\max}$. For the case of $\delta = 0$, the major axis of the foot-point path lies in the horizontal direction, while, for the case of $\delta = \delta_{\max}$, the major axis of the foot-point path tilts from the horizontal direction.

Fig. 4.5(a) shows the crank torque curves of both the initial and optimized Type I mechanisms. We note that the peak crank torque of the optimized mechanism is larger than that of the initial mechanism. Since the initial design does not satisfy all the constraints, the initial design has a smaller crank torque. This indicates that the required crank torque can be reduced, if some of the constraints are relaxed. Fig. 4.5(b) shows the optimized crank torque curves for Type II mechanism. As expected, the absolute value of the optimized crank torque for the case of $\delta = \delta_{\max}$ is much larger than that of $\delta = 0$.

As to the actuating force, since Type I mechanism is a one-DOF mechanism, Fig. 4.6 only shows the actuating force of Type II mechanism. Again, the actuating force at $\delta = 0$ is smaller than the required force at $\delta = \delta_{\max}$.

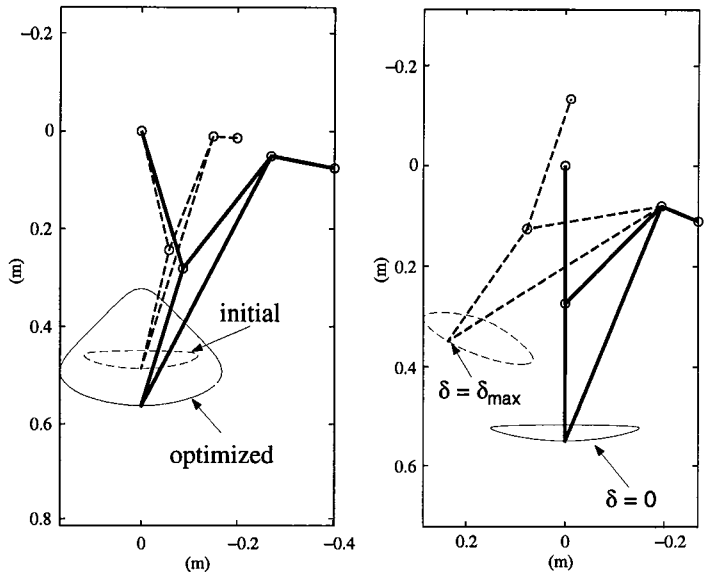

FIGURE 4.4: Optimized four-bar mechanisms, (a) Type I and (b) Type II

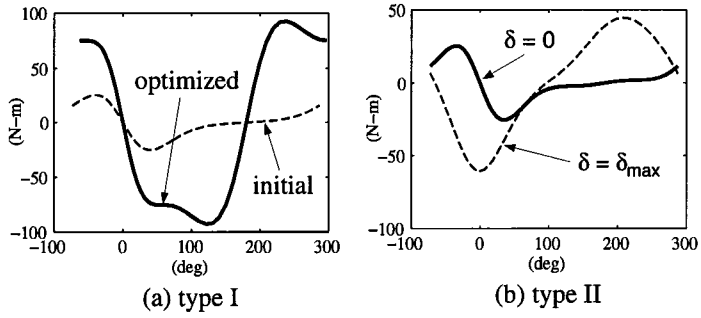

FIGURE 4.5: Crank torque of the optimized four-bar mechanisms, (a) Type I and (b) Type II

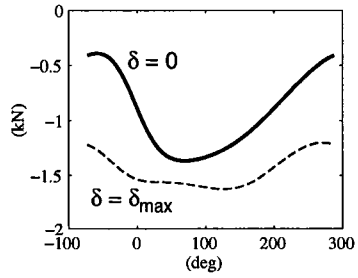

FIGURE 4.6: Actuating force of the optimized four-bar mechanism (Type II)

4.4 Optimization of Six-Bar Leg Mechanisms

4.4.1 Mechanism Description

(a) Type I Mechanism

A planar one-DOF six-bar mechanism with an embedded skew-pantograph, is shown in Fig. 4.7. This mechanism features a symmetrical foot-path with a large path height no smaller than h_p at its foot point. Having such a foot-point path, rotation of the crank link not only produces the back-and-forth motion, but it also enables a walking machine to step over obstacles.

For convenience, an X-Y reference coordinate system with its Y-axis pointing downward in the direction of the symmetrical axis $\overrightarrow{B_0E}$ and with its origin O located at joint B_0 is defined in Fig. 4.7.

In this design, the base-connected four-bar loop A_0AB_0B is selected such that $\overline{AB} = \overline{B_0B} = \overline{BC}$ and the angle between the symmetrical axis $\overrightarrow{Y'}$ (or $\overrightarrow{B_0C}$) and the four-bar linkage baseline $\overrightarrow{B_0A_0}$ is equal to $\phi/2$, where $\phi = \angle ABC$. By reshaping the plate ABC to ABG and adding two links F_0F and FGE in which point F_0 is at B_0, ΔFGE is identical to ΔBCG, and $\overline{F_0F} = \overline{FE} = \overline{BG}$, a skew-pantograph is constructed and embedded into the mechanism [1]. With this embedded skew-pantograph connected to the four-bar linkage at the imaginary coupler point C, the coupler curve is amplified by a factor of n, and rotated by an angle of ψ_2 at point E. Here, $n = \overline{F_0F}/\overline{B_0B}$ and $\psi_2 = \angle GFE$. Hence, the angle $\angle EB_0A_0$, between the symmetrical axis $\overrightarrow{B_0E}$ (i.e., $Y-$axis) and the four-bar linkage baseline $\overrightarrow{B_0A_0}$, is equal to $\phi/2 + \psi_2$ (see Fig. 4.7).

[1] The construction of a six-bar mechanism with an embedded skew-pantograph is discussed in details in Section 3.3.2.

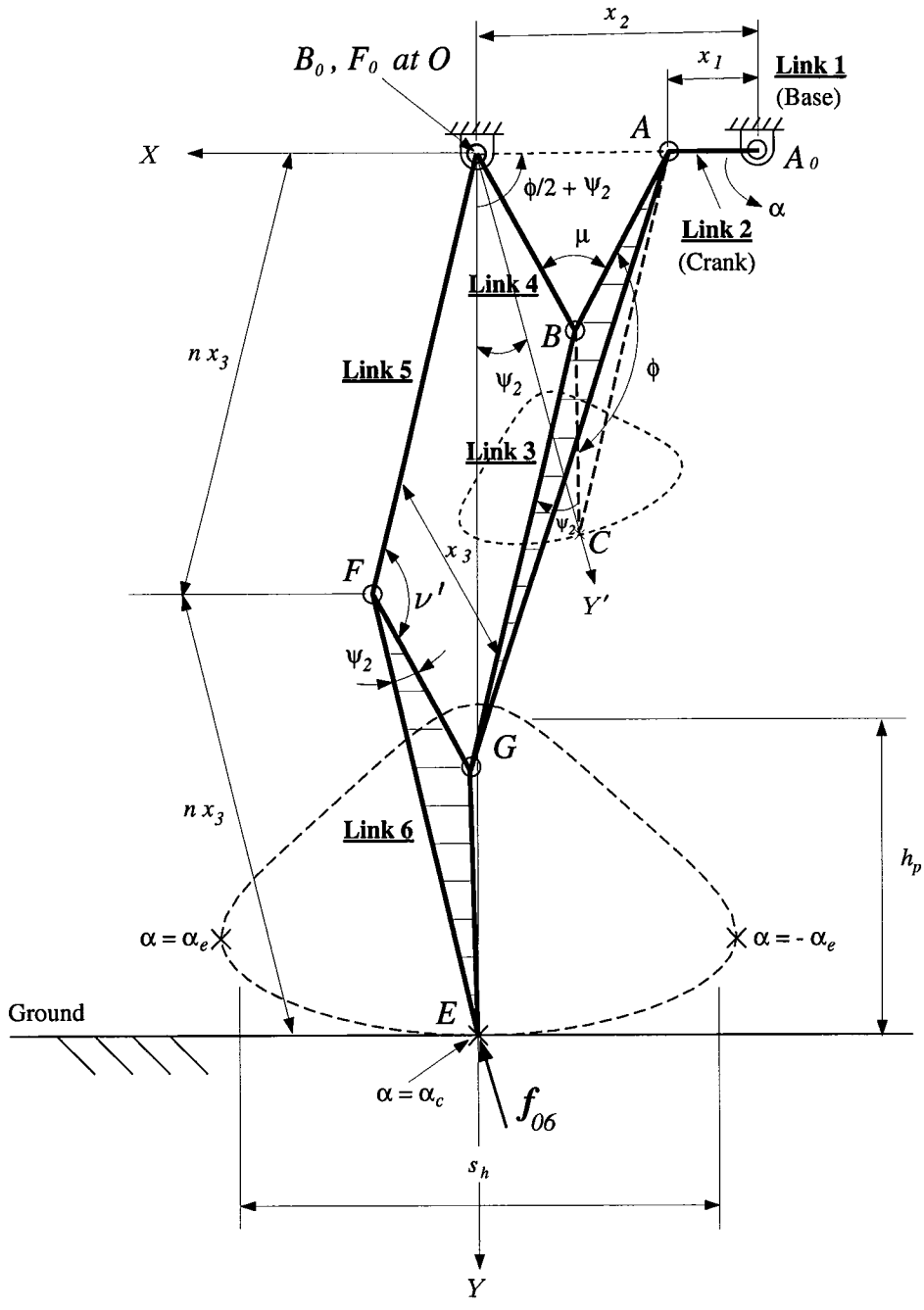

FIGURE 4.7: Type I of the six-bar mechanism

On the foot-path, the distance between the two extreme positions, which are symmetrical about the Y-axis, is referred to as the horizontal stride s_h, as shown in Fig. 4.7.

(b) Type II Mechanism

Type II mechanism is essentially the same mechanism as that shown in Fig. 4.7 except for the following differences. First, Type I mechanism does not have an adjustable pivot, but Type II has. Second, the foot-point path height of Type I mechanism is large for a walking machine to step over obstacles, while that of Type II mechanism is not. Since the mechanism shown in Fig. 4.7 has two concentric pivots, B_0 and F_0, either one or both of them can be used as an adjustable pivot. Thus, we divide Type II mechanism into three sub-cases. Fig. 4.8(a) shows a Type II-A mechanism where pivot F_0 of link 5 can be adjusted between two end positions O and O', while pivot B_0 is fixed at the origin O of the reference coordinate system. Fig. 4.8(b) shows a Type II-B mechanism where pivot B_0 can be adjusted between two end positions O and O', while pivot F_0 is fixed at the origin O of the reference coordinate system. Fig. 4.8(c) shows a Type II-C mechanism where both pivots B_0 and F_0 are adjusted together between two end positions O and O' and hence considered as one adjustable pivot.

For these three sub-cases, linear motion of the adjustable pivot between the two end positions O and O' provides the up-and-down motion, while rotation of the crank provides only the back-and-forth motion of point E. The maximum stroke of the up-and-down motion for Type II-A, -B, and -C is defined as the vertical lift s_v as shown in Figs. 4.8(a), (b), and (c), respectively. It is noted that, for Type II-A and -B mechanisms, as the adjustable pivot moves away from

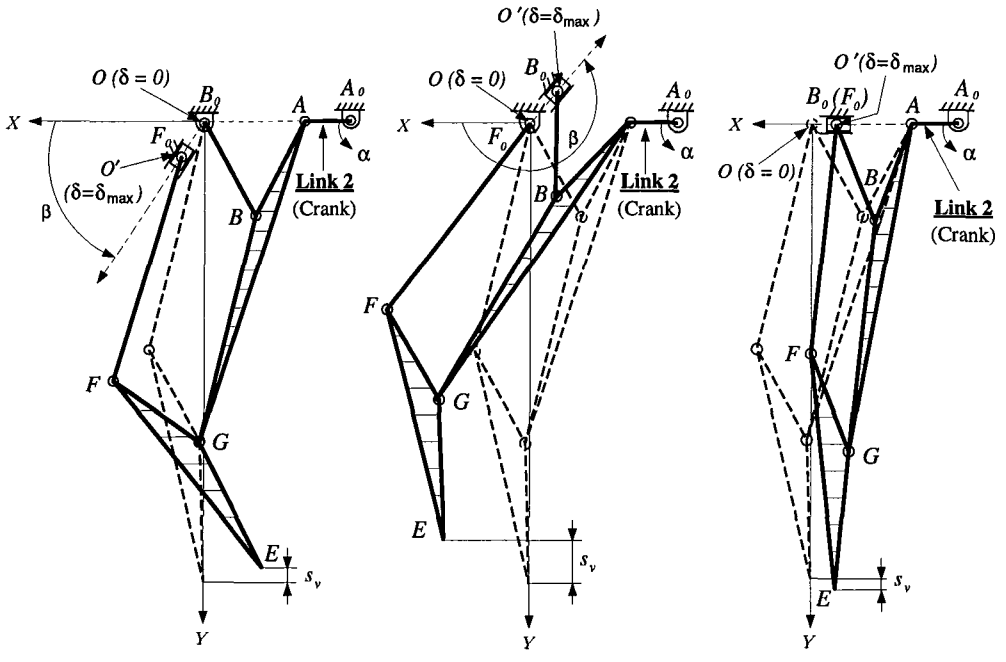

FIGURE 4.8: Six-bar leg mechanism: (a) Type II-A with point F_0 as the adjustable pivot; (b) Type II-B with point B_0 as the adjustable pivot; (c) Type II-C with both points B_0 and F_0 as the adjustable pivot

position O, the foot-path loses its symmetry, while for Type II-C mechanism, the foot-point path remains symmetrical regardlessly.

To avoid confusion, hereafter, positions O and O' will be referred to as the *normal position* and *extreme position* of the adjustable pivot, respectively. Accordingly, a mechanism configuration associated with these two positions are referred to as the *normal configuration* and the *extreme configuration*, respectively.

4.4.2 Optimization Model

Referring to the Type I mechanism in Fig. 4.7, α is the only free variable in the model, while referring to the Type II-A, -B, and -C mechanisms in Figs. 4.7(a), (b), and (c), respectively, α and δ are their two free variables.

(a) Design Variables

Referring to Fig. 4.7, six design variables are required for Type I mechanism: link lengths x_1 through x_3, angles ϕ and ψ_2, and the dimensionless amplification factor n. In addition to these six variables, two additional design variables, δ_{max} and β, are required for Type II-A and II-B mechanisms, while only one additional design variable, δ_{max}, is required for Type II-C mechanism (see Fig. 4.8).

(b) Objective Functions

Similar to the arguments given for both types of the four-bar mechanisms, there are five objective functions for each six-bar Type II mechanism and two objective functions for a Type I mechanism.

Objective 1: minimizing peak crank torque. Providing that transmission loss between the input crank and the output foot point is negligible, we have

$$\begin{aligned} \texttt{FO1} &:= T = -f_{06X}\tfrac{dX_E}{d\alpha} - f_{06Y}\tfrac{dY_E}{d\alpha},\ \forall\, \alpha \in R_p,\ \delta = 0 \qquad \text{(I, II-A, II-B, II-C)} \\ \texttt{FO2} &:= T = -f_{06X}\tfrac{dX_E}{d\alpha} - f_{06Y}\tfrac{dY_E}{d\alpha},\ \forall\, \alpha \in R_p,\ \delta = \delta_{max} \quad \text{(II-A, II-B, II-C)} \end{aligned} \tag{4.20}$$

Hence, the first design objective for Type I mechanism is $\min_{\mathbf{x}} \{\texttt{FO1}\}$, while first and second design objectives for Type II mechanism are $\min_{\mathbf{x}} \{\texttt{FO1}\}$ and $\min_{\mathbf{x}} \{\texttt{FO2}\}$, respectively.

Objective 2: Minimizing vertical actuating force.

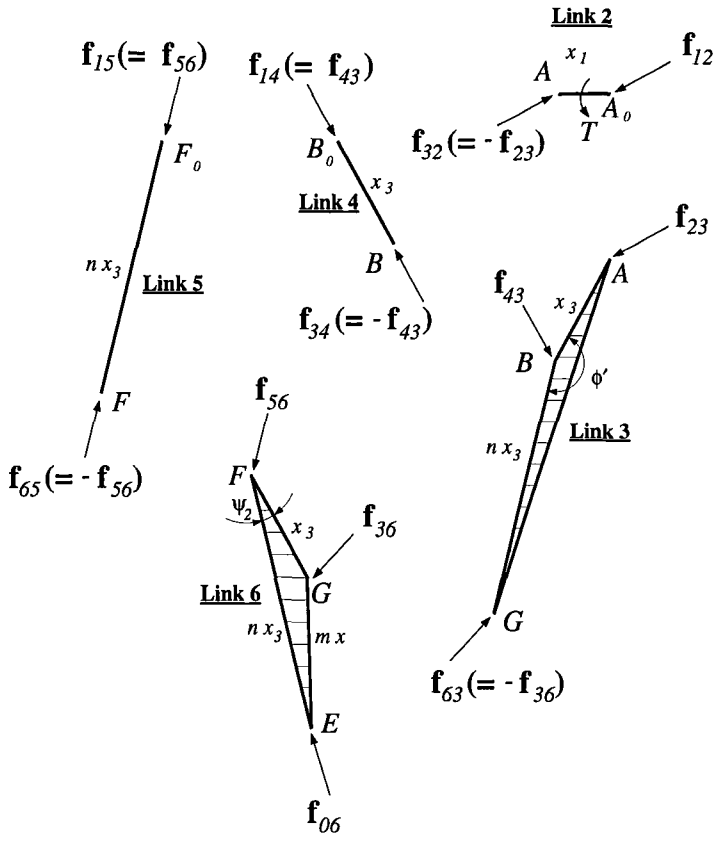

FIGURE 4.9: Free-body diagram analysis of links 2 through 6 for the six-bar mechanism (applicable to both Type I and II mechanisms)

The actuating forces at pivots B_0 and F_0 can be obtained via a free-body diagram analysis of links 2 through 6 as shown in Fig. 4.9. Since both links 4 and 5 are two-force links, we have $\mathbf{f}_{15} = \mathbf{f}_{56}$ and $\mathbf{f}_{14} = \mathbf{f}_{43}$. Balancing the forces and moments acting on links 2, 3, and 4 yields

$$\mathbf{f}_{15} = \mathbf{f}_{56} = f_{56}\,\mathbf{e}_{F_0F} \tag{4.21}$$

$$\mathbf{f}_{36} = -\mathbf{f}_{36} - \mathbf{f}_{06} \tag{4.22}$$

$$\mathbf{f}_{14} = \mathbf{f}_{43} = f_{43}\,\mathbf{e}_{B_0B} \tag{4.23}$$

$$\mathbf{f}_{23} = -\mathbf{f}_{43} + \mathbf{f}_{36} \tag{4.24}$$

$$T = \overline{A_0A}(\mathbf{e}_{A_0A} \times \mathbf{f}_{23}) \tag{4.25}$$

where

$$f_{56} = -\frac{\overline{GE}}{\overline{GF}} \frac{(\mathbf{e}_{GE} \times \mathbf{f}_{06}) \cdot \mathbf{k}}{(\mathbf{e}_{GF} \times \mathbf{e}_{F_0F}) \cdot \mathbf{k}} \tag{4.26}$$

$$f_{43} = \frac{\overline{AG}}{\overline{AB}} \frac{(\mathbf{e}_{AG} \times \mathbf{f}_{36}) \cdot \mathbf{k}}{(\mathbf{e}_{AB} \times \mathbf{e}_{B_0B}) \cdot \mathbf{k}} \tag{4.27}$$

where $\mathbf{e}$ represents an unit vector, $\mathbf{k}$ is an unit vector perpendicular to the plane of the linkage, and '$\times$' means the cross product of two vectors. Note that, since Eq. (4.25) is an alternative way of calculating the value of the crank torque, it can be used to check the values of the functional objectives FO1 and FO2. Since the adjustable pivot of Type II mechanism is adjusted between points O and O', the actuating forces for Type II-A, II-B, and II-C mechanisms can be easily obtained by projecting forces $\mathbf{f}_{56}$, $\mathbf{f}_{43}$, and $(\mathbf{f}_{56} + \mathbf{f}_{43})$ on the direction of $\overrightarrow{OO'}$, respectively. Hence, for Type II-A mechanism, two functional objectives are

$$\begin{aligned} \texttt{FO3} &:= \mathbf{f}_{56} \cdot \mathbf{e}_{OO'}, \quad \forall\, \alpha \in R_p, \delta = 0 \qquad \text{(II-A)} \\ \texttt{FO4} &:= \mathbf{f}_{56} \cdot \mathbf{e}_{OO'}, \quad \forall\, \alpha \in R_p, \delta = \delta_{max} \quad \text{(II-A)} \end{aligned} \tag{4.28}$$

If $\mathbf{f}_{56}$ of Eqs. (4.28) and (4.28) is replaced by $\mathbf{f}_{43}$ and $(\mathbf{f}_{56} + \mathbf{f}_{43})$, the functional objectives of Type II-B and II-C mechanisms can be obtained, respectively. Note that since Type I mechanism does not have an adjustable pivot, its actuating force is not available. Hence, for Type II-A, II-B, and II-C mechanisms, the third and fourth design objectives are: $\underset{\mathbf{x}}{min}\ \{\texttt{FO3}\}$ and $\underset{\mathbf{x}}{min}\ \{\texttt{FO4}\}$, respectively.

Objective 3: minimizing leg size. Since the configuration of the leg mechanism changes as a function of the crank angle and the adjustable pivot location, the problem of computing the leg size will become unnecessarily complex if it is to be calculated at all configurations. For simplicity, the leg size is only calculated at the normal configuration ($\delta = 0$) shown in Fig. 4.7, where point E is

at the center of the propelling portion. At this particular configuration, $\alpha = \alpha_c$ and $\delta = 0$. Thus, the leg height L_h is written as

$$L_h = Y_E|_{\alpha=\alpha_c,\delta=0} \tag{4.29}$$

and the width of leg mechanism, L_w, is defined as the difference between the X coordinates of joint F and A or A_0, i.e.

$$L_w = X_F|_{\alpha=\alpha_c,\delta=0} - \min(X_{A_0}, X_A|_{\alpha=\alpha_c,\delta=0}) \tag{4.30}$$

Normalizing the rectangular leg size with respect to a pre-specified walking area $(s_v s_h)$ yields

$$\texttt{O1} := \frac{L_h L_w}{s_v s_h} \qquad \text{(I, II-A, II-B, II-C)} \tag{4.31}$$

Therefore, the last design objective for all types of mechanisms is: $\min_{\mathbf{x}} \{\texttt{O1}\}$.

(c) Constraint Functions

Stride length. The horizontal stride is defined as the distance between the two extreme positions where $dX_E/d\alpha = 0$. Due to symmetry, $X_E|_{\alpha=\alpha_e} - X_E|_{\alpha=-\alpha_e} = 2X_E|_{\alpha=\alpha_e}$. Hence, the constraint on the stride length is

$$\texttt{C1} := \frac{2X_E|_{\alpha=\alpha_e}}{s_h} \geq \texttt{H}_{\texttt{C1}}, \text{ for } \delta = 0 \quad \text{(I, II-A, II-B, II-C)} \tag{4.32}$$

where the threshold $\texttt{H}_{\texttt{C1}}$ is set to be one.

Vertical Lift. The vertical lift s_v is defined as the maximum change of the foot point E in the $Y-$direction due to the displacement of the adjustable pivot as shown in Figs. 4.8(a), (b), and (c). In those figures, the crank links are held at the angle of $\alpha = \alpha_c$. Therefore, the vertical lift of the foot point is

$$\texttt{C2} := \frac{\|Y_E|_{\alpha=\alpha_c,\ \delta=0} - Y_E|_{\alpha=\alpha_c,\ \delta=\delta_{max}}\|}{s_h} \geq \texttt{H}_{\texttt{C2}} \quad \text{(II-A, II-B, II-C)} \tag{4.33}$$

It is noted that this constraint is not available for Type I mechanism. Here, the value of $\mathtt{H_{C2}}$ is set to be 0.667.

Foot-path height. The foot-path height h_p is defined as the distance between the two intersection points of the $Y-$axis and the foot-point path as shown in Fig. 4.7. The crank angle corresponding to the lower and upper point of intersection are α_c and $\pi - \alpha_c$ [2]. Hence, the constraint of the foot-path height can be written as

$$\mathtt{C3} := \frac{Y_E|_{\alpha=\alpha_c} - Y_E|_{\alpha=\pi-\alpha_c}}{s_h} \geq \mathtt{H_{C3}}, \text{ for } \delta = 0 \text{ (I, II-A, II-B, II-C)} \quad (4.34)$$

As mentioned previously, the value of $\mathtt{H_{C3}}$ for Type I mechanism set to be 0.8 and those for Type II-A, II-B, and II-C mechanisms are set to be 0.1.

Four-bar transmission angle. Referring to Fig. 4.7, since $\overline{AB} = \overline{B_0B} = x_3$, the minimum and maximum transmission angles, $\mu_{\min}$ and $\mu_{\max}$, of the basic four-bar linkage can be written as

$$\mathtt{C4} := \mu_{\min} = 2\sin^{-1}(\frac{x_2 - x_1}{2x_3}) \geq \mathtt{H_{C4}}, \text{ for } \delta = 0 \text{ (I, II-A, II-B, II-C)} \quad (4.35)$$

$$\mathtt{C5} := \mu_{\max} = 2\sin^{-1}(\frac{x_2 + x_1}{2x_3}) \leq \mathtt{H_{C5}}, \text{ for } \delta = 0 \text{ (I, II-A, II-B, II-C)} \quad (4.36)$$

Since the motion of the adjustable pivots of Type II-B and II-C mechanisms changes the characteristics of the basic four-bar linkage, additional transmission angle constraints are imposed:

$$\mathtt{C6} := \mu_{\min} = 2\sin^{-1}(\frac{x'_2 - x_1}{2x_3}) \geq \mathtt{H_{C6}}, \quad \text{for } \delta = \delta_{max} \text{ (II-B, II-C)} \quad (4.37)$$

$$\mathtt{C7} := \mu_{\max} = 2\sin^{-1}(\frac{x'_2 + x_1}{2x_3}) \leq \mathtt{H_{C7}}, \quad \text{for } \delta = \delta_{max} \text{ (II-B, II-C)} \quad (4.38)$$

where $x'_2 = \overline{A_0O'}$. Here, the values of $\mathtt{H_{C4}}$ and $\mathtt{H_{C6}}$ are chosen to be 45 degrees, while those of $\mathtt{H_{C5}}$ and $\mathtt{H_{C7}}$ are selected to be 135 degrees.

[2] See Section 3.1.3 (b), α_c can be either 0 or π.

Skew-Pantograph transmission angle. A skew-pantograph becomes singular when links F_0F and FG are aligned, i.e., ΔF_0FG collapses to a straight line. The singularity of a pantograph is avoided as long as ΔF_0FG remains a bona fide triangle throughout a full crank cycle. To achieve this, the transmission angle $\angle F_0FG$ should not deviate too much from $\pi/2$. Hence, when $\delta = 0$, the minimum and maximum transmission angles of the skew-pantograph, C8 and C9, are

$$\texttt{C8} := \nu'_{\min} \geq \texttt{H}_{\texttt{C8}}, \text{ for } \delta = 0 \text{ (I, II-A, II-B, II-C)} \tag{4.39}$$

$$\texttt{C9} := \nu'_{\max} \leq \texttt{H}_{\texttt{C9}}, \text{ for } \delta = 0 \text{ (I, II-A, II-B, II-C)} \tag{4.40}$$

and, when $\delta = \delta_{\max}$,

$$\texttt{C10} := \nu'_{\min} \geq \texttt{H}_{\texttt{C10}}, \text{ for } \delta = \delta_{\max} \text{ (II-C)} \tag{4.41}$$

$$\texttt{C11} := \nu'_{\max} \leq \texttt{H}_{\texttt{C11}}, \text{ for } \delta = \delta_{\max} \text{ (II-C)} \tag{4.42}$$

Note that C10 and C11 are considered only for Type II-C because points F_0, F, G, B, and B_0 of Type II-A and II-B mechanisms do not form a parallelogram when $\delta \neq 0$ (see Fig. 4.8). The definition of ν' can be found in Eq. (3.58) of Section 3.4.2. Again, the values of $\texttt{H}_{\texttt{C8}}$ and $\texttt{H}_{\texttt{C10}}$ are chosen to be 45 degrees, while those of $\texttt{H}_{\texttt{C9}}$ and $\texttt{H}_{\texttt{C11}}$ are chosen to be 135 degrees.

Orientation angle of the lowest link. In order to prevent link 6 (lowest limb) from bumping into the ground, the orientation of link 6 must be constrained. Since it is desired to have the orientation of link 6 to be as close to $\pi/2$ as possible, we let

$$\begin{aligned} \texttt{FC1} &:= \|\theta_{FE} - \pi/2\| \leq \texttt{H}_{\texttt{FC1}}, \ \forall\alpha, \ \delta = 0 \quad \text{(I, II-A, II-B, II-C)} \\ \texttt{FC2} &:= \|\theta_{FE} - \pi/2\| \leq \texttt{H}_{\texttt{FC2}}, \ \forall\alpha, \ \delta = \delta_{\max} \quad \text{(II-A, II-B, II-C)} \end{aligned} \tag{4.43}$$

where both $\mathtt{H_{FC1}}$ and $\mathtt{H_{FC2}}$ values are set to be 70 degrees, i.e., the minimum angle between the lowest limb and the ground is 20 degrees.

Constraints on the Extreme Position O' Referring to Type II-A mechanism in Fig. 4.8(a), in order to avoid the singular condition, the extreme position O' should be constrained in a way that ΔGFF_0 remains a triangle at all times. Thus, we have

$$\mathtt{FC3} := \cos^{-1}[\frac{(\overline{GF})^2 + (\overline{FF_0})^2 - (\overline{GF_0})^2}{2(\overline{GF})(\overline{FF_0})}] \leq \mathtt{H_{FC3}}, \quad \forall\alpha,\ \delta = \delta_{max} \text{ (II-A) } (4.44)$$

Based on the same reason, ΔGBB_0 of Type II-B mechanism shown in Fig. 4.8(b) must remain a triangle at all times. Thus,

$$\mathtt{FC3} := \cos^{-1}[\frac{(\overline{GB})^2 + (\overline{BB_0})^2 - (\overline{GB_0})^2}{2(\overline{GB})(\overline{BB_0})}] \leq \mathtt{H_{FC3}}, \quad \forall\alpha,\ \delta = \delta_{max} \text{ (II-B) } (4.45)$$

Here, the value of $\mathtt{H_{FC3}}$ is set as 160 degrees.

4.4.3 Results and Discussion

Similar to the synthesis of four-bar mechanisms, the optimization of six-bar mechanisms was carried out based on the design specifications outlined in section 4.2.2 and the assumption of a flat walking terrain.

For Type I and II mechanisms, leg dimensions of the initial and optimized mechanism are shown in Table 4.3, while the values of the optimized objective functions are listed in Table 4.4. Fig. 4.10(a) shows the initial and optimized Type I mechanisms. The optimized mechanism features a $\Delta-$shaped foot-point path with a large path height. The mechanism size is substantially smaller after the optimization. Figs. 4.10(b), (c), and (d) show optimized Type II-A, -B, and -C mechanisms, respectively. For each optimized mechanism, two configurations

Design Variables	Initial Values	Optimized Values			
		Type I Mechanism	Type II Mechanism		
			II-A	II-B	II-C
x_1 (m)	0.050	0.062	0.017	0.044	0.045
x_2 (m)	0.200	0.216	0.146	0.237	0.224
x_3 (m)	0.250	0.145	0.168	0.252	0.233
ϕ (rad)	3	2.410	2.650	2.527	2.498
ψ_2 (rad)	0.094	0.476	0.491	0.630	1.249
n	3	2.766	3.845	1.616	3.163
β (rad)	0	N/A	0.790	-0.768	-0.486
δ_{max} (m)	0.000	N/A	0.182	0.131	0.156

TABLE 4.3: Initial and optimized values of the design variables

are shown: one is at $\delta = 0$ and the other is at $\delta = \delta_{\max}$. At $\delta = \delta_{\max}$, the major axis of the foot-point path of Type II-A mechanism remains close to the horizontal direction, while those of Types II-B and II-C tilt away from the horizontal direction. However, among the three, Type II-A mechanism has the largest size and its crank is too small to be considered as a practical design.

Figs. 4.11(a), (b), (c), and (d) show the crank torque curves for Type I and three Type II mechanisms, respectively. Fig. 4.11 shows that Type I mechanism has the largest crank torque, followed by Type II-B, II-C, and then II-A. For the three Type II mechanisms, the peak crank torques at $\delta = \delta_{\max}$ are larger than those at $\delta = 0$.

Figs. 4.12(a), (b), and (c) show the actuating force for Type II-A, II-B, and II-C mechanism, respectively. In general, the actuating forces at $\delta = \delta_{\max}$ is

Objective Functions		Type I Mechanism	Type II Mechanism		
			II-A	II-B	II-C
Peak crank torque (N-m)	$T\|_{\delta=0}$	72.3	17.0	20.3	21.0
Peak crank torque (N-m)	$T\|_{\delta=\delta_{max}}$	N/A	39.4	67.3	53.4
Maximum actuating force (kN)	$f_a\|_{\delta=0}$	N/A	0.42	0.98	1.05
Maximum actuating force (kN)	$f_a\|_{\delta=\delta_{max}}$	N/A	2.01	2.35	1.79
Normalized leg size		2.34	3.33	2.35	1.79

TABLE 4.4: Values of the optimized objective functions

larger than that at $\delta = 0$. Again, Type II-A mechanism has the smallest, while Type II-B mechanism has the largest actuating force.

In summary, we conclude that, among the type II mechanisms, II-A mechanism has several advantages over the other two cases in terms of the foot-point path, crank torque, and actuating force. However, the shortcoming of Type II-A mechanism is that it has the largest mechanism size and smallest crank size.

4.5 Synthesis of an Eight-Bar Leg Mechanism

4.5.1 Mechanism Description

(a) Type I Mechanism

A planar one-DOF compound mechanism composed of a four-bar linkage A_0ABB_0 and a pantograph $CFGHF_0$ is shown in Fig. 4.13. This mechanism is referred to as Type I mechanism. For this mechanism, one end of the pantograph is driven by the four-bar coupler point C, while the other end F_0 is fixed at the

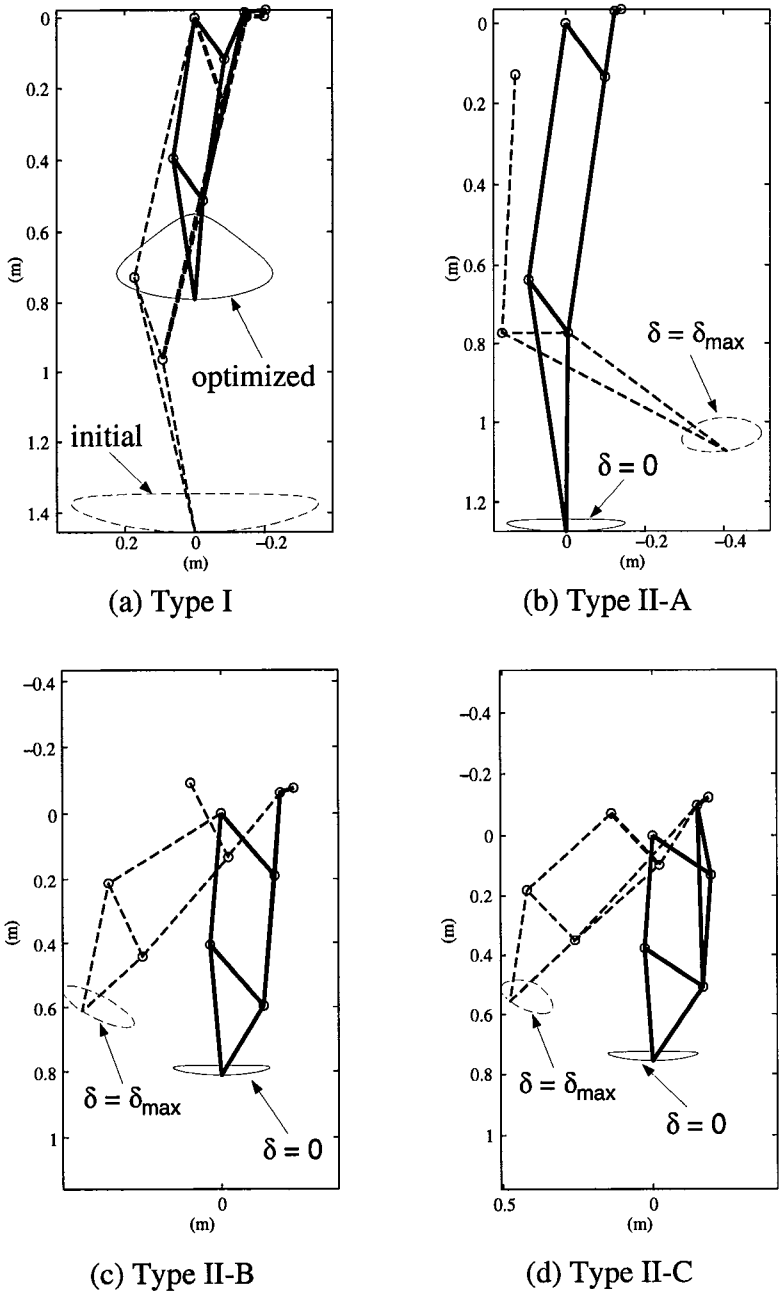

(a) Type I (b) Type II-A

(c) Type II-B (d) Type II-C

FIGURE 4.10: Optimized six-bar mechanisms and their foot path (a) Type I, (b) Type II-A, (c) Type II-B, and (d) Type II-C

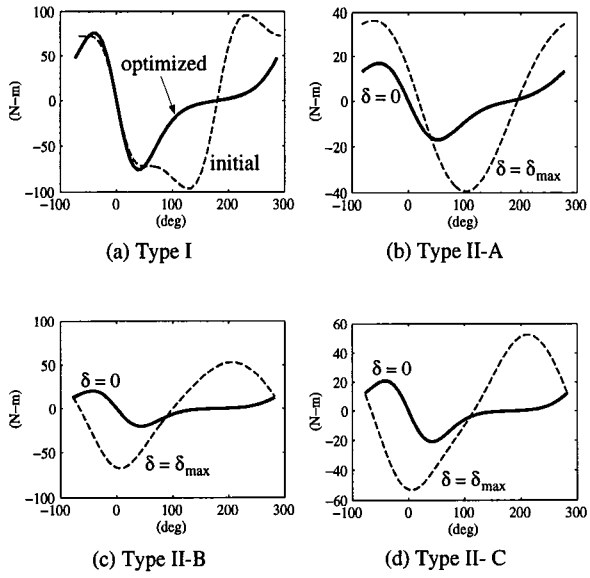

(a) Type I (b) Type II-A

(c) Type II-B (d) Type II- C

FIGURE 4.11: Crank torque of the optimized six-bar mechanisms, (a) Type I, (b) Type II-A, (c) Type II-B, and (d) Type II-C

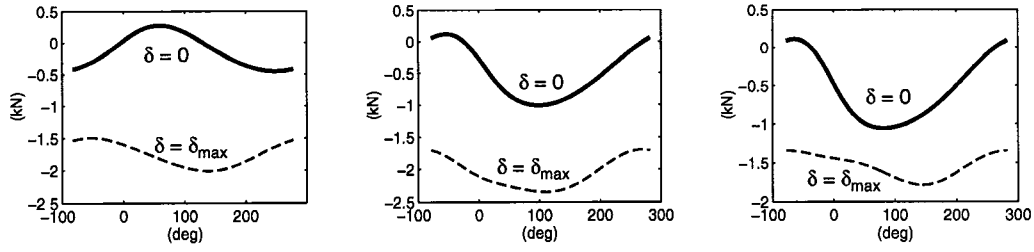

(a) Type II-A (b) Type II-B (c) Type II-C

FIGURE 4.12: Actuating force of the optimized Type II six-bar mechanisms, (a) Type II-A, (b) Type II-B, and (c) Type II-C

base. Since this mechanism is able to generate a foot-point path large enough for the leg mechanism to step over obstacle, rotation of the crank provides a back-and-forth motion as well as an up-and-down motion of the foot point E. For convenience, an X-Y reference coordinate system with its Y-axis pointing downward in the direction of $\overrightarrow{B_0F_0}$ and with its origin located at joint B_0 is defined in Fig. 4.13.

In our design, the four-bar linkage is selected such that $\overline{AB} = \overline{BC} = \overline{B_0B}$ and the angle between the symmetric axis $\overrightarrow{B_0F_0}$ and the four-bar linkage baseline $\overrightarrow{B_0A_0}$ is equal to $\phi/2$, where $\phi = \angle ABC$. It is well known (Hartenberg and Denavit, 1964) that, for this type of four-bar linkage, the coupler curve traced by point C is symmetrical about the axis $\overrightarrow{B_0F_0}$. The pantograph, which is connected to the four-bar linkage at point C, reproduces and amplifies the coupler curve by a factor of $(-x_5/x_4)$ at the foot-point E. The negative sign refers to the inverted shape of the curve generated by point E as compared to that generated by point C. For simplicity, the amplification factor (x_5/x_4) is denoted as n hereafter.

In this design, the height of the path p_h as shown in Fig. 4.13 has to be larger than the vertical lift s_v required by the design specifications. The distance between the two extreme positions of the foot-point path at E, where $dX_E/d\alpha = 0$, is referred to as the horizontal stride. Note that the horizontal stride must be no smaller than the desired stride s_h, as shown in Fig. 4.13.

(b) Type II Mechanism

Fig. 4.14 shows a Type II compound mechanism. This mechanism is identical to that shown in Fig. 4.13, except for the fact that joint F_0 of Type II mechanism is an adjustable pivot. Thus, Type II mechanism is a two-DOF mechanism. For

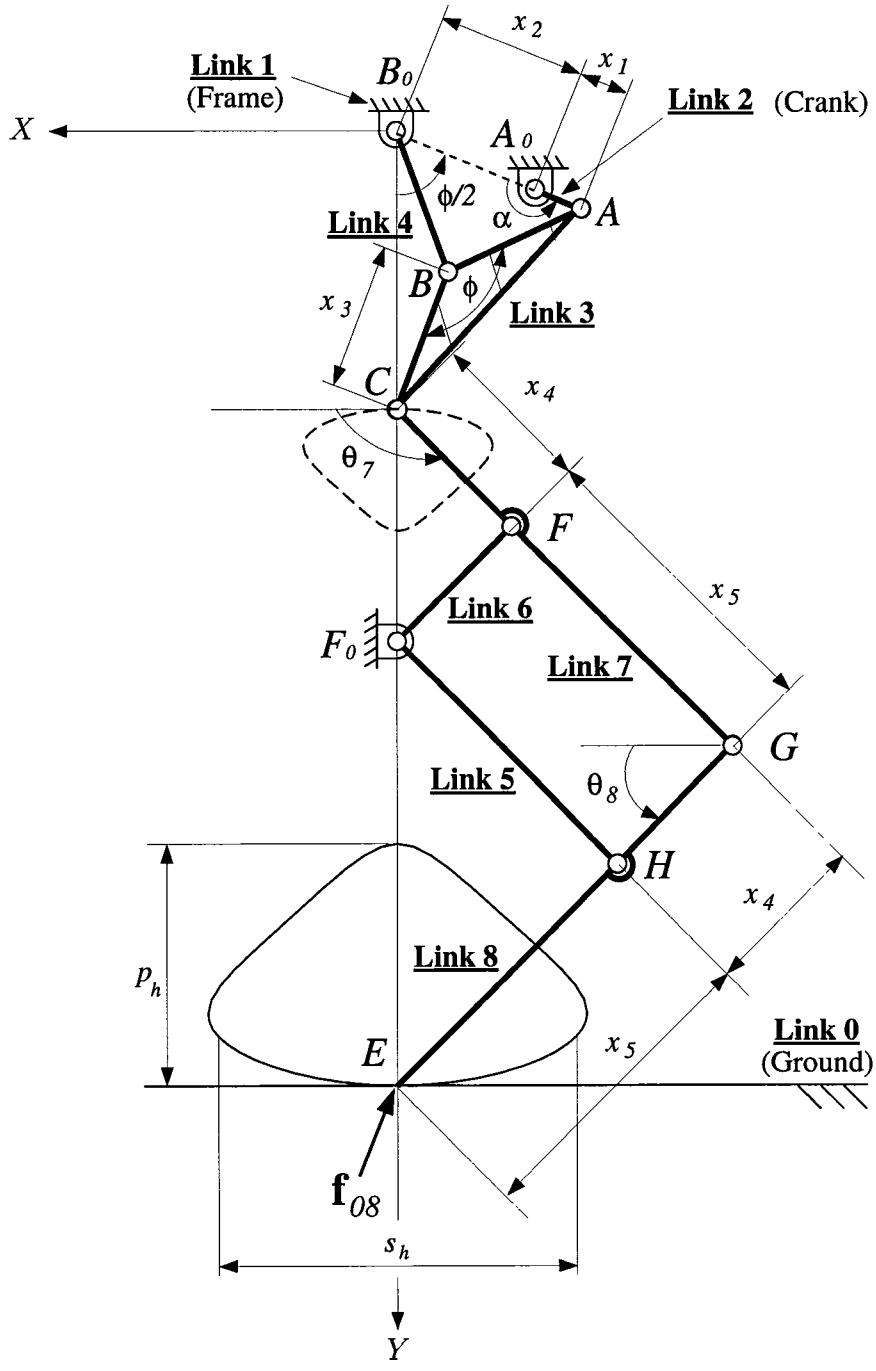

FIGURE 4.13: Type I compound leg mechanism

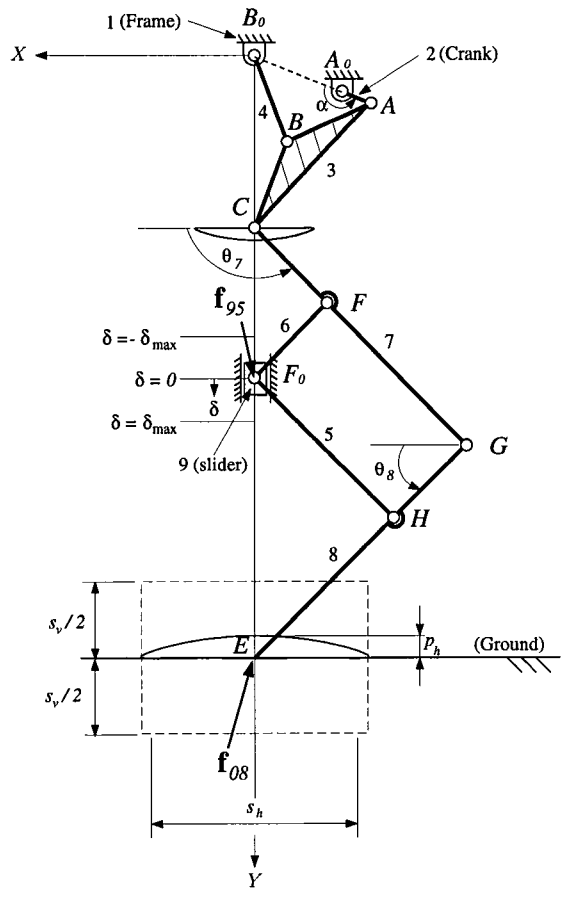

FIGURE 4.14: Type II compound leg mechanism

this mechanism, rotation of the crank provides only the back-and-forth motion, while linear motion of point F_0 provides the up-and-down motion of the foot point E. As shown in Fig. 4.14, when joint F_0 is held at its middle position (i.e., $\delta = 0$), the foot-point path traced by E will be at the mid-level of the walking area. By adjusting joint F_0 to the positions where $\delta = -\delta_{\max}$ and $\delta = \delta_{\max}$, the foot path will be at the upper and lower levels of the walking area. The difference between these two levels is referred to the vertical stride s_v as shown in Fig. 4.14. Similar to Type I mechanism, the horizontal stride must be no smaller than the desired stride s_h, as shown in Fig. 4.14.

4.5.2 Optimization Model (Type II Mechanism)

Since the optimization model for Type I mechanism can be easily obtained from that of Type II mechanism, we only present the latter one in this section.

(a) Design Variable

Referring to Figs. 4.13 and 4.14, six independent design variables, link lengths x_1 through x_5 and the coupler angle ϕ, are included in this model. Crank angle α and joint F_0 displacement δ are the two free variables. Note that, since the quantity $\delta_{\max}$ is related to the vertical stride s_v by

$$\delta_{\max} = s_v/2(1+n), \tag{4.46}$$

quantity $\delta_{\max}$ is not considered as a design variable.

(b) Objective Functions

Three design objectives are simultaneously considered in the optimization model: minimize (i) the peak crank torque, (ii) the vertical actuating force at joint F_0, and (iii) the leg size.

Objective 1: Minimizing peak crank torque. Assuming that the transmission loss between the input crank and the output foot point is negligible, we have a functional objective

$$\texttt{F01} := T = -f_{08X}\frac{dX_E}{d\alpha} - f_{08Y}\frac{dY_E}{d\alpha}, \qquad \forall\, \alpha \in R_p \tag{4.47}$$

where $dX_E/d\alpha$ and $dY_E/d\alpha$ can be found in Chapter 3. Note that the location of the slider does not effect the crank torque. Here, we minimize the crank torque by assuming that the slider is held at its mid-range position. We believe that

this is a reasonable approach, since the slider will be held at this position most of the time during normal walking. Thus our first design objective is: $\min_{\mathbf{x}} \{\mathtt{F01}\}$.

Objective 2: Minimizing vertical actuating force. Since the vertical actuating force f_{91Y} at joint F_0 is related to the ground reaction force f_{08Y} by a factor of $-(1+n)$,

$$\mathtt{01} := f_{91Y} = -(1+n) f_{08Y} \tag{4.48}$$

Hence our second design objective is : $\min_{\mathbf{x}} \{\mathtt{01}\}$. We note that the vertical actuating force, f_{91Y}, is not a function of the slider position nor that of the crank angle α.

Objective 3: minimizing leg size. As previously stated, for simplicity, the leg size is only calculated at the central configuration shown in Fig. 4.14, where point E is at the middle of the propelling portion and joint F_0 at the middle of its vertical operating range, i.e., $\delta = 0$. At this particular configuration, the crank angle α is taken to be π. [3] Since the pantograph as shown in Fig. 4.14 has its two links $\overline{CG} = \overline{GE}$ and the transmission angle of the pantograph at the normal configuration is selected to be $\pi/2$, the leg height L_h can be derived as,

$$L_h = (\overline{B_0 E})_{\alpha=\pi} = Y_C|_{\alpha=\pi} + \sqrt{2}(x_4 + x_5) \tag{4.49}$$

(See Chapter 3 for the formulation of Y_C) The width L_w of leg mechanism is defined as the maximum X coordinate of joint A or G, i.e.

$$\begin{aligned} L_w &= \max(X_A|_{\alpha=\pi}, X_G|_{\alpha=\pi}) \\ &= \max[(x_1 + x_2)\sin(\phi/2), \sqrt{2}(x_4 + x_5)/2] \end{aligned} \tag{4.50}$$

[3] α could be taken to be zero as well.

Normalizing the leg size with respect to a pre-specified walking area ($s_v s_h$) yields

$$\texttt{O2} := \frac{[Y_C|_{\alpha=\pi} + \sqrt{2}(x_4 + x_5)]\max(X_A|_{\alpha=\pi}, X_G|_{\alpha=\pi})}{s_v s_h} \tag{4.51}$$

Therefore, the third design objective is: $\min_{\mathbf{x}} \{\texttt{O2}\}$.

(c) Constraint Functions

There are six simple constraints and three functional constraints in the model. Note that the vertical stride is not considered as a constraint function, because it is indirectly handled by the constraints imposed on the pantograph transmission angle.

Stride length. The horizontal stride is defined as the distance between the two extreme horizontal positions of the foot-point E where $dX_E/d\alpha = 0$ (see Fig. 4.14). The corresponding crank angles at these two positions are denoted as $\alpha = \alpha_e$ and $\alpha = -\alpha_e$, respectively. The angle α_e is obtained numerically by setting $dX_E/d\alpha = 0$. Due to symmetry, the constraint on the stride length is

$$\texttt{C1} := \frac{2X_E|_{\alpha=\alpha_e}}{s_h} \geq \texttt{H}_{\texttt{C1}}. \tag{4.52}$$

Normally the threshold $\texttt{H}_{\texttt{C1}}$ is 1 since the foot-path stride should be no less than a pre-specified stride length s_h.

Foot-path height. The height of the foot path is the difference between the Y coordinate of the foot-point E at $\alpha = 0$ and $\alpha = \pi$,

$$\texttt{C2} := \frac{Y_E|_{\alpha=\pi} - Y_E|_{\alpha=0}}{s_h} \geq \texttt{H}_{\texttt{C2}} \tag{4.53}$$

where the value of $\texttt{H}_{\texttt{C2}}$ is positive.

Four-bar transmission angle. Since $\overline{AB} = \overline{B_0B} = x_3$, the minimum and maximum transmission angles, C3 and C4, of the four-bar linkage, can be written

as

$$\texttt{C3} := 2\sin^{-1}(\frac{x_2 - x_1}{2x_3}) \geq \texttt{H}_{\texttt{C3}} \tag{4.54}$$

$$\texttt{C4} := 2\sin^{-1}(\frac{x_2 + x_1}{2x_3}) \leq \texttt{H}_{\texttt{C4}} \tag{4.55}$$

To achieve efficient force transmission in the four-bar linkage, the transmission angle should not deviate too much from $\pi/2$. Here, $\texttt{H}_{\texttt{C3}}$ and $\texttt{H}_{\texttt{C4}}$ are chosen such that $(\pi/2 - \texttt{H}_{\texttt{C3}}) = (\texttt{H}_{\texttt{C4}} - \pi/2)$. Note that under this constraint the Grashof criteria for the four-bar linkage are automatically satisfied.

Pantograph transmission angle. The pantograph becomes singular when all its links are aligned, i.e., ΔCGE collapses to a straight line. The singularity of a pantograph is avoided as long as ΔCGE remains a bona fide triangle throughout a full crank cycle. Again, to achieve this, the transmission angle $\angle CGE$ should not deviate too much from $\pi/2$. Hence, the minimum and maximum transmission angles of the pantograph, C5 and C6, are

$$\texttt{C5} := \cos^{-1}[\frac{2(x_4 + x_5)^2 - l_{\min}^2}{2(x_4 + x_5)^2}] \geq \texttt{H}_{\texttt{C5}} \tag{4.56}$$

$$\texttt{C6} := \cos^{-1}[\frac{2(x_4 + x_5)^2 - l_{\max}^2}{2(x_4 + x_5)^2}] \leq \texttt{H}_{\texttt{C6}} \tag{4.57}$$

where $l_{\min} = (\overline{CE})_{\alpha=0,\delta=-\delta_{\max}}$ and $l_{\max} = (\overline{CE})_{\alpha=\alpha_e,\delta=\delta_{\max}}$ (referring to Fig. 4.14) are the minimum and maximum distances of $\overline{CE}$, respectively. The thresholds $\texttt{H}_{\texttt{C5}}$ and $\texttt{H}_{\texttt{C6}}$ are chosen such that $(\pi/2 - \texttt{H}_{\texttt{C5}}) = (\texttt{H}_{\texttt{C6}} - \pi/2)$.

Links 7 and 8 orientation angles. In order to prevent link 7 from interfering with the four-bar linkage or link 8 from bumping into the ground, the orientations of these two links must be constrained. Since the link lengths $\overline{CG} = \overline{GE}$, the minimum and maximum angles of θ_8 are equal to those of $\pi - \theta_7$. Therefore

constraints imposed on θ_8 would be enough,

$$\texttt{FC1}: \quad = \quad \|\theta_8 - \pi/2\| \leq \texttt{H}_{\texttt{FC1}}, \qquad \forall\, \alpha \in R_p,\ \delta = -\delta_{\max} \tag{4.58}$$

$$\texttt{FC2}: \quad = \quad \|\theta_8 - \pi/2\| \leq \texttt{H}_{\texttt{FC2}}, \qquad \forall\, \alpha \in R_p,\ \delta = \delta_{\max} \tag{4.59}$$

Note that, the functional constraints FC1 and FC2 are calculated at the upper most and lower most level of the walking area, respectively.

Second derivatives of Y_E. Since the propelling portion of the foot path should be always below the non-propelling portion within the entire stride length, it is desirable to have a concave foot path for the propelling portion, i.e.

$$\texttt{FC3} \quad := \quad \frac{d^2 Y_E}{d\alpha^2} \geq \texttt{H}_{\texttt{FC3}}, \quad \alpha \in [\alpha_e, \pi] \tag{4.60}$$

where $\texttt{H}_{\texttt{FC3}}$ is set to zero. Note that, due to symmetry, Eq. (4.60) only calculates $d^2Y_E/d\alpha^2$ over one-half of the propelling portion.

4.5.3 Results and Discussion

Fig. 4.15(a) shows the initial and optimized Type I mechanisms. The optimized mechanism features an inverted $\Delta-$shaped foot-point path. Such a path does not provide a leg mechanism the capability to step over an obstacle. In addition, it makes a machine hopping up and down when walking. Thus, this type of mechanism is not desirable. Although there is no mathematical proof, it is observed that the propelling portion of the foot-path produced by this type of mechanism tends not to approximate a straight line if a large ratio between the path height and the stride length (i.e., h_p/s_h) is required. In this model, $h_p/s_h = 0.8$ is used. It is also observed that, although numerical results are not shown here, when the ratio h_p/s_h decreases to certain value, the propelling

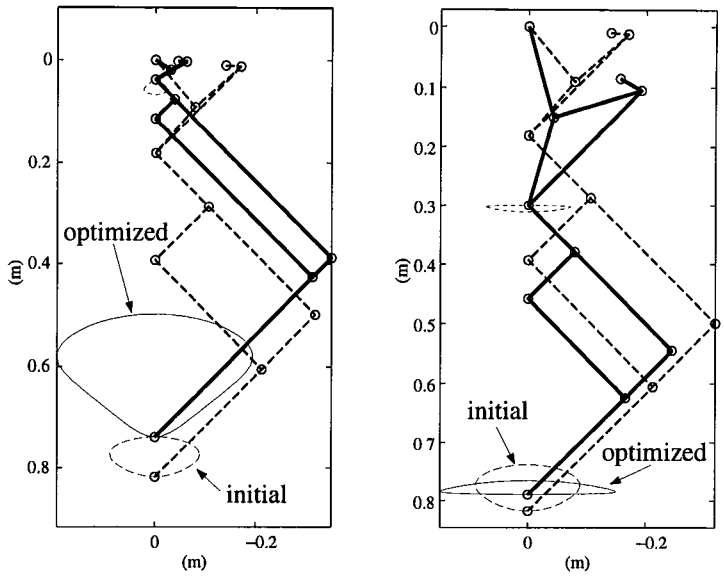

(a) Type I (b) Type II

FIGURE 4.15: Initial and optimized eight-bar mechanisms, (a) Type I, and (b) Type II

portion of Type I mechanism can be flat. This indicates that in order to achieve a large path height with a flat propelling path, the stride length of the foot path have to be much larger than is needed. This, consequently, will make the size of the leg bulky. Therefore, eight-bar Type I mechanism is not unacceptable as a leg design if a large path height is needed.

On the contrary, Fig. 4.15(b) shows an optimized Type II mechanism which does not feature such an undesired path. Instead, Type II mechanism generates a foot-point path featuring a flat propelling portion. From that figure, the path height is obviously small. In addition, from the structure view point, Type II mechanism shows a proper ratio between the sizes of the four-bar linkage and the pantograph, while Type I mechanism has a small four-bar linkage with a comparatively large pantograph.

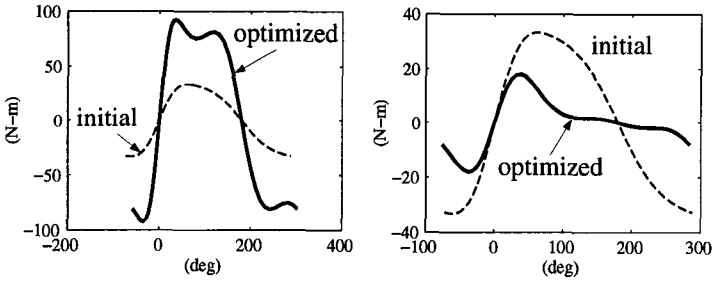

(a) Type I (b) Type II

FIGURE 4.16: Crank torque of the initial and optimized eight-bar mechanisms, (a) Type I, and (b) Type II

Figs. 4.16(a) and (b) shows the crank torque curves of Type I and II mechanisms, respectively. Since the crank torque of Type II mechanism remains constant regardless of the position of the adjustable pivot F_0, only one optimized crank torque curve is shown. As expected from the discussion on the foot-point path, the peak crank torque of the optimized Type I mechanism is not only higher than Type II mechanism, but also higher than the initial mechanism.

Based on the above discussion, if a large up-and-down motion is required, we conclude that the eight-bar Type II mechanism is acceptable, while Type I mechanism is unacceptable, as a leg design, if a large path height is required by its design specification.

For these two types of eight-bar mechanisms, Table 4.5 shows the initial and optimized leg dimensions, while Table 4.6 shows the values of the optimized objective functions. Note that, since the actuating force of Type II mechanism is proportional to $(1 + n)$, it is not a function of the crank angle.

Design Variables	Initial Values	Optimized Values	
		Type I Mechanism	Type II Mechanism
x_1 (m)	0.03	0.010	0.041
x_2 (m)	0.14	0.026	0.178
x_3 (m)	0.12	0.021	0.156
x_4 (m)	0.15	0.030	0.112
x_5 (m)	0.30	0.463	0.234
ϕ (rad)	3.0	2.768	2.140

TABLE 4.5: Initial and optimized design variables

Objective Functions		Type I Mechanism	Type II Mechanism
Peak crank torque (N-m)	T	79.8	7.93
Maximum actuating force(kN)	f_{95Y}	N/A	2.75
Normalized leg size		2.79	2.14

TABLE 4.6: Values of the optimized objective functions

4.6 Remarks on Types I and II of the Four-, Six-, and Eight-Bar Mechanisms

For Type I mechanism (i.e., mechanism without an adjustable pivot), eight-bar mechanism is unacceptable because of its inverted $\Delta-$shaped foot-point path (see Fig. 4.15(a)). Although both the four- and six-bar Type I mechanisms have similar leg sizes and peak crank torque values, the six-bar mechanism is considered to be better than the four-bar mechanism because of the slenderness of the six-bar mechanism. It is worth noting that, for this type of mechanism,

the constraint imposed on the path height are the most crucial constraint. Due to the large path height, the peak crank torque is normally higher than that of Type II mechanism.

Among various Type II mechanisms (i.e., mechanisms with an adjustable pivot), eight-bar mechanism has advantages over the other two mechanisms. The eight-bar Type II mechanism has a small peak crank torque and a compact size compared to the other two mechanisms. Also, as the pivot is adjusted, the eight-bar mechanism always generates a symmetrical foot-point path. Such a feature makes the peak crank torque independent of F_0 position. For the other two mechanisms, the peak crank torques increase as the adjustable pivot moves away from the initial $\delta = 0$ position. Moreover, the eight-bar mechanism features an actuating system for which the up-and-down and the back-and-forth motions can be independently controlled.

Although the six-bar Type I mechanism and the eight-bar Type II mechanism have some essential differences in the mechanism structure, we may compare them in general as follows. The six-bar Type I mechanism has fewer links. Since it is a one-DOF mechanism, it requires only one motor for each leg[4] to provide both back-and-forth, and up-and-down motions. This substantially reduces the overall body weight, which in turn reduces the crank torque requirement. However, Type I six-bar mechanism is less flexible than the eight-bar Type II mechanism. In addition, for walking on a flat ground, the six-bar Type I mechanism hops up-and-down more than the eight-bar Type II mechanism. Moreover, the size of the six-bar Type I is larger than the eight-bar Type II mechanism. The choice between the six-bar Type I and eight-bar Type II mechanism thus

[4]Motor for the turning motion is not counted.

depends on the application.

It is note that the above comparison is based on the results yielded from the multi-objective optimization models formulated according to the user-specified good and bad values of the objective functions and the constraint thresholds defined by the design specifications. Should any of those pre-specified values change, the optimization results may vary. In addition, it is also noted that the results obtained from the optimization models are not global optima. This implies that the changes of the initial conditions (or initial guesses) may result in local optima other than those presented in this chapter.

4.7 Mechanisms with Spring Elements for Force Reduction

Since a large actuator will make the walking machine heavy and this in turn results in high load at the foot point, it is desirable to further reduce the already optimized torque and force obtained from the previous section. For this reason, light weight passive elements such as springs are considered. Among a variety of springs, tension springs are selected for their ease of attachment.

Spring elements have been used in leg mechanism both to store kinetic energy (Alexander, 1990; Dhandapani and Ogot, 1994) and to reduce actuating forces (Shin and Streit, 1993). Shin and Streit (1993) developed a two-phase equilibrator which was connected to two legs and switched its configuration between the two walking phases, the propelling and returning phases. While such an equilibrator allows a significant reduction in actuating forces, the additional mechanism associated to it requires a complicated control algorithm even for flat

terrain walking. In order to keep the leg mechanism and control algorithm simple, we reduce the actuating force and torque by directly placing spring elements on the mechanism.

Since there is no general guideline for mounting springs to a leg mechanism, the spring placement configuration should take the advantage of some of the special features of a mechanism. For our leg mechanism, symmetry is a significant feature. Thus, all of the springs are arranged in such a way that the actuator force and crank torque are reduced in a symmetric manner.

Since the eight-bar compound mechanism with an adjustable pivot (Type II) is judged to be the most suitable mechanism, a study of spring placement is performed on this mechanism. In this section, three possible spring configurations as shown in Fig. 4.17 are presented for further reduction of the actuating force and torque.

To demonstrate the concept, we apply a second-stage optimization from which the spring size and the attachment points are determined for further reduction of the vertical actuating force and crank torque for the entire walking cycle or path. This is in contrast to the approach used by Matthew and Tesar (1977a; 1977b) who developed a formulation to meet external force/torque at a finite number of points along a path.

4.7.1 Configurations of Spring Placements

(a) Configuration I

Fig. 4.17(a) shows two springs attached on the leg mechanism. Spring k_1 (k_1 is the spring constant) is connected at points C and C'. Point C' lies on the axis of symmetry B_0F_0 and point C is the coupler point of the four-bar. Spring

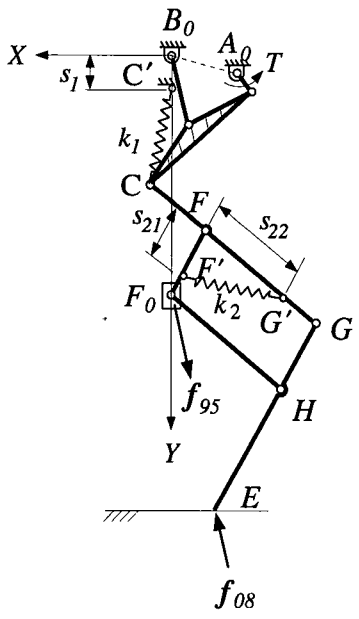

(a) Configuration I

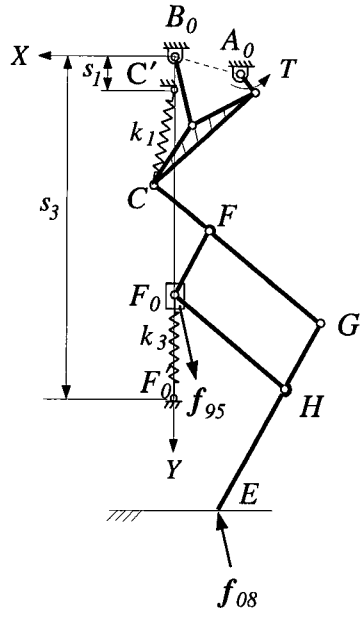

(b) Configuration II

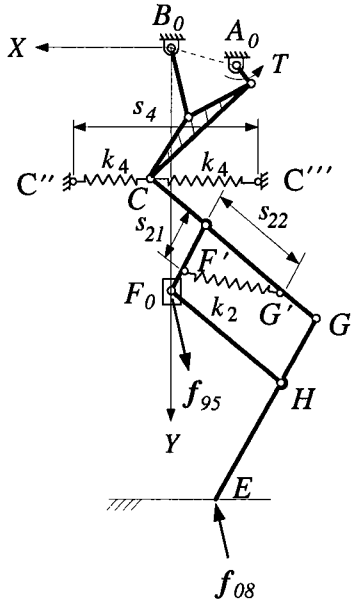

(c) Configuration III

FIGURE 4.17: Three proposed spring configurations

k_2 is attached onto the pantograph at G' and F', where point G' lies on link FG and point F' lies on link F_0F. As a result, the crank torque is reduced by both springs, while the vertical actuating force at point F_0 is reduced by spring k_2 alone.

Without the springs, when the mechanism is subject to a force $\mathbf{f}_{08}$, the pantograph will be under compression, i.e., points C and E tend to approach each other, while the coupler point C of the four-bar linkage tends to move away from its base point B_0. After the springs are attached on the mechanism, spring k_1 will pull the coupler point C toward the base point B_0 and spring k_2 will extend the pantograph. Because of this, force acting on the coupler point C is affected by both springs, resulting in a reduced crank torque. As to the pantograph, a reduced actuating force at point F_0 is obtained due to the fact that the compressive force from the ground is partially balanced by the tension force from spring k_2.

Applying the principle of virtual work (see details in Appendix D), we obtain the crank torque as

$$\begin{aligned} T =& [nf_{08X} + (k_1\kappa_1 - k_2\kappa_2)X_C]\frac{dX_C}{d\alpha} \\ &+[nf_{08Y} + k_1\kappa_1(Y_C - s_1) + k_2\kappa_2(Y_{F_0} - Y_C)]\frac{dY_C}{d\alpha} \end{aligned} \tag{4.61}$$

where $n = x_5/x_4$, $\kappa_1 = (1 - l_{01}/l_1)$, and $\kappa_2 = (s_{21}s_{22}/{x_4}^2)(1 - l_{02}/l_2)$. The coefficients of the $dX_C/d\alpha$ and $dY_C/d\alpha$ in Eq. (4.61) are respectively the X- and Y- forces at joint C. Note that in Eq. (4.61), f_{08Y} is always negative, while $k_1\kappa_1(Y_C - s_1)$ and $k_2\kappa_2(Y_{F_0} - Y_C)$ are always positive. Therefore, the crank torque can be substantially reduced as long as the term $(k_1\kappa_1 - k_2\kappa_2)$ is kept at

a small value. The vertical actuating force at point F_0 is

$$f_{95Y} = -(1+n)f_{08Y} - k_2\kappa_2(Y_{F_0} - Y_C). \tag{4.62}$$

Note that the right hand side of Eq. (4.62) is the difference of two positive quantities (since f_{08Y} is negative).

It can be seen from Eq. (4.61) that the resultant crank torque is affected by both springs. This implies that there are restrictions in the selection of springs, because of their coupling effect on crank torque. Note that in this configuration, an additional reaction force in the X- direction at point F_0 is introduced by spring k_2, which will increase the frictional force of the slider at point F_0.

(b)Configuration II

Fig. 4.17(b) shows an alternative arrangement of the springs. Spring k_1 is attached at points C and C' identical to that shown for the first configuration, while spring k_3 is connected at points F_0 and F_0', where point F_0' lies on the axis of symmetry B_0F_0. The crank torque T for this spring configuration, via a formulation similar to that described in Appendix D, is given by

$$\begin{aligned} T = {} & (nf_{08X} + k_1\kappa_1 X_C)\frac{dX_C}{d\alpha} \\ & +[nf_{08Y} + k_1\kappa_1(Y_C - s_1)]\frac{dY_C}{d\alpha} \end{aligned} \tag{4.63}$$

and the actuating force f_{95Y} is found to be

$$f_{95Y} = -(1+n)f_{08Y} - k_3[(s_3 - Y_{F_0}) - l_{03}]. \tag{4.64}$$

From Eqs. (4.63) and (4.64), it is clear that the crank torque T depends only on spring k_1 and the actuating force f_{95Y} is solely related to spring k_3. Unlike the first configuration, there is no coupling effect between these two springs.

Moreover, k_3 spring will not generate additional side force at point F_0. However, one potential problem with this design is that the attachment point F_0' may come too close to the ground.

(c) Configuration III

The third spring configuration, as shown in Fig. 4.17(c), consists of three springs. Spring k_2 is attached to the pantograph at F' and G' in a manner identical to that of the first configuration. One end of two springs k_4 are attached at point C at one ends, while the other ends are attached at C'' and C''', respectively. Both C'' and C''', which are symmetric about the Y-axis, are located on a horizontal line passing half way between the two extreme Y coordinates of the coupler curve. Since the coupler point C does not change much in its Y coordinate (compared to the change in the X coordinate), the force generated by springs k_4 are mainly in the X-direction. Neglecting the Y-direction force generated by springs k_4, the crank torque T is obtained as

$$\begin{aligned} T = & [nf_{08X} + (k_2\kappa_2 - 2k_4)X_C]\frac{dX_C}{d\alpha} \\ & +[nf_{08Y} + k_2\kappa_2(Y_C - s_1)]\frac{dY_C}{d\alpha} \end{aligned} \tag{4.65}$$

and f_{95Y} is given by Eq. (4.62).

Note that, in this design, points C'' and C''' must be separated far enough for the springs to remain in tension at all times. This may pose a problem in a situation when the available space is limited. Similar to the second configuration, springs k_2 and k_4 are not coupled. Again, spring k_2 generates an additional frictional force on the slider point F_0.

4.7.2 Optimization Model

For the sizing and placement of the springs, an optimization-based model is established. The model is comparably simpler than that for the leg mechanism dimensions and again the software Consol-Optcad (Fan et al., 1990) is used.

The design variables for the three spring configurations include the distances s_1, s_{21}, s_{22}, s_3, and s_4, the spring constants k_1 through k_4, and their unstretched (or free) lengths l_{01} through l_{04}. All of the design variables are assumed to be positive, except s_1 which is allowed to be negative. Here, quantities s_1 and s_3 are measured from point B_0 along the Y-axis direction, while s_{21} and s_{22} are measured from point F along $\overrightarrow{FF_0}$ and $\overrightarrow{FG}$, respectively, and the quantity s_4 is defined as $\overline{C''C'''}$.

The design objectives of the second-stage optimization are the crank torque T and the actuating force f_{95Y}, as described in the previous sections. The constraints can be divided into two groups: constraints on the extension ratios of the springs, and constraints on the location of the spring attachment points. For each spring, two constraints on the extension ratio are imposed. For example, spring k_1 has the following two constraints:

$$\mathtt{SC1} := \frac{\min(l_1)}{l_{01}} \geq \mathtt{H_{SC1}} \tag{4.66}$$

$$\mathtt{SC2} := \frac{\max(l_1)}{l_{01}} \leq \mathtt{H_{SC2}}. \tag{4.67}$$

The quantity $\mathtt{H_{SC1}}$, normally set to one, is the minimum extension ratio. The quantity $\mathtt{H_{SC2}}$, depending on the spring characteristics, is the maximum extension ratio. The stretched lengths l_1 and l_2 and their extreme values can be found in Appendix D, while $\min(l_3) = s_3 - \{Y_{F_{01}} + s_v/[2(1+n)]\}$, $\max(l_3) = s_3 - \{Y_{F_{01}} - s_v/[2(1+n)]\}$, $\min(l_4) = s_4/2 - X_E|_{\alpha=\alpha_x}$ and $\max(l_4) = s_4/2 + X_E|_{\alpha=\alpha_x}$ can be

easily obtained from Fig. 4.17. Here $Y_{F_{01}} = Y_C|_{\alpha=\pi} + \sqrt{2}x_4$, where $Y_{F_{01}}$ is the Y coordinate of the slider F_0 when it is held at its middle position, and $s_v/[2(1+n)]$ is one-half of the vertical displacement of the slider F_0.

As to the constraints on the locations of the spring attachment points, again we take spring k_1 as an example:

$$\texttt{SC3} := s_1 \geq \texttt{H}_{\texttt{SC3}} \tag{4.68}$$

$$\texttt{SC4} := s_1 \leq \texttt{H}_{\texttt{SC4}} \tag{4.69}$$

where $\texttt{H}_{\texttt{SC3}}$ and $\texttt{H}_{\texttt{SC4}}$ are the minimum and maximum values for s_1, respectively. Note that, for spring k_2, it is desirable for the maxima of s_{21} and s_{22} to be smaller than that of x_4 and x_5, respectively. Therefore, a second-stage optimization model can be easily developed for each spring configuration using the objective and constraint functions described in this section.

4.7.3 Results and Discussion

The second-stage optimization results are based on the following assumptions: (i) the maximum spring extension ratio for all springs is 30%; (ii) the spring constants are not to exceed 50 kN/m; (iii) joint F_0 is held at the middle position while the crank torque and actuating force are computed for a full crank cycle; and (iv) leg dimensions obtained from the optimized design in Table 4.5 are used for all three spring configurations.

The spring constants and their unstretched lengths for the three optimized configurations are tabulated in Table 4.7, while the spring locations are listed in Table 4.8. From these two tables, it can be observed that springs k_1 for the first

	Initial	Spring Configuration		
	Guess	I	II	III
l_{01} (m)	0.1	0.130	0.316	N/A
l_{02} (m)	0.1	0.182	N/A	0.186
l_{03} (m)	0.1	N/A	0.216	N/A
l_{04} (m)	0.1	N/A	N/A	0.500
k_1 (kN/m)	0	29.5	10.2	N/A
k_2 (kN/m)	0	50.0	N/A	50.0
k_3 (kN/m)	0	N/A	42.6	N/A
k_4 (kN/m)	0	N/A	N/A	48.8

TABLE 4.7: Design variables of the springs

configuration are shorter than for the second configuration, because spring k_1 in the first configuration must provide a larger side force to cancel that generated by spring k_2. Springs k_2 used in the first and third configurations are attached at almost the same positions, i.e., G' and G coincide. The location of F_0' for spring k_3, which is 0.548 meters below joint B_0, does not come too close to the ground because the leg is about 0.8 meter long. Since s_4 is about 0.576 meter (much larger than the width of the leg), there may not be enough room to attach springs k_4 for the third configuration. Table 4.9 shows the maximal crank torques and actuating forces for the three alternative designs with and without springs. As shown in Table 4.9, the actuating torque and force values for the second configuration have been reduced to about one half of the values without the springs.

From the above discussions, we conclude that the second spring configuration

	Initial	Spring Configuration		
	Guess	I	II	III
s_1(m)	0	0.150	-0.100	N/A
s_{21}(m)	0.1	0.017	N/A	0.038
s_{22}(m)	0.1	0.233	N/A	0.233
s_3(m)	0.35	N/A	0.548	N/A
s_4(m)	0.30	N/A	N/A	0.576

TABLE 4.8: Location variables of the springs

	Without	Spring Configuration		
	Springs	I	II	III
f_{95Y}(kN)	2.75	2.22	1.38	1.69
T (N-m)	7.93	6.44	4.01	4.92

TABLE 4.9: Actuating force and torque with and without springs

is the most promising design. For this configuration, Figs. 4.18(a) and 4.18(b) show the reduction in crank torque and actuating force, respectively, for a full walking cycle. While the crank torque and actuating force in the returning portion have been increased, their largest (absolute) values over a full walking cycle have been significantly reduced.

4.8 Summary

In this chapter, we present the results of an optimization-based dimensional synthesis for the planar four-, six-, and eight-bar leg mechanisms. All mech-

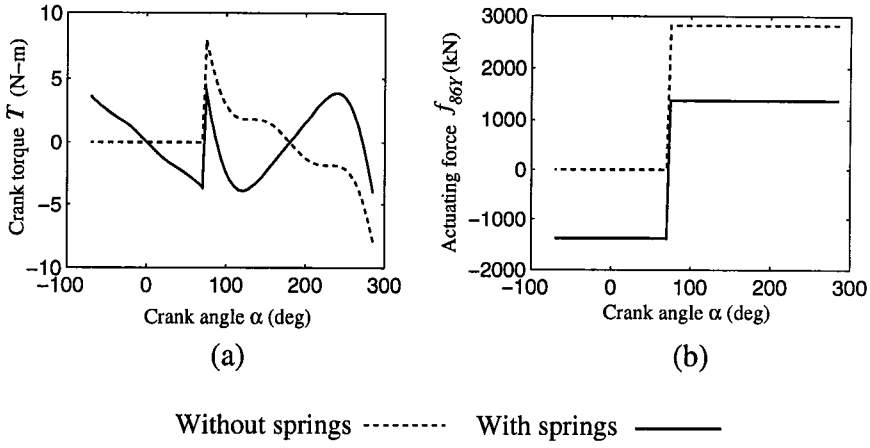

FIGURE 4.18: A comparison of actuating forces and torques: (a) Crank torque vs. crank angle; (b) Actuating force vs. crank angle

anisms are investigated with and without an adjustable pivot. With the requirements that all the design specifications (or constraints) be satisfied, these leg mechanism dimensions are determined via multi-objective optimization with three design goals: minimum leg size, minimum actuating force, and minimum peak crank torque. As a result of the optimization-based methodology, it is shown that these leg mechanisms can be synthesized without the need for a prescribed coupler path.

By comparing the results of those synthesized mechanisms, we conclude that six-bar mechanism without an adjustable pivot is most suitable for a one-DOF leg with a compromise in flexibility. We also conclude that the eight-bar mechanism with an adjustable pivot is most suitable for a two-DOF leg design with two perpendicularly decoupled actuating motions. The advantages and the disadvantages of these two mechanisms are also explored in details.

Finally, tension springs with three different attachment configurations are proposed for the reduction of the actuating force and torque. We demonstrate

that the actuating force and torque can be substantially reduced with the appropriate attachment of tension springs onto the mechanism.

Chapter 5

Conclusion

5.1 Summary

In this study, optimization-based dimensional synthesis of planar leg mechanisms featuring symmetrical foot-point paths are presented. These leg mechanisms are designed in such a way that a walking machine has the flexibility required for walking on a rough terrain, while it can achieve fast locomotion, remains easy to control, and requires minimum actuation torque for walking on a flat ground.

In Chapter 2, a systematic methodology is used for the concept design of a leg mechanism. Since the turning motion of a leg mechanism can be separated from the back-and-forth and the up-and-down motions, only two-DOF planar leg mechanisms are considered. Furthermore, by temporarily excluding the DOF associated with the up-and-down motion of a leg, only one-DOF planar mechanism is considered. In the search for admissible one-DOF planar leg mechanism designs, some of the functional requirements of a leg mechanism are transformed into a set of structural specifications from which all possible candidate mechanisms are enumerated. The remaining functional requirements and

other design guidelines are included in a set of evaluation criteria from which unwanted candidate mechanisms are screened out. Using this methodology, six admissible leg mechanisms are obtained for further studies. These mechanisms include one four-bar, four six-bar, and one eight-bar mechanisms as shown in Figs. 2.7 (a), (b)-(e), and (f), respectively.

In Chapter 3, all admissible leg mechanisms that have the potential to generate a symmetrical foot-point path are studied. For the symmetrical four-bar linkage, the coordinates of the foot point are formulated, the guidelines to prevent double point(s) are derived, and the equation for the crank torque is obtained. The relation between the coupler angle ϕ and the condition used to select the propelling and non-propelling portions of the foot-point path is also established. Based on a symmetrical four-bar mechanism, an eight-bar compound mechanism consisting of a four-bar and a pantograph is constructed.

A new class of six-bar linkages with an embedded (skew-) pantograph is introduced. Two types of such six-bar linkages are constructed, leading to the admissible Watt-I and Stephenson-II and -III type mechanisms as shown in Figs. 2.7(b) through (e). For this class of six-bar mechanisms, design limitations such as the reduction of the admissible range for the transmission angle μ are discussed. The foot-point path generated by such a class of mechanisms is proved to be bounded inside two concentric circles.

In Chapter 4, the results of an optimization-based dimensional synthesis for the planar four-, six-, and eight-bar leg mechanisms are presented. For the dimensional synthesis, each admissible mechanism is investigated with and without an adjustable pivot. For those mechanisms with an adjustable pivot, one DOF is used for normal walking to provide an ovoid path which emulates that of humans

while the other (the motion of an adjustable pivot) is used only when necessary to walk over obstacles. For those mechanisms without an adjustable pivot, the sole DOF motion generates a large Δ-shaped path, which makes a leg mechanism capable of performing both the up-and-down and the back-and-forth motions. To exploit these to the fullest, a multi-objective optimization-based design formulation is proposed to minimize the following three design objectives: (i) peak crank torque, (ii) maximum actuating force, and (iii) leg size.

By comparing the results of the synthesized mechanisms, it is concluded that six-bar mechanism without an adjustable pivot is most suitable for a one-DOF leg. It is also conclude that the eight-bar mechanism with an adjustable pivot is most suitable for a two-DOF leg design with two perpendicularly decoupled actuating motions.

Finally, tension springs with three different attachment configurations are added for the reduction of the actuating force and torque. It is demonstrated that the actuating force and torque can be substantially reduced with the attachment of tension springs to the mechanism.

5.2 Contributions of This Thesis

The major contributions of this thesis can be summarized as follows:

1. Introduction of a new class of six-bar linkages with an embedded (skew-) pantograph which are capable of generating a symmetrical foot-point path:
   (a) two types of such six-bar linkages are constructed, and
   (b) design limitations, in terms of the transmission angle, are explored and that foot-point path is shown to be bounded between two con-

centric circles.

2. Investigation of a symmetrical four-bar coupler curve, in which

   (a) guidelines to exclude double point(s) are derived, and

   (b) conditions for selecting the propelling and non-propelling portions are established.

3. Reduction of the actuating force/torque in a symmetric manner by adding tension springs to an existing mechanism

4. Performance of a comparative study among the leg mechanisms with and without an adjustable pivot.

5. Dimensional synthesis of the leg mechanism via a multiobjective optimization model without the need of a prescribed coupler curve.

5.3 Recommendations for the Future Work

As an extension of this study, the following problems are recommended for future investigation:

1. Some problems regarding a symmetrical four-bar coupler curve have not been fully addressed:

   (a) Referring to Fig. 3.1, it is well known that the sufficient condition for a four-bar linkage to trace a symmetrical coupler-curve is $\overline{B_0B} = \overline{AB} = \overline{BC}$. However, research for deriving a set of necessary conditions for a four-bar linkage to generate a symmetrical coupler curve still remains

unsolved. If this problem can be solved, potentially a new class of four-bar linkages will be available for the design of leg mechanisms.

(b) Although a $\Delta-$shaped curve can be obtained via an optimization formulation, the necessary and sufficient conditions for producing such a curve is not yet well understood.

(c) In the optimization procedure, it is observed that for the type I mechanisms (mechanisms without an adjustable pivot), the constraint on the path height is always an active constraint, while that on the stride length is not. The relation between these two quantities has not been established yet and requires further explanation.

2. In this study, friction, inertia force, and the dynamic coupling effects are all neglected. However, these effects can become important depending on the type of application or environment that a walking machine is operating in. Therefore, an extension of this study, not neglecting the above mentioned effects is warranted.

3. An experimental verification of the results presented in this thesis should provide additional insights for improvements in the leg designs studied here.

4. Path planning and control of such a leg mechanism should be studied.

Appendix A

Coefficients of the Polynomial in Eq. (3.22)

(I) In Eq. (3.22), the coefficients, a_i, $i = 1, ..., 6$, of the sixth-degree polynomial are:

$$a_6 = 16x_1^4x_2^4 \tag{A.1}$$

$$a_5 = -32x_1^4x_2^3 - 32x_1^3x_2^5 + 32x_1^3x_2^3x_3^2 \tag{A.2}$$

$$\begin{aligned} a_4 = {} & 24x_1^4x_2^2 + 48x_1^3x_2^4 + 24x_1^2x_2^6 - 48x_1^3x_2^2x_3^2 - 16\sin^2(\phi/2)x_1^3x_2^2x_3^2 \\ & -48x_1^2x_2^4x_3^2 - 16\sin^2(\phi/2)x_1^2x_2^4x_3^2 + 16\sin^2(\phi/2)x_1^2x_2^2x_3^4 \end{aligned} \tag{A.3}$$

$$\begin{aligned} a_3 = {} & -8x_1^4x_2 - 24x_1^3x_2^3 - 24x_1^2x_2^5 - 8x_1x_2^7 + 24x_1^3x_2x_3^2 \\ & +16\sin^2(\phi/2)x_1^3x_2x_3^2 + 48x_1^2x_2^3x_3^2 + 32\sin^2(\phi/2)x_1^2x_2^3x_3^2 \\ & +32\sin^2(\phi/2)x_1^3x_2^3x_3^2 + 24x_1x_2^5x_3^2 + 16\sin^2(\phi/2)x_1x_2^5x_3^2 \\ & -32\sin^2(\phi/2)x_1^2x_2x_3^4 - 32\sin^2(\phi/2)x_1x_2^3x_3^4 \end{aligned} \tag{A.4}$$

$$\begin{aligned} a_2 = {} & x_1^4 + 4x_1^3x_2^2 + 6x_1^2x_2^4 + 4x_1x_2^6 + x_2^8 - 4x_1^3x_3^2 - 4\sin^2(\phi/2)x_1^3x_3^2 \\ & -12x_1^2x_2^2x_3^2 - 12\sin^2(\phi/2)x_1^2x_2^2x_3^2 - 32\sin^2(\phi/2)x_1^3x_2^2x_3^2 \\ & -12x_1x_2^4x_3^2 - 12\sin^2(\phi/2)x_1x_2^4x_3^2 - 32\sin^2(\phi/2)x_1^2x_2^4x_3^2 - 4x_2^6x_3^2 \\ & -4\sin^2(\phi/2)x_2^6x_3^2 + 16\sin^2(\phi/2)x_1^2x_3^4 + 32\sin^2(\phi/2)x_1x_2^2x_3^4 \\ & +32\sin^2(\phi/2)x_1^2x_2^2x_3^4 + 16\sin^2(\phi/2)x_2^4x_3^4 \end{aligned} \tag{A.5}$$

$$a_1 = 8\sin^2(\phi/2)x_1^3x_2x_3^2 + 16\sin^2(\phi/2)x_1^2x_2^3x_3^2 + 8\sin^2(\phi/2)x_1x_2^5x_3^2$$
$$-32\sin^2(\phi/2)x_1^2x_2x_3^4 - 32\sin^2(\phi/2)x_1x_2^3x_3^4 \quad \text{(A.6)}$$

$$a_0 = 16\sin^2(\phi/2)x_1^2x_2^2x_3^4 \quad \text{(A.7)}$$

(II) If α is equal to π, Eq. (3.22) degenerates into a third-degree polynomial, where its the coefficients, a_i, $i = 1, ..., 3$, are:

$$a_3 = 4x_1^2x_2^2 \quad \text{(A.8)}$$

$$a_2 = -4x_1^2x_2 - 4x_1x_2^3 + 4x_1x_2x_3^2 \quad \text{(A.9)}$$

$$a_1 = x_1^2 + 2x_1x_2^2 + x_2^4 - 4x_1x_3^2 - 4x_2^2x_3^2 \quad \text{(A.10)}$$

$$a_0 = 4x_1x_2x_3^2 \quad \text{(A.11)}$$

$$\text{(A.12)}$$

Note that, because Eq. (3.22) in case **(I)** has been rationized by squaring both sides of the equation during the derivation, the degree of the equation in case **(I)** is six, but that in case **(II)** is only three.

Appendix B

First and Second Derivatives of Coupler-Point C

From Eqs. (3.18) and (3.19), we may rewrite the coordinate of the foot point C as

$$X_C = x_1 \sin\alpha(\cos\frac{\phi}{2} + p\sin\frac{\phi}{2}) \tag{B.1}$$

$$Y_C = (x_2 - x_1\cos\alpha)(\cos\frac{\phi}{2} + p\sin\frac{\phi}{2}) \tag{B.2}$$

where

$$p = (\frac{4x_3^2}{q} - 1)^{1/2} \tag{B.3}$$

$$q = x_2^2 + x_1^2 - 2x_1x_2\cos\alpha \tag{B.4}$$

The first derivatives of the coordinate with respect to α can be found as

$$\frac{dX_C}{d\alpha} = x_1[\cos\alpha\cos(\frac{\phi}{2}) + (p\cos\alpha + \frac{dp}{d\alpha}\sin\alpha)\sin(\frac{\phi}{2})] \tag{B.5}$$

$$\frac{dY_C}{d\alpha} = X_C + \sin(\frac{\phi}{2})(x_2 - x_1\cos\alpha)\frac{dp}{d\alpha} \tag{B.6}$$

and their second derivatives are

$$\frac{d^2X_C}{d\alpha^2} = -X_C + x_1\sin(\frac{\phi}{2})(2\cos\alpha\frac{dp}{d\alpha} + \sin\alpha\frac{d^2p}{d\alpha^2}) \tag{B.7}$$

$$\frac{d^2Y_C}{d\alpha^2} = \frac{dX_C}{d\alpha} + x_1\sin\alpha\sin(\frac{\phi}{2})\frac{dp}{d\alpha} + \sin(\frac{\phi}{2})(x_2 - x_1\cos\alpha)\frac{d^2p}{d\alpha^2} \tag{B.8}$$

The first and second derivatives of p are obtained as

$$\frac{dp}{d\alpha} = -4x_1x_2x_3^2\sin(\alpha)q^{-2}p^{-1} \quad \text{(B.9)}$$

$$\frac{d^2p}{d\alpha^2} = 4x_1x_2x_3^2q^{-2}p^{-1}[-\cos\alpha + 4x_1x_2\sin^2(\alpha)q^{-1} + \sin(\alpha)p^{-1}\frac{dp}{d\alpha}] \quad \text{(B.10)}$$

Therefore, the first and second derivatives of the coordinates of the coupler point C can be obtained by substituting Eqs. (B.1-B.4) and (B.9-B.10) into Eqs. (B.5-B.6) and (B.7-B.8), respectively.

Appendix C

Three Six-bar Mechanisms with Symmetrical Foot-Point Paths

C.1 Hain's Mechanism

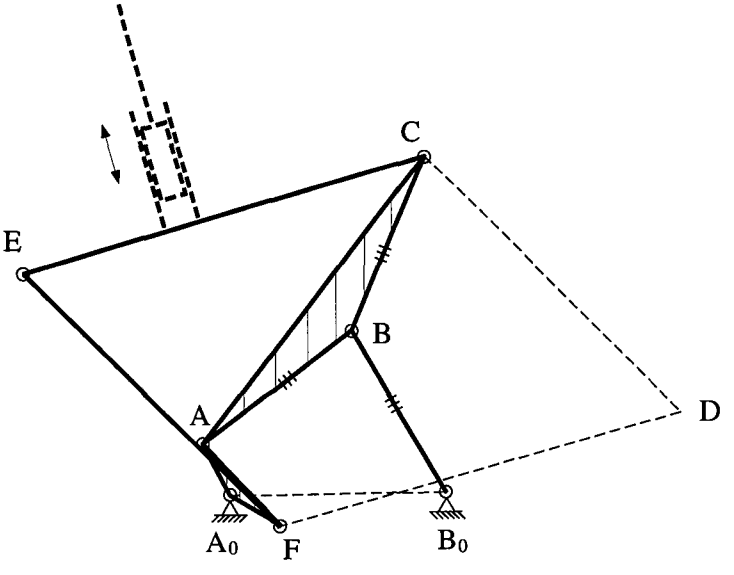

FIGURE C.1: Six-bar linkage using Hain's translation bar concept

Fig. C.1 shows the six-bar linkage invented by Hain (Dijksman, 1976) for which any point on link EC will trace an identical symmetrical curve as that

traced by point C. Here is the procedure to construct Hain's mechanism:

1. Construct a four-bar linkage $A_0 - ABC - B_0$ such that $\overline{AB} = \overline{BC} = \overline{BB_0}$.

2. Stretch-rotate the four-bar linkage A_0ABB_0 about point A until point B coincides with point C such that $\Box FACD \sim \Box A_0ABB_0$ as shown in Fig. C.1.

3. Make triangle A_0AF as a ternary link.

4. Construct a four-bar parallelogram $CDFE$ and obliterate the redundant dyad CDF.

Note that the Hain's mechanism as shown in Fig. C.1 is not unique, other curve-cognate mechanisms are possible see (Dijksman, 1976).

Since there are two common links shared by $\Box FACD$ and $\Box A_0ABB_0$, all the corresponding links in these two four-bar linkages must have the same angular velocity. Thus, the angular velocities of links FD, EC and A_0B_0 (ground) are all equal to zero. Hence, translation is the sole planar motion for link EC, which implies that all the points on link EC will trace identical curves as point C, e.g., if point C traces a symmetrical curve, so does point E.

C.2 Dijksman's Mechanism

Starting from a symmetrical arrangement of Kempe's overconstrained focal mechanism as shown in Fig. C.2(a), Dijksman (1980a; 1984) obtained a six-bar mechanism, through the Robert's law, to trace a symmetrical curve. Note that, in the Kempe's focal mechanism shown in Fig. C.2(a), point K is the mid-point of link AB, point D is at one of the intersections of $\overline{KA_0'}$ and half circle BDB_0

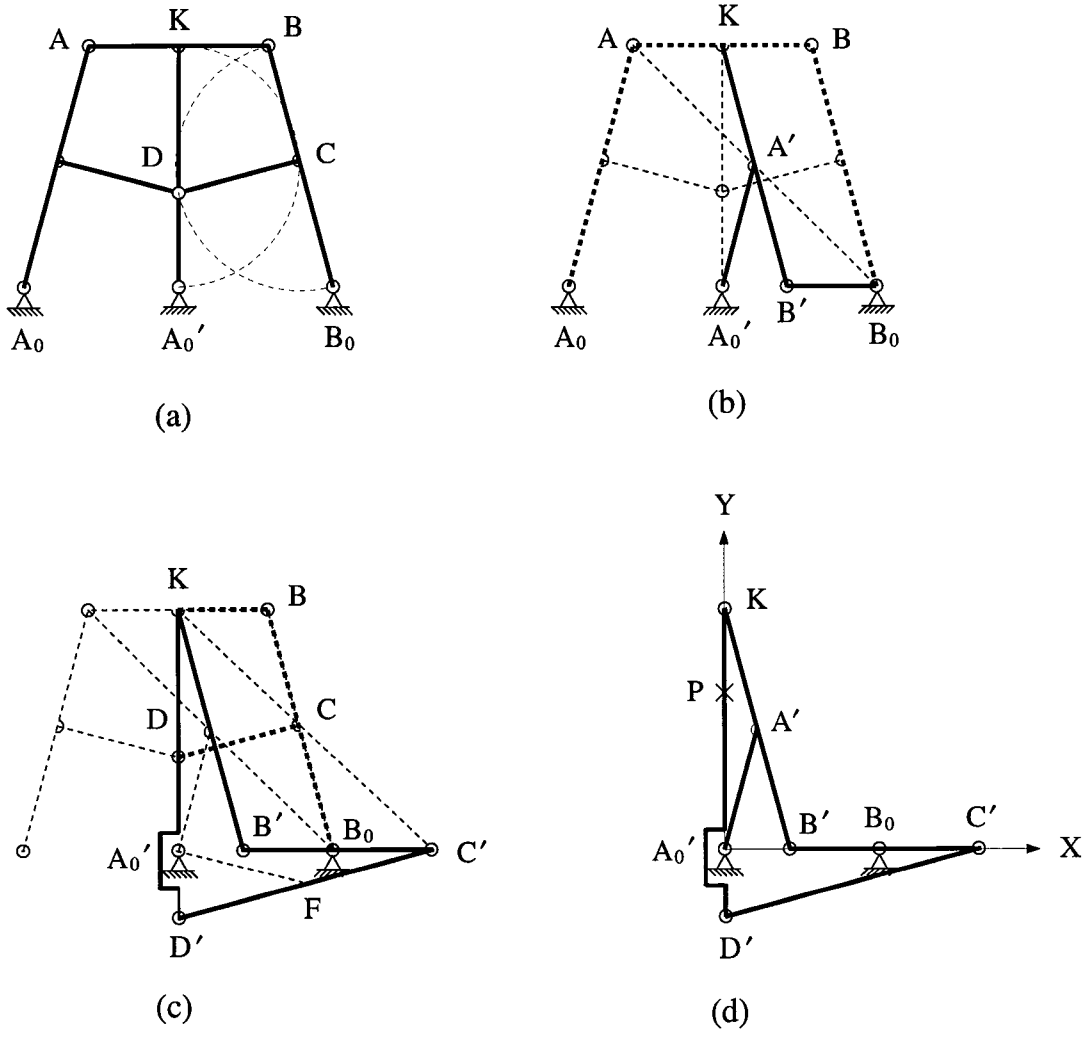

FIGURE C.2: Six-bar cognate linkage derived from the Kempe's focal mechanism. (a) Kempe's focal mechanism (b) First Robert's cognate linkage (c) Second Robert's cognate linkage (d) 'Double-Roberts' six-bar cognate linkage

(whose diameter is $\overline{BB_0}$), and point C is at one of the intersections of $\overline{BB_0}$ and half circle KCA_0' (whose diameter is $\overline{KA_0'}$). Dijksman's six-bar mechanism is constructed as follows:

1. Replace the four-bar trapezium $A_0 - AKB - B_0$ by its curve cognate $A_0' - A'KB' - B_0$ according to Robert's law, see Fig. C.2(b). Points A_0, A, and B have been substituted by A_0', A', and B', respectively. Note that, because K is at the mid-point of link AB, A' is also at the mid-point of link KB', As a result, the mechanism $A_0' - A'KB' - B_0$ is a symmetrical four-bar linkage.

2. Applying Robert's law again, the four-bar $K - BCB_0 - D$ is replaced by its curve cognate $K - B'B_0C' - D'$, see Fig. C.2(c). Here, points D, C, and B have been substituted by D', C', and B', respectively. Note that since the mid-point F of link $D'C'$ traces a circle about A_0' (Dijksman, 1975), the mechanism $K - B'B_0C' - D'$ is also a symmetrical four-bar linkage.

3. Combine the two opposite symmetrical four-bar linkages into a six-bar linkage, see C.2(d).

Consequently, the focal mechanism is replaced by a six-bar linkage in which both ends of the floating link $D'K$ trace four-bar symmetrical curves about axis Y.

Theorem C.1 *Referring to the six-bar linkage as shown in Fig. C.2(d), any point P on the link $D'K$ or its extension would trace a curve that is symmetrical about axis Y.*

Proof:

If a Cartesian coordinate system is attached to the six-bar linkage with its origin at A_0' and its $Y-$axis on the axis of symmetry as shown in Fig. C.2(d), the

coordinates of points D', K, and P can expressed as $(X_{D'},Y_{D'})$, (X_K,Y_K), and (X_P,Y_P), respectively, where $X_P = aX_{D'} + (1-a)X_K$, $Y_P = aY_{D'} + (1-a)Y_K$ and a is a real number.

Assume D'' and K' are the symmetrical points of D' and K with respect to the axis of symmetry Y, respectively. As points D' and K move to D'' and K', point P moves to P'. Since $X_{D''} = -X_{D'}$ and $X_{K'} = -X_K$, the X-coordinate of point P' becomes $X_{P'} = aX_{D''} + (1-a)X_{K'} = -[aX_{D'} + (1-a)X_K] = -X_P$. (QFD)

This theorem also shows that the curve generated by any point on link $D'K$ is a linear combination of the two four-bar symmetrical curves at D' and K.

C.3 Mechanisms Derived From Chebychev's Dyad

Referring to the six-bar linkage as shown in Fig. C.3, the dyad $D_0 - DCE$ with the lengths $\overline{D_0D} = \overline{DC} = \overline{DE}$ is a so-called Chebychev's dyad.

Theorem C.2 *Referring to the Chebychev's dyad in Fig. C.3, if point C trace a symmetrical curve about axis Y_1 on which the fixed pivot D_0 is located, then point E will trace a curve which is symmetrical about an axis Y_2 and the angle from axis Y_2 to Y_1 is equal to $\phi_2/2$, where $\angle CDE = \phi_2$.*

Proof:

(i) Assume subscripts r and l represent the two positions of Chebychecv's dyad when point C is in the right- and left-hand side of the symmetrical axis Y_1, respectively. In Fig. C.3, only the 'r' position is shown.

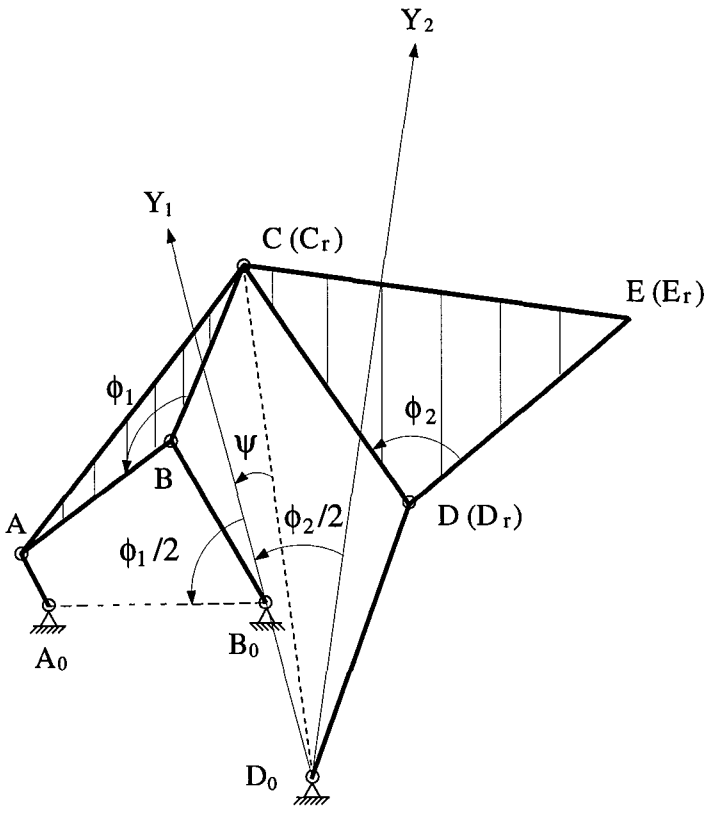

FIGURE C.3: Six-bar linkage using Chebychev's dyad to trace a symmetrical curve at E

If D_0 is on the axis of symmetry Y_1, it can be shown that $\overline{D_0C_r} = \overline{D_0C_l}$. This, in turn, shows that $\overline{D_0E_r} = \overline{D_0E_l}$ because $\Delta E_l D_0 D = \Delta E_r D_0 D$.

(ii) Assume the angles measured from $\overrightarrow{D_0C_r}$ and $\overrightarrow{D_0C_l}$ to $\overrightarrow{Y_1}$ are equal to ψ and $-\psi$, respectively. Because $\angle CD_0E = \angle CDE/2 = \phi_2/2$, the angles measured from $\overrightarrow{D_0E_r}$ and $\overrightarrow{D_0E_l}$ to $\overrightarrow{Y_1}$ are equal to $\phi/2 + \psi$ and $\phi/2 - \psi$, respectively.

From (i) and (ii), it is, therefore, proved that the positions E_r and E_l are symmetrical about axis Y_2 and the angle from Y_2 to Y_1 is equal to $[(\phi/2 + \psi) + (\phi/2 - \psi)]/2 = \phi_2/2$. (QFD)

Therefore, if the point C traces a curve which is symmetrical about $\overrightarrow{Y_1}$, point E would also trace a symmetrical curve about $\overrightarrow{Y_2}$.

It is obvious that more Chebychev's dyad chains can be added to the linkage shown in Fig. C.3 to trace a symmetrical curve by a mechanism which is more than six links. It is to be noted that the curve that is generated by the linkage of this type has higher order than that of the four-bar linkage curve.

Appendix D

Derivation of Crank Torque T and Force f_{95} for the First Spring Configuration

From the principle of virtual work and stationary energy,

$$\delta W = \delta P \tag{D.1}$$

where δW is the virtual work and δP is the virtual potential energy. The potential energy stored by the springs is

$$P = 1/2\, k_1(l_1 - l_{01})^2 + 1/2\, k_2(l_2 - l_{02})^2. \tag{D.2}$$

Differentiating Eq. (D.2) results in

$$\delta P = k_1(l_1 - l_{01})\delta l_1 + k_2(l_2 - l_{02})\delta l_2. \tag{D.3}$$

The square of l_1 can be written from Fig. 4.17(a), as

$${l_1}^2 = [X_C^2 + (Y_C - s_1)^2] \tag{D.4}$$

while the square of l_2 can be obtained by applying the cosine law to $\Delta F'FG$ and ΔCF_0F as

$${l_2}^2 = {s_{21}}^2 + {s_{22}}^2 - \frac{s_{21}s_{22}}{{x_4}^2}[(Y_{F_0} - Y_C)^2 + {X_C}^2 - 2{x_4}^2]. \tag{D.5}$$

From Eqs. (D.4) and (D.5) $\min(l_1)$, $\min(l_2)$, $\max(l_1)$, and $\max(l_2)$ could be obtained. Differentiating Eqs. (D.4) and (D.5) and substituting the resulting equations in Eq. (D.3), yields

$$\begin{aligned}\delta P = k_1\kappa_1[X_C\frac{dX_C}{d\alpha} + (Y_C - s_1)\frac{dY_C}{d\alpha}]\delta\alpha - k_2\kappa_2(Y_{F_0} - Y_C)\delta Y_{F_0} \\ +k_2\delta_2[-X_C\frac{dX_C}{d\alpha} + (Y_{F_0} - Y_C)\frac{dY_C}{d\alpha}](\delta\alpha)(\delta Y_{F_0})\end{aligned} \tag{D.6}$$

where $\kappa_1 = 1 - l_{01}/l_1$ and $\kappa_2 = (s_{21}s_{22}/{x_4}^2)(1 - l_{02}/l_2)$. Now, consider the virtual work of the leg mechanism,

$$\delta W = T\delta\alpha + \mathbf{f}_{08}\cdot\delta\mathbf{r}_{B_0E} + \mathbf{f}_{95}\cdot\delta\mathbf{r}_{B_0F_0}. \tag{D.7}$$

Since $\mathbf{f}_{08} = f_{08X}\mathbf{e}_X + f_{08Y}\mathbf{e}_Y$, $\mathbf{f}_{95} = f_{95X}\mathbf{e}_X + f_{95Y}\mathbf{e}_Y$, $\mathbf{r}_{B_0E} = -nX_C\mathbf{e}_X + [(1+n)Y_{F_0} - nY_C]\mathbf{e}_Y$, and $\mathbf{r}_{B_0F_0} = Y_{F_0}\mathbf{e}_Y$, the virtual work is given:

$$\begin{aligned}\delta W =& (T - nf_{08X}\frac{dX_C}{d\alpha} - nf_{08Y}\frac{dY_C}{d\alpha})\delta\alpha + \\ & [(1+n)f_{08Y} + f_{95Y}]\delta Y_{F_0}.\end{aligned} \tag{D.8}$$

Substituting Eqs. (D.8) and (D.6) into (D.1) and set the coefficients of $\delta\alpha$ and δY_{F_0} to zero, yields

$$\begin{aligned}T &= [nf_{08X} + (k_1\kappa_1 - k_2\kappa_2)X_C]\frac{dX_C}{d\alpha} \\ &+[nf_{08Y} + k_1\kappa_1(Y_C - s_1) + k_2\kappa_2(Y_{F_0} - Y_C)]\frac{dY_C}{d\alpha}\end{aligned} \tag{D.9}$$

and

$$f_{95Y} = -(1+n)f_{08Y} - k_2\kappa_2(Y_{F_0} - Y_C). \tag{D.10}$$

The side force f_{95X} can be found by taking the moment about point C of the forces acting on the pantograph,

$$f_{95X} = -(1+n)f_{08X} + k_2\kappa_2 X_C. \tag{D.11}$$

Finally, summing all the forces acting on pantograph, yields

$$\begin{aligned} f_{37X} &= n f_{08X} - k_2 \kappa_2 X_C \\ f_{37Y} &= n f_{08Y} + k_2 \kappa_2 (Y_{F_0} - Y_C). \end{aligned} \tag{D.12}$$

Bibliography

Adachi, H., Koyachi, N., Nakamura, T., and Homma, K., 1990, "Develpoment of a Quadruped Walking Machine and Its Adaptive Crawl Gait," *1990 Japan-USA Symposium on Flexible Automation - A Pacific Rim Conference*, pp. 91–94, Iscie, Kyoto, Japan.

Akhras, R., and Angeles, J., 1990, "Unconstrained Nonlinear Least-Square Optimization of Planar Linkages for Rigid-Body Guidance," Mechanism and Machine Theory, Vol. 25, No. 1, pp. 97–118.

Alexander, R. M., 1990, "Three Uses for Springs in Legged Locomotion," The International Journal of Robotics Research, Vol. 9, No. 2, pp. 53–61.

Antuma, H. J., 1978, "Triangular Nomograms for Symmetrical Coupler Curves," Mechanism and Machine Theory, Vol. 13, No. 3, pp. 251–267.

Bekker, M. G., 1969, *Introduction to Terrain-Vehicle Systems*, University of Michigan Press, Ann Arbor, Michigan.

Bhatia, D. H., and Bagci, C., 1977, "Optimum Synthesis of Multiloop Planar Mechanisms for the Generation of Paths and Rigid-Body Positions by the Linear Partition of Design Equations," ASME Journal of Engineering for Industry, pp. 116–123.

Bonnans, J. F., Panier, E., Tits, A. L., and Zhou, J., 1992, "Avoiding the Maratos Effect by Means of a Nonmonotone Line Search: II. - Feasible Iter-

ates," SIAM J. Numerical Analysis, Vol. 29, No. 4, pp. 1187–1202.

Byrd, J. S., and DeVries, K. R., 1990, "A Six-Legged Telerobot for Nuclear Applications Development," The International Journal of Robotics Research, Vol. 9, No. 2, pp. 43–52.

Chen, N. X., and Song, S. M., 1992, "Optimal Synthesis and Analysis of a New Leg Mechanism: The Planetary Gear Leg," *Proc. of ASME: Robotics, Spatial Mechanisms, and Mechanical Systems.* ASME DE-Vol. No. 45, pp. 155-161.

Dhandapani, S., and Ogot, M. M., 1994, "Modeling of a Leg System to Illustrate the Feasibility of Energy Recovery in Walking Machines," *Advances in Design Automation.* DE-Vol. No. 69-2, ASME Pub., pp. 429-436.

Dijksman, E., 1976, *Motion Geometry of Mechanisms*, Cambridge University Press, 4th Eds., London, UK.

Dijksman, E. A., 1975, "Kempe's (Focal) Linkages Generalized, Particularly in Connection with Hart's Second Straight-Line Mechanism," Mechanism and Machine Theory, Vol. 10, No. 6, pp. 445–460.

Dijksman, E. A., 1979, "Symmetrical Coupler Curves, Produced by a 6-Bar Linkage of Type Stephenson-I," *Proceedings of Fifth World Congress on Theory of Machine and Mechanism*, pp. 537–540.

Dijksman, E. A., 1980a, "Half-Symmetrical 6-Bar Curves Produced by Focal Linkages or Their Derivatives," Mechanism and Machine Theory, Vol. 15, No. 3, pp. 221–228.

Dijksman, E. A., 1980b, "Highest-Order Coupler Points of Watt-I Linkages, Tracing Symmetrical 6-Bar Curves," Mechanism and Machine Theory, Vol. 15, No. 6, pp. 421–434.

Dijksman, E. A., 1981, "Watt-I Linkages with Shunted Chebyshev-Dyads, Pro-

ducing Symmetrical 6-Bar Curves," Mechanism and Machine Theory, Vol. 16, No. 2, pp. 153–165.

Dijksman, E. A., 1984, "An Unsymmetrical Watt-I Linkage Generating A Family of Symmetrical Curves," Mechanism and Machine Theory, Vol. 19, No. 3, pp. 297–306.

Fan, M. K. H., Wang, L. S., Koninckx, J., and Tits, A. L., 1990, *CONSOLE - User's Manual*, Version 1.1, SRC-TR-87-212r2, Institute for Systems Research, University of Maryland, College Park, Maryland.

Freudenstein, F., and Sandor, G. N., 1961, "On the Burmester Points of a Plane," ASME Journal of Applied Mechanics, pp. 41–49.

Funabashi, H., Ogawa, K., Gotoh, Y., and Kojima, K., 1985a, "Synthesis of Leg-Mechanisms of Biped Walking Machines (Part I, Synthesis of Ankle-Path-Generator)," Bulletin of JSME, Vol. 28, No. 237, pp. 537–543.

Funabashi, H., Ogawa, K., Gotoh, Y., and Kojima, K., 1985b, "Synthesis of Leg-Mechanisms of Biped Walking Machines (Part II, Synthesis of Foot-Driving Mechanism)," Bulletin of JSME, Vol. 28, No. 237, pp. 544–549.

Han, C., 1966, "A General Method for the Optimum Design of Mechanisms," Journal of Mechanisms, Vol. 1, pp. 301–313.

Hartenberg, R., and Denavit, J., 1964, *Kinematics Synthesis of Linkages*, McGraw-Hill Inc., New York, New York.

Hirose, S., 1984, "A Study of Design and Control of a Quadruped Walking Vehicle," The International Journal of Robotics Research, Vol. 3, No. 2, pp. 113–133.

Hirose, S., and Kunieda, O., 1991, "Generalized Standard Foot Trajectory for a Quadruped Walking Vehicle," The International Journal of Robotics Re-

search, Vol. 10, No. 1, pp. 3–12.

Hirose, S., and Umetani, Y., 1980, "The Basic Motion Regulation System for a Quadruped Walking Machine," ASME Paper No. 80-DET-34, delivered at the ASME Design Engineering Technical Conference, Los Angeles, California.

Huang, C., and Roth, B., 1993, "Dimensional Synthesis of Closed-Loop Linkages to Match Force and Position Specification," ASME Journal of Mechanical Design, Vol. 115, pp. 194–198.

Huang, C., and Roth, B., 1994, "Position-Force Synthesis of Closed-Loop Linkages," ASME Journal of Mechanical Design, Vol. 116, pp. 155–162.

Klein, C. A., Olson, K. W., and Pugh, D. R., 1983, "Use of Force and Attitude Sensors for Locomotion of a Legged Vehicle Over Irregular Terrain," The International Journal of Robotics Research, Vol. 2, No. 2, pp. 3–17.

Koyachi, N., Adachi, H., Nakamura, T., and Nakano, E., 1990, "Stair Adapting Control of Semi-Fixed Gait Hexapod Walking Robot," *1990 Japan-USA Symposium on Flexible Automation - A Pacific Rim Conference*, pp. 95–98, Iscie, Kyoto, Japan.

Matthew, G. K., and Tesar, D., 1977b, "Synthesis of Spring Parameters to Balance General Forcing Functions in Plannar Mechanisms," ASME Journal of Engineering for Industry, pp. 347–352.

Matthew, G. K., and Tesar, D., 1977a, "Synthesis of Spring Parameters to Satisy Specified Energy Levels in Plannar Mechanisms," ASME Journal of Engineering for Industry, pp. 341–346.

McLarnan, C. W., 1963, "Synthesis of Six-Link Plane Mechanisms by Numerical Analysis," ASME Journal of Engineering for Industry, pp. 5–11.

Morecki, A., Bianchi, G., and Kedzior, K., 1985, "Theory and Practice of Robots

and Manipulators," Proc. of Romansy 1984: The Fifth CISM-IFToMM Symposium, Hermes Publishing, Kogan Page, London, pp. 403.

Mosher, R. S., 1968, "Test and Evaluation of a Versatile Walking Truck,". Proceedings of Off-Road Mobility Symposium, International Society for Terrain Vehicle Systems, Washington, D.C., pp. 359-379.

Nye, W. T., and Tits, A. L., 1986, "An Application-Oriented Optimization-Based Methodology for Interactive Design of Engineering Systems," International Journal of Control, Vol. 43, No. 6, pp. 1693–1721.

Panier, E., and Tits, A. L., 1993, "On Combining Feasibility, Descent and Superlinear Convergence in Inequality Constrained Optimization," J. of Mathematical Programming, Vol. 59, No. 2, pp. 261–276.

Pugh, D. R., Ribble, E. A., Vohnout, V. J., Bihari, T. E., Walliser, T. M., Patterson, M. R., and Waldron, K. J., 1990, "Technical Description of the Adaptive Suspension Vehicle," The International Journal of Robotics Research, Vol. 9, No. 2, pp. 24–42.

Roth, B., 1967, "Finit-Position Theory Applied to Mechanism Synthesis," ASME Journal of Applied Mechanics, pp. 599–605.

Roth, B., and Freudenstein, F., 1963, "Synthesis of Path-Generating Mechanisms by Numerical Methods," ASME Journal of Engineering for Industry, pp. 298–306.

Russell, M., 1983, "Odex I: The First Functionoid," Robotics Age, Vol. 5, No. 5, pp. 12–18.

Ryan, A. D., and Hunt, K. H., 1985, "Adjustable Straight-Line Linkages - Possible Legged-Vehicle Applications," ASME Journal of Mechanisms, Transmissions, and Automation in Design, Vol. 107, pp. 256–261.

Sarkisyan, Y. L., Gupta, K. C., and Roth, B., 1972, "Kinematic Geometry Associated with the Least-Square Approximation of a Given Motion," ASME Paper No. 72-Mech-14, delivered at the Mechanisms Conference, San Francisco, California.

Shieh, W. B., Tsai, L. W., Azarm, S., and Tits, A. L., 1995, "Multiobjective Optimization of a Leg Mechanism with Various Spring Configurations for Force Reduction,". Advances in Design Automation, DE-Vol. No. 82, ASME Pub., pp. 811-818 (also, accepted in the Trans. ASME, Journal of Mechanical Design).

Shin, E., and Streit, D. A., 1993, "An Energy Efficient Quadruped with Two-Stage Equilibrator," ASME Journal of Mechanical Design, Vol. 115, No. 1, pp. 156–163.

Song, S. M., Lee, J. K., and Waldron, K. J., 1987, "Motion Study of Two- and Three-Dimensional Pantograph Mechanisms," Mechanism and Machine Theory, Vol. 22, No. 4, pp. 321–331.

Suh, C. H., and Radcliffe, C. W., 1967, "Synthesis of Plane Linkages with Use of the Displacement Matrix," ASME Journal of Engineering for Industry, pp. 206–214.

Sutherland, G. H., and Roth, B., 1974, "An Improved Least-Square Method for Designing Function-Generating Mechanisms," ASME Paper No. 74-Det-4, delivered at the Mechanisms Conference, New York, New York.

Sutherland, I. E., and Ullner, M. K., 1984, "Footprints in the Asphalt," The International Journal of Robotics Research, Vol. 3, No. 2, pp. 29–36.

Thompson, B., 1975, "A Survey of Analytical Path-Synthesis Techniques for Plane Mechanisms," Mechanism and Machine Theory, Vol. 10, pp. 197–205.

Todd, D. J., 1985a, "A Pneumatic Walking Robot," Robotics Age, Vol. 7, No. 1, pp. 31–35.

Todd, D. J., 1985b, *Walking Machines - An Introduction to Legged Robots*, First Eds., Krogan Page, Ltd., London, UK.

Tsai, L., 1995, *Systematic Design of Mechanisms*, Classnote of ENME 604, Dept. of Mechanical Engineering, University of Maryland, College Park, Maryland.

Tsai, L. W., and Lu, J.-J., 1990, "Coupler-Point-Curve Synthesis Using Homotopy Methods," ASME Journal of Mechanical Design, Vol. 112, No. 3, pp. 384–389.

Tull, H., and Lewis, D., 1968, "Three Dimensional Kinematic Synthesis," ASME Journal of Engineering for Industry, Vol. 90, pp. 481–484.

Waldron, K. J., Vohnout, V. J., Pery, A., and McGhee, R. B., 1984, "Configuration Design of the Adaptive Suspension Vehicle," The International Journal of Robotics Research, Vol. 3, No. 2, pp. 37–48.

Zhou, J. L., and Tits, A. L., 1993, "Avoiding the Maratos Effect by Means of a Nonmonotone Line Search: II. - Feasible Iterates," J. of Optimization Theory and Application, Vol. 76, pp. 455–476.